

UNIVERSITY OF CALIFORNIA

Santa Barbara

Photochemical and Photophysical Investigations of Newly Designed
Supramolecular Structures Composed of Quantum Dots and Nitric Oxide Donors

A Dissertation submitted in partial satisfaction of the
requirements for the degree Doctor of Philosophy
in Chemistry

by

Daniel Neuman

Committee in charge:

Professor Peter C. Ford, Chair

Professor Richard J. Watts

Professor Steven K. Buratto

March 2007

The dissertation of Daniel Neuman is approved.

Richard J. Watts

Steven K. Buratto

Peter C. Ford, Committee Chair

January 2007

Photochemical and Photophysical Investigations of Newly Designed
Supramolecular Structures Composed of Quantum Dots and Nitric Oxide Donors

Copyright © 2007

by

Daniel Neuman

ACKNOWLEDGEMENTS

There are countless people to whom I am indebted for helping me breakthrough and realize my full potential.

First and foremost, I must thank my parents, Andrei and Anca Neuman, without whose encouragement and continued support none of this would have been possible. They came to a foreign land to provide a better life for me and for this I promise to carry the torch and maintain the family honor!

Thank you also to my advisor Professor Peter Ford who has molded me into the scientist I am today. Professor Ford, whom I'll always remember for declaring "...I'm not in the business of training monkeys..." allowed me to follow my own passions and interests, but made sure to keep me focused on the work at hand. Besides the intellectual freedom provided by Professor Ford, he could always be counted on to have an "open door" policy when it came to dealing with the countless frustrations that are all too common in a graduate student's career. Thanks for everything and I look forward to working with you as a colleague in the future.

I must say something about the wonderful members, both present and past, of the Ford group. Graduate school can be a hard and frustrating ordeal and would be much more difficult to bear without so many great individuals working around you on a daily basis. I especially want to thank Alexis Ostrowski, whom even after the many warnings and disclaimers about the potential perils of taking on my

project, has worked very hard to help me push this work to where it is today. Much of the work presented in chapters IV and V was done in collaboration with Alexis, and I am indebted to her for her drive and perseverance. The studies presented here are based on the earlier investigations by Dr. Malcolm De Leo and Dr. Frank DeRosa, both recent graduates of the Ford group and I must thank them for the hard work they committed to this project. I would also like to thank the other current members of the Ford Group for putting up with me over the past several years. Thank you Ryan Absalonson for being a great lab mate; I hope you find your inspiration buddy!

Many thanks also to my committee members Professor Steve Buratto and Professor Richard Watts for always being critical of my research ideas and propositions. I would also like to thank Professor Geoff Strouse whom sparked my interest in the exciting world of nanotechnology.

I likely would never have gotten a “Ton-20” the hard hard way if I hadn’t been introduced to playing darts by Gary Braun. Besides being a great dart player and talented musician, Gary is a brilliant scientist. On top of that, he has been a great friend. Thank you for all the intellectual conversations and technical help. Trudging through the world of nanotech would have been much more difficult without you.

I owe a lot to Dr. Steve Wecksler for inspiring me to stay motivated in the face of seeming endless frustration and to keep my eyes on the goal. I see great wines

in our future. Also, Dr. Travis Jennings and Dr. Mia Berrettini, I truly value the great times we had together and look forward to our paths crossing again soon.

Within the Chemistry department at UCSB, there are countless support staff that truly keep the motor running smoothly. Thank you to Skip Touponce and Neil Hicks in the Research Storeroom, Luis Pratt of the electronics shop, Richard Bock in the glass shop, Art Ramirez in purchasing, Tom Wise in IT, and of course the team in the machine shop Terry Hart, Bruce Dunson, and Mike Johnson. Thanks also to Dr. James Pavlovich in the mass spectrometry laboratory and Dr. Ata Shirazi of the NMR facility for helping me with instrumental and experimental troubleshooting.

Dr. Jerry Hu of the NMR facility in the Materials Research Laboratory at UCSB supplied his knowledge and expertise for the solid state NMR studies presented here and I thank him for this.

Special thanks also to Dr. Alexander Mikhailovsky with whom I collaborated for the ultrafast spectroscopy studies presented here. Thank you for all the stimulating discussions and advice.

To all my friends whom I've met here in Santa Barbara outside of graduate school, you guys have kept me grounded and I hope the music never stops! Special thanks to Kevin and Amy Donnelly for all of your support and helping me break out of my shell..."P-A-N-A-M-A!!"

And my beautiful fiancée Tess Hartwell, I cannot even begin to describe how indebted I feel to you for your endless support over the last three years. You have

been my inspiration to move forward and do something truly wonderful with my life. These have been times that have truly tested the ties that bind us, and we are only stronger now. Your everlasting love is a fire that keeps me burning. We will do great things in this life together!

To my parents Andrei and Anca Neuman, this one is for you!

VITA OF DANIEL “NANO” NEUMAN

Education

- Ph.D in Inorganic Chemistry, University of California, Santa Barbara, Santa Barbara, CA. **January 2007**.
Thesis: *Photochemical and Photophysical Investigations of Newly Designed Supramolecular Structures Composed of Quantum Dots and Nitric Oxide Donors*
Advisor: Professor Peter C. Ford
- B.A. in Chemistry (*cum laude*), Boston University, (MA), **2000**
Project Title: *Synthesis and Characterization of Trinuclear Rhenium Clusters Based on the $[Re^{III}_3(\mu-Cl)_3]$ Core Unit*
Advisor: Professor Pericles Stravropoulos

Experience

- 2004-Present Graduate Research Assistant, University of California (Santa Barbara)
Advisor: Professor Peter C. Ford
- 2000-2004 Graduate Research Assistant, University of California (Santa Barbara)
Advisors: Professor Peter C. Ford
Professor Geoffery F. Strouse (moved to FSU, 01/2004)
- 1998-2000 Undergraduate Research Assistant, Boston University (MA)
Advisor: Pericles Stravropoulos

Affiliations

- American Chemical Society
- Materials Research Society

Publications

- “*Photosensitized NO Release from Water Soluble Nanoparticle Assemblies*” Neuman, D.; Ostrowski, A. D.; Absalonson, R. O.; Strouse, G. F.; Ford, P. C. submitted to *J. Am. Chem. Soc.*, **2007**
- “*Electrostatic Assemblies Between Quantum Dots and Chromium (III) Complexes Probed by Photoluminescence Quenching. Demonstration of the Sensitized Release of Nitric Oxide*” Neuman, D.; Ostrowski, A. D.; Mikhailovsky, A. A.; Absalonson, R. O.; Strouse, G. F.; Ford, P. C. *in preparation*.

- “*Decoration of Quantum Dot Surfaces with Photo-active Chromium (III) Cyclam Complexes*” Neuman, D.; Strouse, G. F.; Ford, P. C. *in preparation*.
- “*Structural and Functional Characteristics of Rhenium Clusters Derived from Redox Chemistry of the Triangular [Re^{III}₃(μ-Cl)₃] Core Unit*” Neuman, D.; Paraskevopoulou, P.; Psaroudakis, N.; Mertis, K.; Staples, R.; Stavropoulos, P. *Inorg. Chem.*, **2000**, *39*, 5530-5537.

Presentations

- **Oral Presentation** - “*New Quantum Dot Based Supramolecular Structures for Photochemical Drug Delivery*”, Neuman, D.; Strouse, G. F.; Ford, P. C. Materials Research Society National Meeting, **2005** (Boston, MA).
- **Poster Presentation** - “*Investigating the luminescent properties of CdSe quantum dots: photo-enhancement and quantum yield fluctuations*” Neuman, D. N.; Strouse, G. F.; Ford, P. C. American Chemical Society National Meeting, **2004** (Philadelphia, PA).
- **Poster Presentation** - “*Optical Properties of CdSe Nanoparticle Doped Sol-Gels*” Neuman, D.; Ford, P. C.; Strouse, G. F. Materials Research Society Spring Meeting, **2002** (San Francisco, CA).
- **Oral Presentation** - “*CdSe Glasses: Sensitivity to Biological Molecules*” Neuman, D.; Ford, P. C.; Strouse, G. F. Southern California Inorganic Photochemistry Conference, **2001** (Catalina Islands, CA).
- **Poster Presentation** - “*Trinuclear Rhenium Clusters as Catalysts in Hydrocarbon Oxidations.*” Neuman, D.; Stavropoulos, P. American Chemical Society National Meeting, **2000**, (San Francisco, CA).

This material is based upon work supported by the National Science Foundation
under Grant No. 0352650.

ABSTRACT

Photochemical and Photophysical Investigations of Newly Designed
Supramolecular Structures Composed of Quantum Dots and Nitric Oxide Donors

by

Daniel Neuman

Nitric oxide (NO), a ubiquitous messenger molecule in mammalian physiology, is also known to act as a potent γ -radiation sensitizer. For this reason, there is considerable interest in the development of thermally stable compounds capable of controllably releasing NO. Such compounds could see broad application for the enhancement of existing cancer treatment strategies. In this context, photochemically activated NO precursors are attractive given the opportunity to control the location and timing of the signal leading to release of NO. With this in mind, the work described here exploits the extraordinary light absorbing capabilities of semiconductor quantum dots (QDs) both in the single photon excitation (SPE) and two photon excitation (TPE) regimes and demonstrates their potential applicability as photosensitizers for NO releasing prodrugs.

In this dissertation, new supramolecular structures will be described that are composed of chromium(III) complexes of cyclam (cyclam = 1,4,8,11-tetraazacyclotetradecane) both covalently bound to and electrostatically assembled on the surface of water soluble CdSe/ZnS QDs. Previous studies on the nitrito (ONO) derivatives of the chromium cyclam complexes indicated that they are photo-labile towards release of NO with quantum yields as high as 50 %. However, these complexes lack absorption at long wavelengths (>600 nm) where biological tissue penetration is enhanced. Investigations of the electrostatic assemblies in aqueous solution demonstrate that the Cr(III) complexes quench the QD photoluminescence (PL) obtained via either SPE (366-546 nm) or TPE (800 nm) excitation in a concentration dependent manner. Furthermore, in the electrostatic assemblies containing the dinitrito *trans*-Cr(cyclam)(ONO)₂⁺ cation and CdSe/ZnS QDs, photolysis of the assembly results in enhanced photochemical NO release (up to 50 fold more) as compared to the Cr(III) complexes alone. The photophysical and photochemical properties of these QD/chromium(III) cyclam structures are the subjects of this dissertation..

TABLE OF CONTENTS

1. Chapter I. Background	1
A. Biology of NO	2
i. Discovery of NO Synthesis in the Body: Vasodilation	2
ii. NO in Immune Response	9
iii. NO in Cancer Therapy	10
B. Photochemical NO Donors	13
i. Photodynamic Therapy (PDT)	13
ii. Design of Photochemical NO donors	15
iii. Chromium(III) Nitrito Complexes	18
C. Semiconductor Nanoparticles (Quantum Dots)	33
i. What are Quantum Dots?	33
ii. QD synthesis	35
iii. QD Optical Properties	38
iv. QD Surface Functionalization	41
D. Current Studies	44
i. New Quantum Dot Based Supramolecular Structures for Photochemical Nitric Oxide Delivery	44
ii. Photoenhancement of QDs in the Presence of Nitric Oxide	49
E. References	51
2. Chapter II. Experimental	58
A. Reagents and Instrumentation	58

i. Reagents.....	58
ii. Solvents.....	59
iii. Gases.....	60
iv. Instrumentation and Methods.....	60
B. Synthesis	70
i. Cadmium Selenide (CdSe) Nanocrystal Quantum Dots (QDs).....	70
ii. Growth of a Zinc Sulfide (ZnS) shell to give CdSe/ZnS Core/Shell QDs.....	75
iii. QD Surface Ligand Exchange to Give Water Soluble QDs.....	81
iv. Preparation of Silica based Sol-Gels Embedded with CdSe-HDA.	84
v. Simple Chromium(III) Cyclam Complexes	85
vi. C-Substituted Cyclam Complexes.....	85
vii. Coupling Reactions of QDs and Various Cyclam Complexes	93
C. References.....	96
3. Chapter III. Conjugation of Various Cyclam Analogues to	
 Quantum Dot Surfaces.....	98
A. Introduction.....	98
B. Thiol Functionalized Cyclams for Binding to QD Surfaces.....	99
i. Functionalization of Chromium(III) Cyclam with Lipoic Acid.....	100
ii. Functionalization of Chromium Cyclam with DHLA: Surface Exchange of QDs	108
C. Surface Conjugation Reactions Between Water Soluble QDs and	
 Chromium (III) Cyclam Complexes.....	111
i. CdSe-MPA Conjugated with hbc (6) or Cr(hbc)Cl ₂ ⁺ (7)	111
ii. Conjugation of Cr(abc)Cl ₂ ⁺ to the Surface of DHLA Coated CdSe/ZnS QDs.....	120

D. Future Potential	128
E. References.....	131
4. Chapter IV. Photophysical Investigations of Electrostatic Assemblies Between Quantum Dots and <i>trans</i>-Dichloro Chromium(III) Cyclam.....	134
A. Introduction.....	134
B. Experimental	135
C. Results and Discussion	137
i. Photoluminescence Quenching of QDs by [trans-Cr(cyclam)Cl ₂]Cl.....	137
ii. Femtosecond Transient Absorbance of 1S Transition in the QDs.....	145
iii. Mechanism for Quantum Dot PL Quenching.....	146
iv. Complications Due to “Surface Effects”?	152
D. Conclusions.....	154
E. References.....	156
5. Chapter V. Photochemistry of Electrostatic Assemblies Between Quantum Dots and [trans-Cr(cyclam)(ONO)₂]BF₄. Sensitized Release of Nitric Oxide.....	159
A. Introduction.....	159
B. Experimental	160
i. Materials	160

ii. Single and Two Photon Excited Photoluminescence	161
iii. Continuous Wave Photolysis and Nitric Oxide Detection	162
C. Results and Discussion	163
i. Photoluminescence Quenching of QDs by 2.....	163
ii. Electrochemical Detection of Sensitized NO Production	168
iii. Two Photon Sensitization in Assemblies of QDs with Cr(cyclam)(ONO) ₂ ⁺	176
D. Conclusions.....	180
E. References.....	182
6. Chapter VI. Conclusions and Future Potential.....	185
References.....	190
I. Appendix I. Photoenhancement in CdSe QDs in the Presence	
of NO	192
A. Introduction.....	192
B. Experimental	195
C. Results and Discussion	195
D. References.....	201

LIST OF FIGURES

Figure 1.1. Synthesis of nitric oxide and its action in vasodilation.	7
Figure 1.2. Potential fates of carbon centered radicals formed during γ -radiation therapy.....	12
Figure 1.3. Strategies for photochemical generation of nitric oxide presented with the dinitrito <i>trans</i> - Cr(III) cyclam model system.	17
Figure 1.4. Energy level diagram for a d^3 metal system in octahedral and reduced symmetries.	19
Figure 1.5. Demonstration of Adamson's rules for photoaquation of coordination complexes of chromium(III) in pseudo-octahedral ligand fields.	20
Figure 1.6. Effects of stereorigidity of the non-labilized axis on the photoaquation quantum yield of <i>trans</i> -Cr(III) dichloro complexes.	21
Figure 1.7. Photochemistry of nitritometalloporphyrins as outlined by Hoshino. ⁵¹	23
Figure 1.8. Extinction spectrum of <i>trans</i> -[Cr(cyclam)(ONO) ₂] ₂ BF ₄ in aqueous solution.....	24
Figure 1.9. Photochemistry of <i>trans</i> -[Cr(cyclam)(ONO) ₂](BF ₄) in aqueous solution.....	26
Figure 1.10. Nickel templated synthesis for "C-substituted" cyclam analogues. .	29
Figure 1.11. NO amperogram demonstrating enhanced NO production from appended conjugated organic functionalities. All solutions had equal starting concentrations (990 nM). Reprinted in modified form with permission from(DeRosa, F.; Bu, X.; Ford, P. C. <i>Inorg. Chem.</i> 2005, 44, 4157-4165. Copyright 2007 American Chemical Society.....	31
Figure 1.12. Size tuned optical properties of CdSe QDs A) Absorbance spectra of different sized CdSe QDs in toluene. B) Image showing photoluminescence from solid sol gels embedded with 3 different QD sizes. (Blue background is due to UV hand lamp used to illuminate the sol-gels)..	34
Figure 1.13. CdSe QD photoluminescence brightening data obtained by Dr. Leroy Laverman upon continuous laser irradiation of a sol gel doped with CdSe QDs in the presence of a nitric oxide atmosphere.	50

Figure 2.1. Example of use of absorbance to monitor the CdSe-HDA QD growth. Also shown (green dashed line) is the PL spectrum of the last aliquot (~3.7 nm QDs).....	72
Figure 2.2. Comparison of the optical properties (absorbance and PL) of 3.8 nm core CdSe QDs (black circles) grown by the hot injection route and the corresponding CdSe/ZnS core/shell QDs (blue squares) grown via the slow addition of organometallic shell precursors. Inset: Absorbance of “out-of-batch” aliquots diluted in hexanes removed during shell growth to monitor progression of the 1S transition.	77
Figure 2.3. Optical properties (absorbance and PL) of 3.0 nm CdSe-HDA cores (grey circles) and corresponding CdSe/ZnS core/shell QDs (red squares) shelled via SILAR. Inset: Absorbance of “out-of-batch” aliquots diluted in hexanes following each injection and following sample annealing, demonstrating red shift and broadening of 1S transition (red tail in the later injections is due to a scattering edge from particulates in the samples.)	80
Figure 3.1. Functionalized C-substituted <i>trans</i> -chromium(III) cyclam complexes.	99
Figure 3.2. Potential reactions for the generation of a DHLA functionalized <i>trans</i> -chromium cyclam complex.....	101
Figure 3.3. ESI (+) mass spectrum of 11.	103
Figure 3.4. UV-vis extinction spectrum of 11 in methanol.....	104
Figure 3.5. Absorbance spectra over the course of 170 min. reaction of 11 with 3.6 equiv. of NaBH ₄ in methanol.....	106
Figure 3.6. ESI (+) mass spectrum of an aliquot removed following 170 min. during the reduction of 11 with NaBH ₄ in methanol.	107
Figure 3.7. Surface exchange and surface conjugation of CdSe QDs to form mQDs.....	113
Figure 3.8. Infrared absorbance spectra of starting materials and surface conjugated mQDs in KBr. Line indicates ν_{CO} at 1710 cm ⁻¹	114
Figure 3.9. Solid state CPMAS ¹³ C NMR spectra of B) CdSe-MPA, C) hbc (6), and D) mQD coupling product of CdSe-MPA and 6. Dashed line indicates shoulder at 170-175 ppm assigned to the ester product in D). The spectrum in A) is a ¹³ C NMR of the QD ligand MPA in CDCl ₃	116
Figure 3.10. False color image taken of the electrophoresis gel comparing electrophoretic mobility of the QD-DHLA and the modified QD-PEG	

conjugates towards the positive electrode (up) in a 1.5% agarose gel. Lane 3 (mQD with mPEG-NH₂), Lane 5 (DHLA coated QD starting material), and Lane 12 (6 nm gold nanoparticles used as an imaging standard).....123

Figure 3.11. False color image comparing electrophoretic mobility of QD-DHLA and indicated purified QD conjugates towards the positive electrode (up) in a 1.5 % agarose gel. Lane 2 (DHLA coated QD starting material), Lane 3 (mQDs modified with mPEG-NH₂), Lane 4 (mQDs modified with a 100:1 mixture of mPEG-NH₂ and 9), and Lane 7 (6 nm gold nanoparticle standard used for imaging purposes).125

Figure 3.12. PL spectra of absorbance matched phosphate buffered solutions (15 mM, pH 8.2) of the two conjugates QD-mPEG and QD-mPEG-Cr(abc)Cl₂. Spectra were excited at 450 nm.126

Figure 4.1. Spectrum showing the overlap of the water soluble core/shell CdSe/ZnS QD photoluminescence with the Q₁ absorbance band of [*trans*-Cr(cyclam)Cl₂]Cl in aqueous solution.136

Figure 4.2. A) Top: Photoluminescence spectra of the QDs showing changes due to increasing concentration of 1. Each trace represents an independently prepared sample having a constant QD concentration (190 nM) and varied 1 concentration (0–1000 μM). The QD PL is excited at 460 nm where the absorbance of 1 is negligible at the concentrations used here. Inset shows the UV-vis absorbance of each sample. Arrow indicates increasing [1]. B) Bottom: Stern Volmer type plot where I is the PL intensity of the QDs at the PL λ_{max} and I₀ is the PL intensity of the QDs in the absence of 1. The upper set of points (red dots) indicate samples which were acquired in 15 mM phosphate buffer, while the lower set (blue squares) were acquired under otherwise identical solutions with 250 mM added KCl.....138

Figure 4.3. Time resolved PL of water soluble QDs used in this study in aqueous solution (190 nM). QDs are excited with ~ 120 fs pulses tuned to 460 nm. QD PL is monitored at λ_{max} = 570 nm. The trace through the data represents a fit according to Eq. 4.1 with n = 4 (see text). A residual plot above the data demonstrates the “goodness of fit”.139

Figure 4.4. Comparison of QD time resolved PL as a function of increasing concentrations of 1 (same samples used to generate steady state data in Figure 4.2).....141

Figure 4.5. Stern-Volmer type plot showing the effect of increasing KCl concentration on the PL intensity of aqueous solutions of QDs. Each point represents an individual sample of QDs diluted to 190 nM in 15 mM

phosphate buffer solution (pH 8.2) having various concentrations of KCl added.	144
Figure 4.6. TA dynamics of the QDs measured at 530 nm for 190 μM solutions of QDs with varied concentrations of 1. The data sets are 0 mM (filled circles), 5 mM (filled squares), and 10 mM (filled triangles) 1. The lines represent double exponential fits to the data. Inset shows the spectral data for the recovery of the bleach of the QD 1S transition (<i>without</i> 1 added) at various delay times after the pump pulse.....	146
Figure 4.7. Idealized drawing of <i>trans</i> -Cr(cyclam)Cl ₂ ⁺ cations electrostatically assembled within the hydration sphere of DHLA coated CdSe/ZnS QDs...	149
Figure 5.1. Diagram of continuous wave photolysis and NO detection experimental set-up.....	162
Figure 5.2. Optical data for solutions of QDs (190 nM) mixed with varied concentrations of 2 (0-1000 μM). A) Absorbance data for mixtures of QDs (190 nM) and 2 (0-630 μM). Arrows indicate 366 nm excitation used in B) and 546 nm excitation used in C). B) PL spectra of QDs (190 nM) and mixed with varied concentrations of 2 (0-630 μM) obtained with 366 nm excitation. Spectra have been corrected for inner-filter effects due to absorbance of 2 at this wavelength. C) PL spectra of QDs (190 nM) and mixed with varied concentrations of 2 (0-1000 μM) obtained with 546 nm excitation.	164
Figure 5.3. Spectra comparing the PL of phosphate buffered solutions (15 mM, pH 8.2) of QDs alone (190 nM, solid circles) or mixed with 2 (630 μM , open squares). Inset is a blow up showing the spectra normalized to the peak maxima.....	165
Figure 5.4. Stern-Volmer plot for solutions of QDs in phosphate buffer (15 mM, pH 8.2) at constant concentration (\sim 190 nM) with varied concentrations of Cr(III) complex. I is the PL intensity at the λ_{max} and I_0 is the corresponding PL intensity of QDs without any complex added.	166
Figure 5.5. Spectral overlap of the DHLA coated CdSe/ZnS QDs PL with the absorbance of 1 and 2. All spectra taken in phosphate buffer (15 mM, pH 8.2).	167
Figure 5.6. Photoreaction of 2 under aerated conditions.	168
Figure 5.7. NO amperograms comparing electrode response to continuously stirred and irradiated (320-390 nm BP) phosphate buffered solutions with (solid circles) or without (empty circles) QDs (100 nM) following injection	

of 2 to give a final concentration of 200 μM . Injection is indicated by dashed arrow.	169
Figure 5.8. Photochemical release of NO from electrostatic assemblies of QDs and <i>trans</i> -Cr(cyclam)(ONO) ₂ ⁺	170
Figure 5.9. Absorbance spectra of a sample of 2 (221 μM) irradiated (320-390 nm BP) until a limiting spectra was reached. Inset shows the corresponding changes observed for a sample irradiated for only 30 s.	171
Figure 5.10. The diffusion limited reaction of the superoxide anion with NO forming the peroxy nitrite anion which spontaneously rearranges to the nitrate anion.	171
Figure 5.11. NO amperograms for three continuously stirred, irradiated (320-390 nm BP) solutions of 2 (221 μM) generated using <i>Procedure B</i> . Sharp lines mark the light “on” and “off” points. For one sample (open circles), following decay of the initial signal, a second irradiation period was conducted.	173
Figure 5.12. NO amperograms obtained during ~20 s irradiation period of dilute phosphate buffered solutions of 2 (221 μM) with (filled squares) and without (open circles) the presence QDs (120 nM). Sharp features are marks indicating the light was turned “on” at 0 s and light “off” at ~20s.	174
Figure 5.13. Comparison of the absorbance spectra of phosphate buffered solutions of 100 nM QDs (circles) and 200 μM 2. Inset shows blow up of 300–600 nm spectral range.	175
Figure 5.14. Comparison of the SPE (400 nm, cw; blue open circles) and TPE (800 nm, 120 fs pulses; red open squares) generated photoluminescence of the DHLA coated CdSe/ZnS QDs used in this study. Both samples were diluted in phosphate buffer (15 mM, pH 8.2).	177
Figure 5.15. A) TPE-PL spectra of solutions of QDs (120 nM) with varied concentrations of 2 (220 and 600 μM) generated by excitation with 120 fs pulses of 800 nm light (80 MHz). (*) Astrisk marks an instrumental artifact present in all of the TPE-PL data. Inset compares normalized TPE-PL spectra of the QDs in the absence of (black filled circles) and presence of 2 at a concentration of 600 μM (red open squares) exemplifying red shift that accompanies quenching. B) Stern-Volmer type plot comparing the TPE-PL quenching data generated with pulsed NIR excitation, to the analogous experiments using cw excitation in the UV and visible range.	179

Figure I.1. Change in the PL quantum yield of a ~ 350 nM solution of CdSe-HDA QDs in toluene with 12 mM dissolved nitric oxide (NO). The sample is continuously stirred while being irradiated with the 488 nm line of an Ar ⁺ laser (13 mW average power). Inset shows the PL spectrum before and after 865 s of continuous photolysis.....	196
Figure I.2. Spectral data comparing effects of light irradiation (800 s, 488 nm at 13 mW) followed by a period of darkness (2490 s) on a ~ 350 nM solution of CdSe-HDA QDs dissolved in toluene with 12 mM NO.....	197
Figure I.3. PL lifetimes measured for a solution of ~350 nM CdSe-HDA QDs dissolved in toluene initially under argon (blue triangles) and following cw photolysis (865 s, 488 nm at 13 mW) with 12 mM dissolved NO added (black squares). Samples were excited with 120 fs pulses tuned to 400 nm (2 MHz).....	198

1. Chapter I. Background

Cancer has become the leading killer of people under the age of 85 in the United States, even surpassing deaths due to heart disease.¹ The “war on cancer” officially began in 1971 with the adoption of the National Cancer Act, and while deaths due to heart disease have decreased dramatically over the past several decades, the numbers that are cancer related remain largely unchanged. An initiative started by the National Cancer Institute (NCI) entitled the “NCI Alliance for Nanotechnology in Cancer” signifies the current drive to develop new strategies in combating this pandemic using the exciting advances being made in the field of nanotechnology.¹

The focus of this dissertation describes the use of semiconductor nanocrystal quantum dots (QDs) as sensitizers for photochemically active transition metal based nitric oxide (NO) donor complexes. The next section will describe the biological significance of NO as well as provide some background describing the potential use of this small molecule as a gamma radiation sensitizer in cancer therapy. I will then provide some background in recent work by our group highlighting one strategy for the controlled delivery of nitric oxide for medical applications, namely, the development of transition metal based molecules that photochemically decompose to release one or more equivalents of NO. Finally, I will describe the reasons why and how semiconductor nanocrystal QDs, one of the most thrilling new chromophores available to the modern scientific investigator,

can be used to enhance the light absorbing properties of existing photo-active NO-donors for the purpose of designing new photochemotherapeutics.

A. Biology of NO

i. Discovery of NO Synthesis in the Body: Vasodilation

Historically, nitrogen monoxide (nitric oxide or simply NO) had a bad reputation as a toxic gas found in nasty places such as greenhouse gas and cigarette smoke. However, the attitude towards this small molecule (weighing in at just 30 amu) began to change drastically in the late 1980's and early 1990's with the discovery that it is not only found in virtually every tissue of human physiology, but in fact is synthesized in many of these tissues constitutively as well as in response to certain biochemical triggers.² By 1992, NO had been classified as the "...smallest, lightest molecule – and the first gas – known to act as a biological messenger in mammals", and named Science magazine's "Molecule of the Year".³

The events leading to the discovery of NO's biological role truly began back in the late 19th century with the use of amyl nitrite and nitroglycerin for treatment of angina pectoris (pain in the heart muscle from lack of oxygen).^{2,4} Based on extensive work by Dr. T. Lauder Brunton, a pioneer of modern experimental pharmacology, amyl nitrite was found to relieve angina pectoris by decreasing tension in arteries delivering blood to the heart.⁴ Over the next century, this led to the increasingly common practice of administering organic nitrates, and more

recently the inorganic nitro- containing molecule sodium nitroprusside (SNP), for the treatment of a variety of disorders including angina, acute congestive heart failure, and in hypertensive emergencies.⁵

It was not until the 1970's that several independent studies, originally directed at discerning the involvement of cyclic radionucleotides in the mechanical action of smooth muscle, demonstrated that the therapeutic effect of vasodilators was linked to the activation of guanylate cyclase⁶, an enzyme in smooth muscle tissue that catalyzes the production of guanosine 3',5'-cyclic monophosphate (cGMP) from guanosine triphosphate (GTP). By monitoring tissue levels of cGMP, Dr. Ferid Murad *et al* demonstrated that like other vasodilators, infusions of NO alone can activate guanylate cyclase^{6d}, and hypothesized that organic nitrates and other nitro-containing compounds likely functioned by release of NO. The role of nitro-containing vasodilators was ascertained in 1981, when Dr. Louis Ignarro and co-workers identified that the activity of guanylate cyclase in the presence of these complexes was mediated by the presence of thiol (-SH) containing molecules including the ubiquitous cysteine residues found on proteins in all tissues.⁵ S-nitrosothiols were identified as the unstable intermediates that lead to release of NO, which activates guanylate cyclase with concomitant relaxation of smooth muscle.

Meanwhile in the early 1980's a mysterious molecule known as endothelial dependent relaxing factor (EDRF) began to draw the attention of many researchers in the field of cardiovascular pharmacology. The discovery of EDRF originated

from research by Robert F. Furchgott at the department of pharmacology at SUNY Medical Center in Brooklyn, work that was directed at understanding the mechanisms involved in maintaining vascular tone in mammalian blood vessels. Furchgott and his students were studying the mechanism of acetylcholine (ACh) induced arterial smooth muscle relaxation in helical strips and ring preparations of rabbit descending thoracic aorta.⁷ As in many scientific investigations, Furchgott's group was plagued by irreproducibility in their measurements. Specifically, it was found that where-as *in vivo*, ACh is a potent vasodilator, in the *in vitro* preparations of helical strips of rabbit aorta, the researchers observed only contractile responses, and only at much higher ACh concentrations than were required in the *in vivo* experiments. This apparent discrepancy was solved when it was found that if great care was taken to protect the intimal surface of the helical strips during sample preparation, ACh elicited the expected relaxation response. After careful investigation using a silver staining procedure in conjunction with scanning electron microscopy, it was shown that the degree of relaxation response to ACh was directly proportional to the amount of intact endothelial cells that remained on the intimal surface of the aorta tissue samples.^{7a} Samples that were intentionally rubbed to remove the endothelial cells did not elicit relaxation in response to ACh. In a landmark experiment, the response to ACh of a transverse helical strip which had had its intimal surface rubbed (cleared of endothelial cells) was compared with and without the presence of a longitudinal strip (with its intimal surface intact) in a "sandwich" structure with the intimal surfaces facing

each other. Whereas without the presence of the proximal longitudinal strip the transverse strip did not relax, in its presence in the “sandwich” structure, the transverse strip, although devoid of endothelial cells, was observed to relax. This result led the researchers to postulate that some factor derived from the intact endothelial cells on the longitudinal strip was released in response to ACh and diffused to the proximal transverse strip, triggering activation of guanylate cyclase, and finally leading to a relaxation response in that tissue. Based on these results, Furchgott first hypothesized in 1981 that EDRF was a labile hydroperoxide or free radical that diffused from the endothelium to proximal smooth muscle cells, thereby activating guanylate cyclase.⁸

NO, given its small size and lipophilicity, was an obvious choice for a molecule that can easily diffuse through cell membranes. Indeed, there was already clear evidence that NO itself could activate soluble guanylate cyclase and effect relaxation with the concomitant increase in cGMP levels.^{6d,9} An important milestone was the discovery in 1983 that, like NO, endothelium dependent smooth muscle relaxation induced by EDRF led to elevation of tissue cGMP levels, and further that the potent vasodilator and NO-donor SNP caused the same effect in an endothelium *independent* manner.¹⁰ Furchgott’s lab went on to show that the action of EDRF is strongly inhibited by hemoglobin⁸, a protein that has an extremely high affinity for NO.¹¹ The final pieces to the puzzle was put in place in the later half of 1980’s, largely based on the independent findings of Gryglewski *et al* and Rubanyi *et al* showing that superoxide dismutase (SOD)

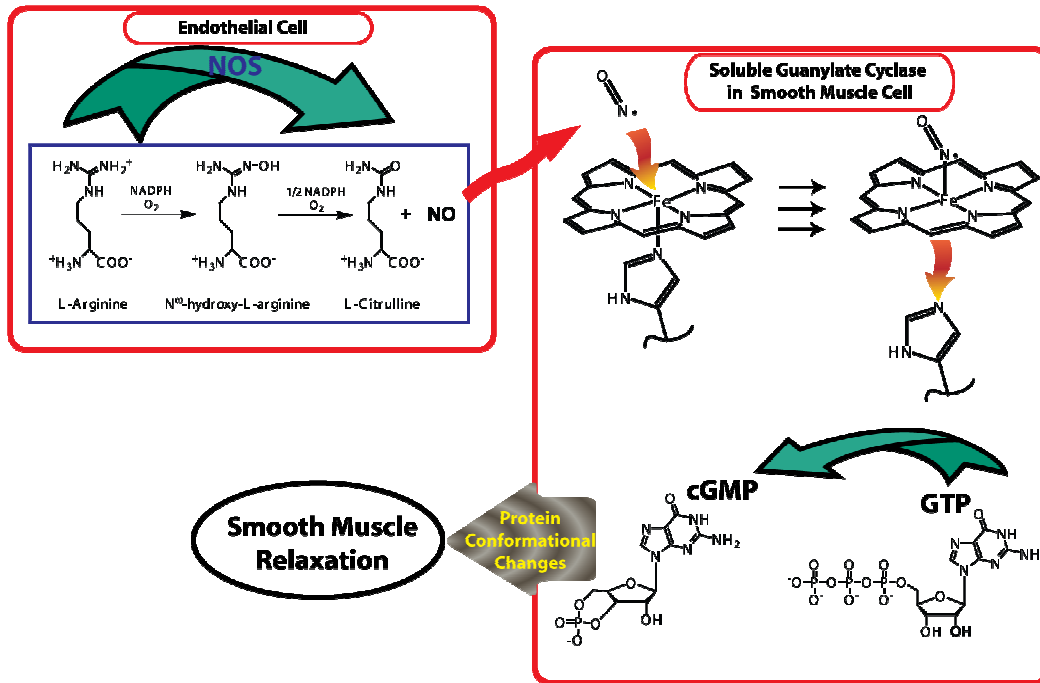
extends the lifetime of EDRF, and thus that O_2^- is a potent deactivator of EDRF.¹² Similar protection by SOD was shown for NO itself¹³, and this of course is due to the diffusion limited reaction between NO and O_2^- to produce the peroxynitrite anion (OONO⁻). Ultimately, these and other similarities led both Furchgott and Ignarro to independently propose that EDRF was NO at a symposium in July of 1986.⁸

Finally, in 1987, quantitative chemical evidence that NO was being produced by the endothelium was obtained using methods to detect its chemiluminescent product upon reaction with ozone.¹⁴ Dr. Richard Palmer *et al* used this method to show that after administration of bradykinin, a protein that induces release of EDRF, NO release was detected in a concentration dependent manner.¹⁵ Most importantly, the amount of NO detected was sufficient to account for the relaxation response attributed to EDRF.¹⁵ This chemical evidence, in conjunction with the great deal of pharmacological data that indicated that EDRF and NO were indistinguishable in their biology established NO as a biological messenger molecule.¹⁶ Although extensive work by many investigators in various fields led to this spectacular discovery, three investigators, Ferid Murad, Louis J. Ignarro, and Robert F. Furchgott were awarded the 1998 Nobel Prize in physiology or medicine for their contributions.

The biological origin of NO was soon explored by Palmer *et al*.¹⁷ Initial studies showed that vascular endothelial cells cultured without the presence of L-arginine released less NO when stimulated by bradykinin, and that re-exposure to

L-arginine (but not D-arginine or any of a large number of other arginine-analogues) restored NO release to normal levels.¹⁷ Although these experiments indirectly pointed towards involvement of L-arginine in cellular NO synthesis, the authors used [¹⁵N]-L-arginine to show that L-arginine itself is the chemical precursor to NO. Mass spectrometry was used to show that stimulated cells exposed to [¹⁵N]-L-arginine produced ¹⁵NO, and that the same amount of ¹⁵NO was produced if only the guanidino nitrogen(s) were labeled.¹⁷

Figure 1.1. Synthesis of nitric oxide and its action in vasodilation.



It is now known that endogenous NO is synthesized by an enzyme known as nitric oxide synthase (NOS). This enzyme catalyzes a two step reaction in which L-arginine is converted to L-citrulline with the concomitant release of one molecule of NO (Figure 1.1).² The first form of NOS (also called Type-I NOS or

*n*NOS) to be isolated and characterized was detailed in a report by Dr. David Bredt and Solomon Snyder on extracts obtained from rat brain tissue.¹⁸ Type II-NOS, or *i*NOS was soon found in isolated macrophages, followed by Type III NOS (*e*NOS) from endothelial cells.¹⁹ The three isoforms have only 50-60% structural homology, however for each particular isoform, homology from species to species can be nearly 90%.²⁰

Type I and III NOS, those enzymes found in neuronal tissue and endothelial cells respectively, are constitutive, meaning they are constantly producing NO in a regulatory manner at basal levels, typically at picomolar concentrations. In the endothelium for example, steady basal levels of NO are needed in order to maintain controlled blood pressure, without which life-threatening hypertension would result. Ignarro and co-workers were the first to offer a mechanism for the physiological activity of NO as a vasodilator.²¹ They postulated that once NO is produced by NOS, it diffuses from the endothelium into a smooth muscle cell where it binds to the heme center of soluble guanylate cyclase in the smooth muscle, causing release of the distal histidine (Figure 1.1). The protein conformational change induced by this ligand exchange at the heme center goes on to activate another portion of the protein responsible for catalytic conversion of guanosine triphosphate (GTP) to cyclic guanosine monophosphate (cGMP); this goes on to initiate a sequence of events leading to smooth muscle relaxation.

ii. NO in Immune Response

Mitchell in 1916 was the first to make a claim that the amount of nitrite (NO_2^-) and nitrate (NO_3^-) excreted by humans was more than could be accounted for by diet alone. In the late 70's and early 80's, Dr. S. Tannenbaum and coworkers suggested that a mammalian metabolic pathway for endogenous NO_3^- synthesis existed based on mass balance studies with humans and mice.²³ Drs. Dennis Stuehr and Michael Marletta showed that the source of endogenous $\text{NO}_2^-/\text{NO}_3^-$ was activated macrophages of the immune system.²⁴ Macrophages, a type of white blood cell, are locally activated by the immune system in the presence of an intracellular pathogen and thus activated become cytotoxic. Dr. John Hibbs observed that the deleterious effect of cytotoxic activated macrophages (CAM) is nonspecific, requires that the target cell be in close proximity, and its mode of action is nonphagocytic.²⁵ In the late 1980's, while similar discoveries were occurring in the field of vasodilation, both Hibbs²⁶ and Dr. Radha Iyengar²⁷ published reports establishing a correlation between macrophage synthesis of $\text{NO}_2^-/\text{NO}_3^-$ and L-citrulline production. It is now clear that the source of these NO_x species is the terminal guanidino nitrogen(s) of L-arginine, and that NO is an intermediate in their formation. Once activated, *i*NOS expression begins in CAM, resulting in the production of large local concentrations of NO (nanomolar), which readily diffuses from the macrophage to the surrounding target cells. The cytotoxic activity of NO depends largely on the particular concentration and cellular environment. NO itself can form complexes with iron in iron-sulfur

complexes of Complex I and II of the mitochondrial transport chain as well as the heme in cytochrome c oxidase.²⁵ Hibbs suggested that NO can disrupt DNA replication by also interacting with the non-heme iron center of ribonucleotide reductase, the rate-limiting enzyme involved in DNA synthesis.²⁸ If the superoxide anion is present, NO and superoxide quickly react to form peroxynitrite, another reactive species that can, for instance, promote the formation of mutagenic hydroxyl radical. In this way, the immune system uses highly localized bursts of large amounts of NO to ward off potential pathogens, and the activity of the NO is regulated by other cellular cofactors including the presence of superoxide.

iii. NO in Cancer Therapy

During their investigations of NO production in macrophages, Stuehr and Dr. Carl Nathan showed that CAM displayed tumoricidal activity, and that the affected tumor cells showed evidence of cessation of DNA synthesis and mitochondrial respiration.²⁹ Hibbs *et al* studied the extracts of CAM, which themselves become susceptible to the same cytotoxic effects as their targets.³⁰ Using electron paramagnetic resonance (EPR) spectroscopy, iron nitrosyl (Fe-NO) species were detected in the CAM, lending support to the hypothesis that the cytotoxic effects of CAM were due to loss of intracellular iron and inhibition of non-heme iron containing enzymes via complexation of iron by NO. In fact, to date studies have shown that NO can have both tumoricidal and protective effects, largely depending on the particular tumor environment and the relative amounts of

NO.³¹ The apparent “double-faced” nature of NO stems from its diverse chemistry in the biological milieu.³² At low concentrations NO can react directly (the direct pathway) with a variety of metal based targets including the heme center of sGC. However, at higher concentrations, reactions of reactive nitrogen oxide species become important due to the reaction of NO with oxygen or superoxide. Intensive research continues to this day to investigate the diverse effects of NO in tumor biology. In general, however, large amounts of NO (for example as produced by CAM in the studies discussed above) tend to be cytotoxic leading to tumor cell apoptosis, while lower levels increase vascularity and promote tumor growth.^{17b}

An area of rather intense research involving high local concentrations of NO and tumor biology is that of gamma-radiation sensitizers. The cytotoxic effects obtained by radiation therapy are postulated to be due to the production of carbon centered radicals in cellular DNA.³³ It is well established that O₂ is a potent radiation sensitizer, an effect attributed to the affinity of molecular oxygen’s unpaired electrons for the carbon centered radicals produced during radiation (Figure 1.2).³⁴ However, the fact that approximately one third of human tumor tissue is hypoxic (oxygen deficient) imparts an underlying limitation to the effectiveness of radiation therapy for the treatment of cancer.^{34c, 35} In fact, this outlines a major drawback to radiation therapy, since under these conditions, nearby normal cells are more sensitive than are the hypoxic tumor cells. A variety of techniques are being studied to circumvent this inherent limitation.

Figure 1.2. Potential fates of carbon centered radicals formed during γ -radiation therapy.

Radiation Induced Damage: Carbon Centered Radicals in Cellular DNA



Damage Repair by Endogenous Reducing Species



Damage Fixation: Aerobic vs. Hypoxic Cell Conditions



In 1957, Dr. P. Howard-Flanders was the first to show that exposure to gaseous NO is almost as effective as oxygen in sensitizing radiation of bacteria cells, and Dr. D. Dewey soon showed that this was the case for mammalian cells as well.^{35b,36} Dr. James Mitchell *et al* demonstrated that NO could be used to radiosensitize tumor cells *in vitro* in 1993.³⁷ Analogous to O₂, NO, itself a stable radical with one unpaired electron, when administered immediately following (or during) radiation, could trap carbon centered radicals before DNA repair proteins could repair them. In addition to administration of NO itself to the target cells, a variety of thermal NO-donors, molecules that thermally decompose to release NO over a prolonged time-scale, were shown to be effective as well.^{37,38} This latter discovery is especially notable due to the inherent problems associated with delivering gaseous NO to a remote tumor location, and the fact that inhaling large quantities of NO damages lung tissues.³⁷

A potential pitfall of administering NO as therapeutic *in vivo* via a NO-donor of the “thermal” type discussed above is the potential for inducing potentially fatal hypotension in regions other than the target tumor. A variety of strategies continue to be explored to deliver NO specifically and controllably within a tumor cell including gene therapy for injection of the iNOS gene into the tumor³⁹, selective activation of macrophages to produce NO within tumors⁴⁰, and the development of NO-donors that are selectively activated within the tumor.⁴¹ The last strategy is the focus of this dissertation. Here-in a novel strategy for photochemical activation of an NO-donor is investigated.

B. Photochemical NO Donors

i. Photodynamic Therapy (PDT)

Although the practice of using light therapy for healing dates back thousands of years to the ancient Egyptian, Chinese, and Indian cultures, its use in western medicine did not advance until the pioneer work of Niels Finsen in the late 19th century.⁴² Finsen, who received the Nobel Prize for his work in 1903, found that red light could be used for the treatment of small pox, while UV light from the sun was an effective treatment for cutaneous tuberculosis. In the same year, Herman von Tappeiner and A. Jesionek discovered that skin tumors could be treated with a topical application of Eosin in combination with light irradiation, a technique they dubbed “photodynamic action”.⁴²

Fast-forward to 1993, when the drug Photofrin, a mixture of porphyrin oligomers, was approved for clinical use in Canada for the treatment of bladder cancer. Photodynamic therapy (PDT), as it is now called, with Photofrin is now approved across the Americas, Europe and Asia for the clinical treatment of a variety of pre-cancer and cancer diseases, as well as for macular degeneration.⁴² PDT uses a photo-active molecule that once optically excited, undergoes efficient intersystem crossing to an excited triplet state which can then sensitize the promotion of nearby oxygen molecules ($^3\text{O}_2$) to the highly reactive, excited singlet oxygen form ($^1\text{O}_2^*$). $^1\text{O}_2^*$ produces a variety of reactive oxygen species (ROS) which damage biological tissue in the area that has been irradiated. Because the damaging effects of ROS are non-specific, a key requirement for PDT is the use of a photosensitizer that localizes in the target tissue under treatment. Further, the photosensitizer itself must be non-toxic. Porphyrin based systems like Photofrin, were initially the most heavily studied because porphyrins are found to localize in tumor cells and are otherwise benign.⁴²

A key component of the PDT strategy is the light activation step. A variety of studies have shown that the penetration of light through human tissue is limited by competitive absorption of tissue constituents (bilirubin, oxyhemoglobin, and water) and scattering effects. In fact, a relatively narrow window exists in the red to near infrared (NIR) range where tissue penetration is appreciable.⁴³ In this window, the penetration depth of light increases with increasing wavelength, with maximal penetration (≥ 6 mm) occurring in the NIR (700-1000 nm).⁴⁴ The

biological activity can extend to 2-3 times this depth, where the light density falls to 3-10%. Photofrin, and the majority of other clinically approved PDT photosensitizer absorb in the 600-750 nm range, leaving a large window for improvement.⁴²

One key drawback of traditional PDT is its reliance upon the local oxygen tension (pO_2) of target tissues. As was discussed previously, a large percentage of human tumor tissue is hypoxic, which makes traditional PDT largely ineffective in these areas. Furthermore, even in well oxygenated tissues, the PDT process itself rapidly consumes available oxygen, resulting in the need for delay times during treatment in which the tissue is allowed to reoxygenate.⁴² These problems open the door for new strategies utilizing light in combination with chemical agents other than oxygen (a strategy sometimes referred to as photochemotherapy) as more effective alternatives to traditional PDT, especially in the hypoxic tumor environment.

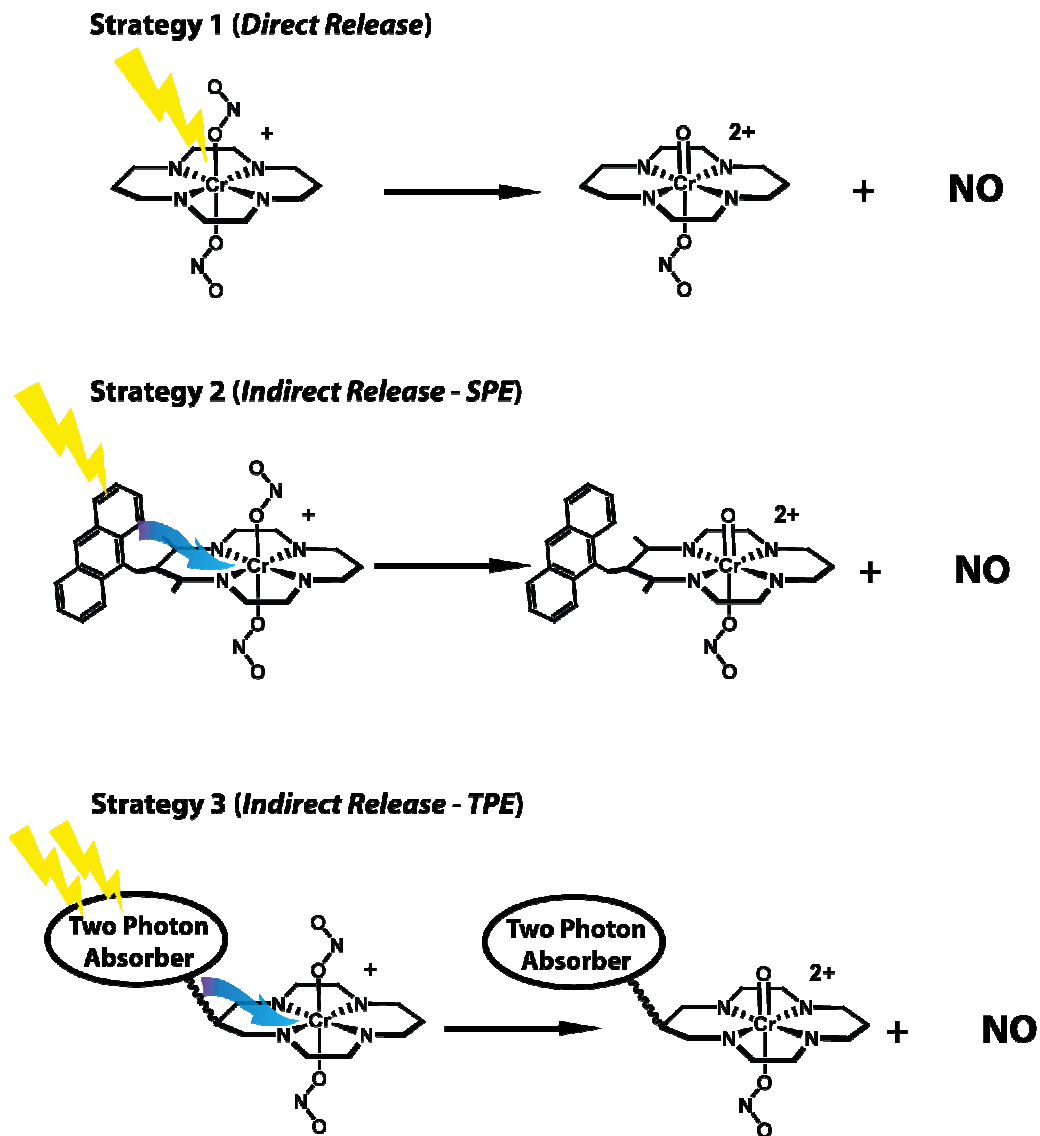
ii. Design of Photochemical NO donors

Since the discovery of NO's ubiquitous role in mammalian biology, the development of photochemically active compounds that can be used to deliver NO in a controlled manner has received considerable attention.⁴¹ This laboratory has been concerned specifically with metal bound nitrosyl and nitrito compounds because they provide the possibility of tuning both the light absorbing properties as well as the excited state reactivities by careful choice of metal and ligand combinations. Over the past decade, a variety of complexes studied by the Ford

group at UCSB have shown considerable potential including ruthenium-salen-nitrosyls⁴⁵, iron sulfur nitrosyl clusters ($\text{Fe}_x\text{S}_y(\text{NO})_z$) known as the Roussin's salts⁴⁶, and both simple and modified dinitrito *trans*- chromium(III) cyclams⁴⁷. All of these complexes release NO, differing mainly in the mechanism for release, the efficiency, and the light absorbing properties of the complex. In particular, the Roussin's red salt (RRS) cluster investigated by Bourassa *et al* was studied in collaboration with the Radiation Biology Branch at the National Cancer Institute to show that photochemically generated NO from RRS effectively sensitizes γ -radiation in hypoxic cell cultures.^{46a} Although this was an important "proof of concept", the RRS suffers from poor thermal stability as well as lack of light absorption in the red, both factors that preclude its use as a cancer drug.

Several factors require optimization in designing a photochemical NO donor that will be a successful cancer drug. First, the compound must be thermally stable in order that it arrive to the target intact without "premature" loss of NO, thus avoiding the potential for fatal hypotension induced by NO's vasodilatory properties. The drug must have some form of tissue specificity so that the therapeutic effect is realized in the target tissue/cell only. Finally, the photochemical NO donor must have strong light absorbing capability, preferably in the 700-1000 nm range where tissue penetration is greatest. With regards to the photochemical process, our studies have investigated three main strategies summarized in Figure 1.3. Using the direct release mechanism, the photochemically active complex is excited directly, resulting in labilization of

Figure 1.3. Strategies for photochemical generation of nitric oxide presented with the dinitrito *trans*- Cr(III) cyclam model system.



NO. In the second and third strategies, a chromophore such as a dye molecule having strong light absorbing properties is attached to the photochemically active core to function as a light harvesting antenna. Much like in the photosynthetic reaction centers of plants, light is collected by antenna and efficiently transferred to the photochemically active metal center, resulting in NO release. Energy

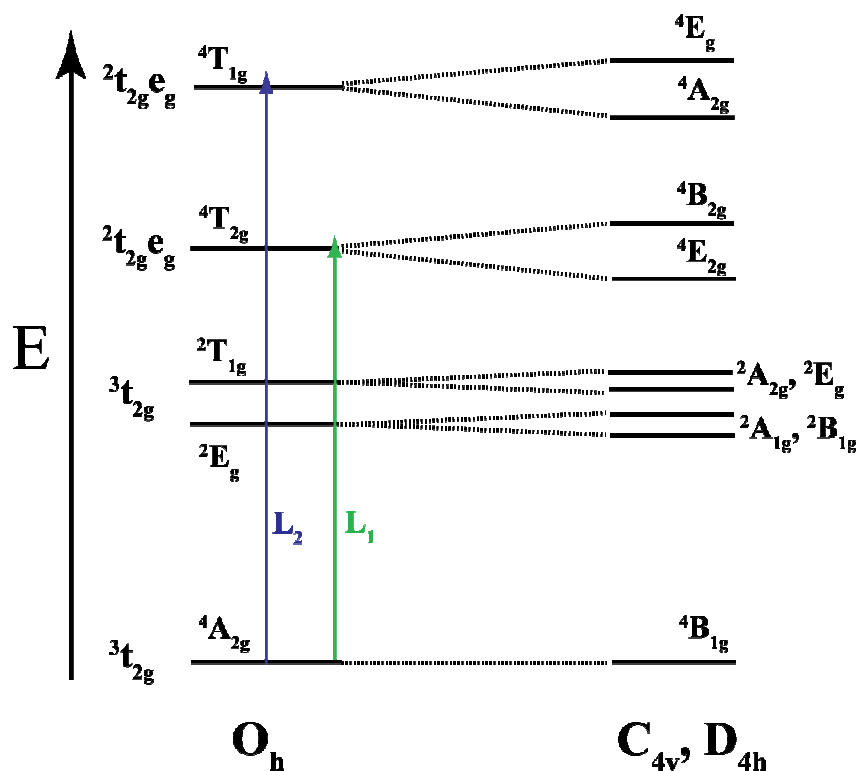
conservation requires that for this strategy to be effective, the excited state of the metal complex responsible for NO release must lie lower in energy than that of the excited chromophore. This presents a potential problem with the need for NO donors that can be activated with NIR light as single photons having wavelengths in this range may not be energetic enough to populate the NO labilizing states. The third strategy circumvents this issue by utilizing chromophores with substantial two photon absorption (TPA) cross-sections. For these chromophores, absorption of two photons of NIR light populates excited states at higher energy, allowing sensitization of the attached photochemically active NO donor with low energy light having high tissue penetration. Dr. Stephen Weckler *et al* recently exploited this strategy in our laboratory by demonstrating the two photon sensitized release of NO from Roussin's red salt esters derivatized with protoporphyrin IX^{48a} or fluorescein^{48b} dye molecules, where irradiation of the appended dye molecule(s) at 800 nm affected release of NO from the iron sulfur nitrosyl core.

iii. Chromium(III) Nitrito Complexes

a) Chromium(III) Photochemistry

The photochemistry of chromium(III) complexes has been explored extensively for several decades.⁴⁹ A wealth of information has been gathered from the simple photoaquation reactions observed upon irradiation into the ligand field transitions of these complexes in aqueous solutions. In octahedral symmetry

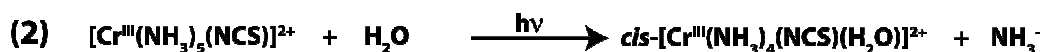
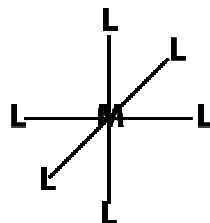
Figure 1.4. Energy level diagram for a d^3 metal system in octahedral and reduced symmetries.



(ML_6), the observed ligand field absorption bands are $^4A_{2g} \rightarrow ^4T_{2g}$ (L_1) and $^4A_{2g} \rightarrow ^4T_{1g}$ (L_2), and typically lie in the visible and near UV respectively (Figure 1.4). Irradiation into either of these bands results in photoaquation with quantum yields in the range of 0.1-0.5 irrespective of the wavelength irradiated.^{49a} This last point is consistent with photochemistry originating from the lowest energy excited state, which in octahedral symmetry is either the $^4T_{2g}$ state or the spin forbidden 2E_g state.

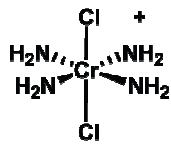
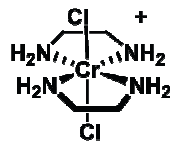
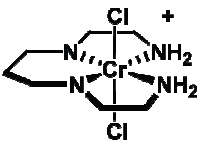
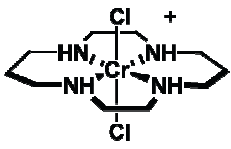
More diverse photochemistry results in molecules of lower symmetry (D_{4h} or C_{4v}) as in those having the general forms *trans*- ML_4X_2 or *trans*- ML_4XY . Adamson studied these systems extensively and generated a set of three rules

Figure 1.5. Demonstration of Adamson's rules for photoaquation of coordination complexes of chromium(III) in pseudo-octahedral ligand fields.



(known as Adamson's Rules) for predicting the products of photoaquation (Figure 1.5).^{49a} First, when considering the six ligands as lying in pairs along 3 mutually perpendicular axes, the axis having the lowest average ligand field strength will be the one that is labilized. Second, if the ligands on the labilized axis are different, then the one having the higher field strength is aquated. And finally, the effects governed by the first two rules are amplified if irradiating into the L_1 band rather than the L_2 band (see Figure 1.4). Additionally, photoaquation according to Adamson's rules was observed to be accompanied by change in the stereochemistry. Thus in reaction (1) in Figure 1.5, photoaquation results in *trans* to *cis* isomerization, a condition that is demonstrated by the decrease in ϕ_{Cl} with increasing stereoridity of the non-labilized axes in a series of *trans*-chromium(III) dichloro complexes (Figure 1.6).

Figure 1.6. Effects of stereorigidity of the non-labilized axis on the photoaquation quantum yield of *trans*-Cr(III) dichloro complexes.

Complex	Photoaquation Quantum Yield
	0.37
	0.32
	0.060
	0.00033

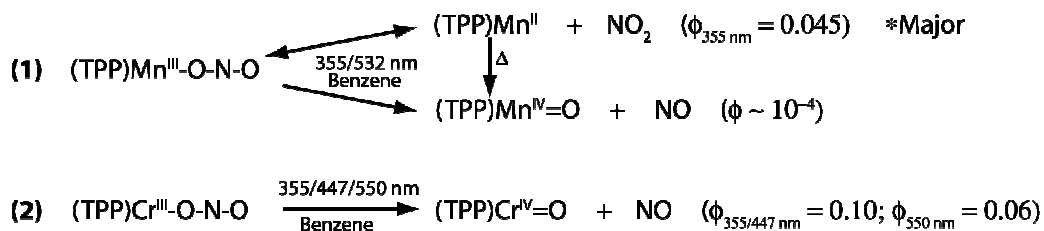
b) Photochemistry of Chromium(III) Nitrito Complexes

Our current interest in the photochemistry of chromium(III) nitrito complexes was stimulated, at least in part, by a study of $\text{Mn}^{\text{III}}(\text{TPP})(\text{ONO})$ (where TPP = 5,10,15,20-tetraphenylporphyrinate(2-)) in 1991.⁵⁰ In that work, Drs. Kenneth Suslick and Randall Watson claimed that photolysis of solutions of $\text{Mn}^{\text{III}}(\text{TPP})(\text{ONO})$ in benzene in the 350–420 nm range led to homolytic β -cleavage of the MnO-NO bond and formation of the $\text{Mn}^{\text{IV}}(\text{TPP})\text{O}$ species with a quantum yield of 5.3×10^{-4} . Following this report, in the same year Suslick *et al* published results of photolysis of the same complex imbedded in frozen glass/polymer matrices.^{50b} In this case however, completely different results were

reported as compared to the earlier study in solution, namely no $\text{Mn}^{\text{IV}}(\text{TPP})\text{O}$ was observed. Instead, the sole product seen following photolysis of the complexes in the solid state was the reduced $\text{Mn}^{\text{II}}(\text{TPP})$ species formed from homolytic α -cleavage of the Mn-ONO bond. In 1992, a re-investigation of photochemistry of $\text{Mn}^{\text{III}}(\text{TPP})(\text{ONO})$ in solution by Dr. Minaro Yamaji *et al* in Japan conflicted with Suslick's initial report.⁵¹ In a flash photolysis experiment irradiating at either 355 or 532 nm, the only transient observed was that due to $\text{Mn}^{\text{II}}(\text{TPP})$. The confusion surrounding the photochemistry of $\text{Mn}^{\text{III}}(\text{TPP})(\text{ONO})$ was resolved several years later in a comprehensive flash photolysis study by Dr. Mikio Hoshino *et al* in conjunction with Dr. Malcolm De Leo in our laboratory.⁵² The main photoproduct following irradiation of $\text{Mn}^{\text{III}}(\text{TPP})(\text{ONO})$ at 355 or 532 nm was shown to be *reversible* cleavage of the Mn-ONO bond to form $\text{Mn}^{\text{II}}(\text{TPP})$ and NO_2 (Upper part of reaction 1 in Figure 1.7). This major pathway had a wavelength dependent quantum yield as high as 0.045 at 355 nm. The photodecomposition product observed after continuous photolysis of the complex was identified as $\text{Mn}^{\text{IV}}(\text{TPP})\text{O}$. Due to the comparatively low quantum yield ($\sim 10^{-4}$), the formation of this minor product was attributed to either a secondary thermal reaction of $\text{Mn}^{\text{II}}(\text{TPP})$ or a low yield photochemical cleavage of the MnO-NO bond (Figure 1.7).

Hoshino *et al* also studied the photochemistry of the analogous $\text{Cr}^{\text{III}}(\text{TPP})(\text{ONO})$ complex.⁵¹ It turned out that the behavior of this complex was markedly different than that of the $\text{Mn}^{\text{III}}(\text{TPP})(\text{ONO})$ analogue. Namely,

Figure 1.7. Photochemistry of nitritometalloporphyrins as outlined by Hoshino.⁵¹

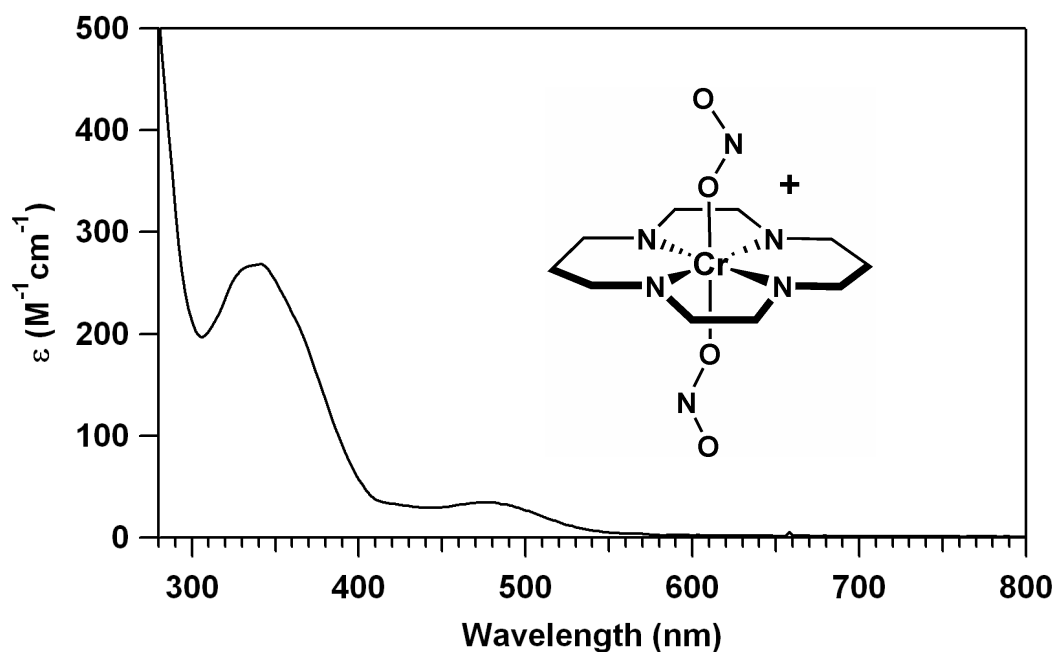


photolysis of $\text{Cr}^{\text{III}}(\text{TPP})(\text{ONO})$ led to the *irreversible* formation of $\text{Cr}^{\text{IV}}(\text{TPP})\text{O}$ and NO with relatively high quantum yields (reaction 2, Figure 1.7). Interestingly, in contrast to the simple photoaquation reactions discussed previously, the quantum yield for this reaction was observed to vary with wavelength (0.10 ± 0.01 at 355 and 447 nm which correspond to the charge transfer and Soret bands, respectively; 0.06 ± 0.01 at 550 nm corresponding to the Q-band). The reason for this dependence may be in analogy to similar behavior in the manganese system where it was postulated that the higher energy bands allow for higher excess energy for bond dissociation.⁵²

Based on Hoshino's work, the chromium(III) nitrito system presented itself as a good candidate for further study as a photochemical NO-donor as it released NO *irreversibly*, and did so with relatively high quantum yields upon irradiation with visible light. In order to study this "nitrito" mechanism in further detail, De Leo chose to study the simpler *trans*- $[\text{Cr}^{\text{III}}(\text{cyclam})(\text{ONO})_2]\text{BF}_4$ system (cyclam = 1,4,8,11-tetraazacyclotetradecane). As discussed earlier, the chromium(III) cyclam complexes are resistant to photoaquation due to the stereoridity of the cyclam macrocycle (Figure 1.6). Furthermore, in contrast to the absorbance spectrum of porphyrin, cyclam has no UV-visible absorbance bands. These

attributes allow the detailed photochemical investigation of the chromium(III) nitrito system while both excluding complications due to other photosubstitution reactions and allowing one to probe the photochemistry of the ligand field excited states directly. Additionally, *trans*-[Cr^{III}(cyclam)(ONO)₂]BF₄ is soluble in aqueous solution, making it a prime candidate for biomedical applications.

Figure 1.8. Extinction spectrum of *trans*-[Cr(cyclam)(ONO)₂]BF₄ in aqueous solution.

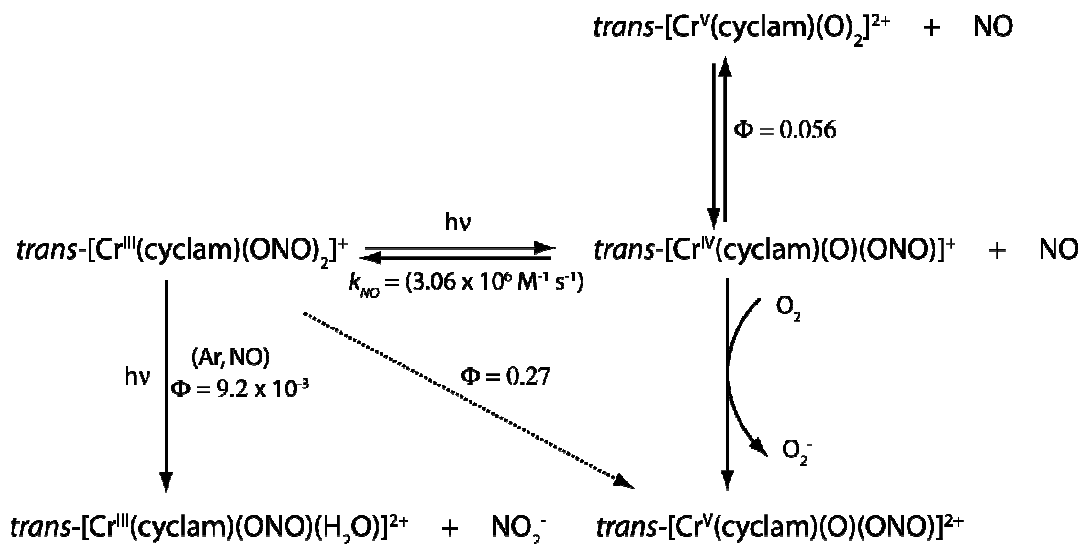


As shown in Figure 1.8, *trans*-[Cr^{III}(cyclam)(ONO)₂]BF₄ has a broad absorbance band due to the ⁴A_{2g} → ⁴T_{2g} transition centered at 476 nm ($\epsilon = 40 \text{ M}^{-1} \text{ cm}^{-1}$) and a transition centered at 336 nm ($\epsilon = 267 \text{ M}^{-1} \text{ cm}^{-1}$) attributed to an n- π^* intraligand transition of the coordinated nitrite. The latter likely obscures the second ligand field quartet transition (⁴A_{2g} → ⁴T_{1g}) typically observed in the near-UV. De Leo explored the photochemistry of this molecule under a variety of conditions and found its behavior to be quite diverse.^{47a-c} Under deaerated

conditions (argon or NO atmospheres), continuous photolysis into the ligand field bands leads to slow conversion to the photoaquated product, $\text{Cr}^{\text{III}}(\text{cyclam})(\text{H}_2\text{O})(\text{ONO})^{2+}$. As expected, the quantum yield for this process is very low (0.0092 ± 0.0008) due to the low photoreactivity of complexes in the $\text{Cr}^{\text{III}}(\text{cyclam})\text{X}_2^+$ series. However, under *aerated* conditions, continuous photolysis in the wavelength range of 366–546 nm led to the formation of the oxidized chromium(V) oxo species, $\text{Cr}^{\text{V}}(\text{cyclam})(\text{O})(\text{ONO})^{2+}$. The absorbance spectrum changes drastically with a large quantum yield of 0.27 ± 0.03 (irradiating at 436 nm), shifting to a new species with a $\lambda_{\text{max}} = 364$ nm ($\epsilon = 2600 \text{ M}^{-1} \text{ cm}^{-1}$). Notably, the quantum yield varies with the intensity of irradiating light, I_a , ranging from 0.14 at the high I_a of 1×10^{19} quanta $\text{l}^{-1} \text{ s}^{-1}$ to as large as 0.50 at a low I_a of 4×10^{17} quanta $\text{l}^{-1} \text{ s}^{-1}$. This behavior suggested that the back-reaction of photochemically produced intermediates was in competition with the formation of the final Cr(V) oxo species. In addition, the release of NO during the photolysis was detected electrochemically. These results allowed De Leo *et al* to postulate a mechanism for the photochemical behavior of *trans*- $[\text{Cr}^{\text{III}}(\text{cyclam})(\text{ONO})_2]\text{BF}_4$ (Figure 1.9).^{47b-c} Irradiation of the complex leads to homolytic β -cleavage of one of the CrO-NO bonds producing $\text{Cr}^{\text{IV}}(\text{cyclam})(\text{O})(\text{ONO})^+$ (or the nitro isomer) and NO. Under deaerated conditions, these two intermediates quickly back-react ($k_{\text{NO}} = (3.06 \pm 0.07) \times 10^6 \text{ M}^{-1} \text{ s}^{-1}$) to form the starting material, a reaction that was quantified using nanosecond flash photolysis techniques under varied NO concentrations. Under

these conditions the net photo-product is the photoaquated species, $\text{Cr}^{\text{III}}(\text{cyclam})(\text{H}_2\text{O})(\text{ONO})^{2+}$. However under air, the initial photoproduct is

Figure 1.9. Photochemistry of $\text{trans}[\text{Cr}(\text{cyclam})(\text{ONO})_2](\text{BF}_4)$ in aqueous solution.



irreversibly trapped by oxygen (O_2), forming $\text{Cr}^{\text{V}}(\text{cyclam})(\text{O})(\text{ONO})^{2+}$ and leading to net release of NO. In reality, the photochemistry of the $\text{trans}[\text{Cr}(\text{cyclam})(\text{ONO})_2]^+$ chromophore is complicated by a delicate balance between reactant concentration, light intensity, and oxygen concentration. One outcome of these complications is further photochemical reaction of the reaction intermediate under low O_2 concentrations. As shown in Figure 1.9, De Leo found that the Cr^{IV} intermediate is susceptible to further photoreaction and observed signals by EPR and mass spectrometry consistent with the loss of a second NO molecule and formation of the di-oxo species, $[\text{Cr}^{\text{V}}(\text{cyclam})(\text{O})_2]^+$.^{47c} In this context, the mechanism in Figure 1.9 supports the observed data and accounts for the main products, but as alluded to by De Leo, further rigorous kinetic studies would be

required to elucidate all of the side-reactions taking place in this system. For a more detailed discussion of the intricacies of this system, the interested reader is directed towards the doctoral dissertation of Dr. Malcolm A. De Leo.^{47a}

Thus, *trans*-[Cr^{III}(cyclam)(ONO)₂]BF₄ presented itself as an effective photochemical NO donor. However its potential as a new photochemotherapeutic is limited by its poor light absorbing properties. Because the visible bands are ligand field in character, the extinction coefficients are quite low (<20 M⁻¹ cm⁻¹ at wavelengths longer than 500 nm) and there is zero absorbance in the red. Although a poor candidate for the *direct* release strategy in terms of biomedical applications, this system turns out to be well suited for the *indirect* release strategy described earlier (Figure 1.3).

c) Functionalized Chromium(III) Cyclam Complexes

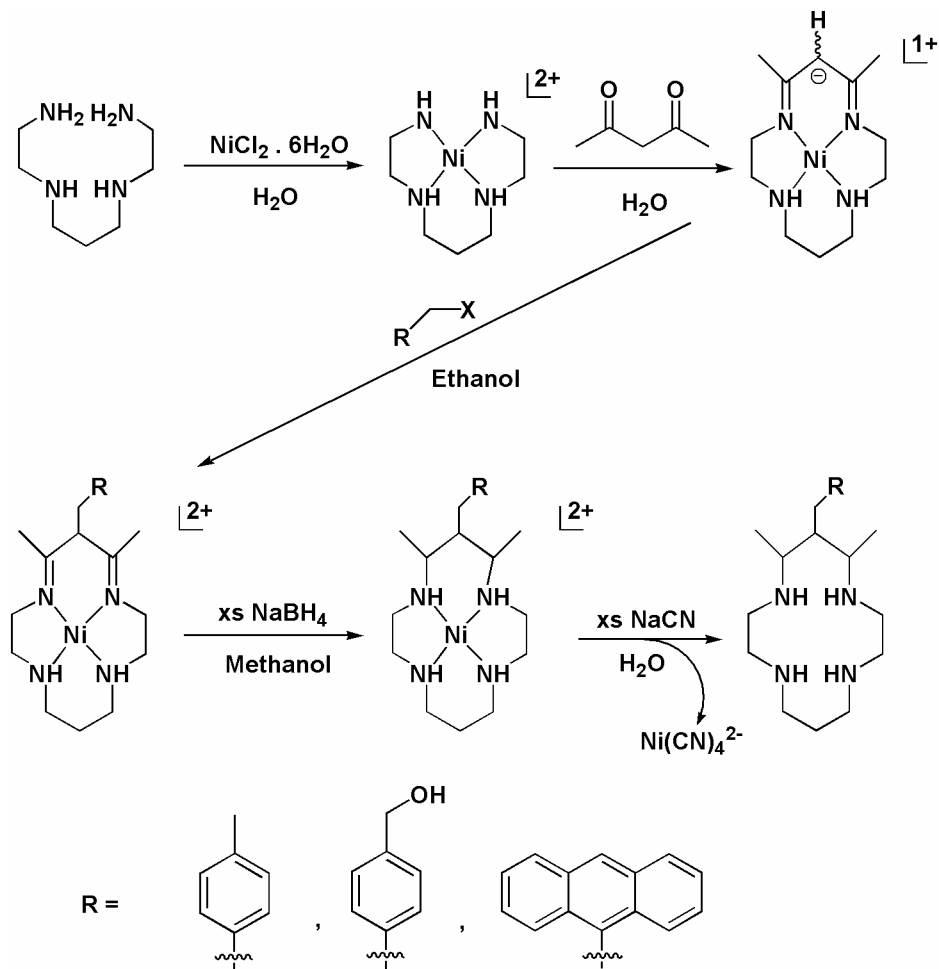
The ability to append a strongly absorbing chromophore to the Cr^{III}(cyclam)X₂⁺ core was investigated by Dr. Frank De Rosa *et al* in the Ford laboratory.^{47d-g} In these studies, it was determined that the complexes could be functionalized either at the 1,8 nitrogens of the cyclam ring (so called N-substituted) or at a ring carbon (so called C-substituted).

In the former case, the Cr(III) complexes, *cis*-[Cr(R₂cyclam)Cl₂]Cl, were synthesized with R = methyl, benzyl, naphthyl, and anthracenyl from the reaction of CrCl₃·3THF and the corresponding R₂cyclam. Unfortunately, these complexes completely resisted attempts made to effect *cis* to *trans* isomerization. The *cis*

isomer is kinetically favored and is formed first, but conversion to the more stable *trans* isomer can usually be accomplished by base catalysis, presumably via deprotonation of the secondary amines along the ring's folding axis. Crystallographic data indicated that in all four N-substituted species, the substituted tertiary amines define this folding axis preventing the *cis* to *trans* isomerization.^{47f} However, photophysical investigations of these complexes indicated efficient intersystem crossing/internal conversion occurred from the higher energy excited states of the appended chromophore to the Cr(III) localized ligand field states. The lowest energy excited state is the doublet state and radiative relaxation (phosphorescence) from this excited state is observed at 77 K as a sharp band near 700 nm with vibronic structure tailing to lower energy. The photoluminescence excitation spectra of the N-substituted complexes closely tracked the absorbance spectra for these complexes including the bands associated with π - π^* transitions from the benzyl, naphthyl, and anthracenyl appendages.^{47f}

De Rosa and co-workers then synthesized the C-substituted cyclams with the goal of obtaining the more thermally stable *trans*- isomers.^{47d,e} Utilizing a nickel template strategy allowed the production of a variety of C-substituted cyclams by a facile Schiff base condensation with the appropriate alkyl halide substituent. Reactions of the free cyclams with $\text{CrCl}_3 \cdot 3\text{THF}$ gave the analogous *trans*- $[\text{Cr}(\text{L})\text{Cl}_2]\text{Cl}$ isomers exclusively, a result that the authors attributed to disfavorable steric interactions between the substituents of the modified cyclam at the 5, 6, and 7 positions and the coordinated chlorides (Figure 1.10). Similar to

Figure 1.10. Nickel templated synthesis for “C-substituted” cyclam analogues.



the N-substituted analogues, investigations of the low temperature Cr(III) doublet state phosphorescence of these complexes showed efficient intersystem crossing/internal conversion from the high energy excited states of the appended aromatic groups to the lowest energy ligand field state.^{47e} Notably, in the anthracyl analogue, in addition to phosphorescence from the doublet state, fluorescence characteristic of the anthracene chromophore was detected at 416, 442, and 466 nm. Comparison with the fluorescence signal of an equimolar

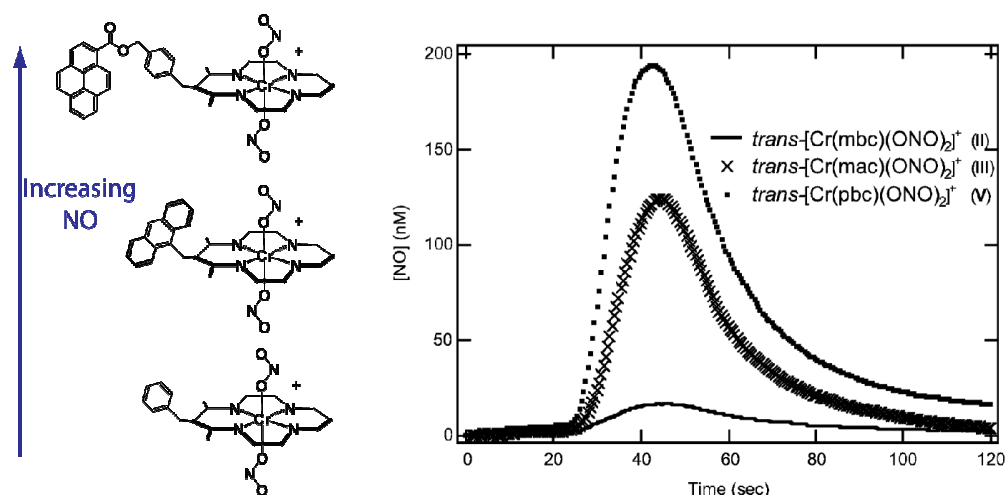
sample of the free ligand indicated that nearly all (>99%) of the anthracyl singlet excited state is quenched by the metal center.

Another C-substituted analogue synthesized by De Rosa *et al* was the *p*-hydroxymethylbenzyl- derivative, *trans*-[Cr(hbc)Cl₂]Cl. This complex could be further modified to the *p*-bromomethylbenzyl- derivative, *trans*-[Cr(bbc)Cl₂]Cl, and the *p*-aminomethylbenzyl- derivative, *trans*-[Cr(abc)Cl₂]Cl, via successive treatments with 48% HBr and aqueous ammonia (NH₄OH), respectively. Each of these three species presents a backbone for further functionalization of the cyclam ring. This was exploited in the case of the amino group of *trans*-[Cr(abc)Cl₂]Cl through the formation of an amide linkage to the dye molecule gallocyanine (7-dimethylamino-4-hydroxy-3-oxo-3*H*-phenoxazine-1-carboxylic acid). Although purification problems precluded a detailed photophysical investigation of this complex, the dye added a strong absorbance band at 610 nm ($\epsilon > 10^4 \text{ M}^{-1} \text{ cm}^{-1}$), presenting a key step forward in improving the light absorbing properties of the Cr(cyclam)X₂⁺ system at longer wavelengths.^{47g}

According to the procedures established by De Leo *et al*, the C-substituted dichloro complexes can be converted to their *trans*-[Cr(L)(ONO)₂]⁺ analogues by reaction with AgNO₂.^{47d} In *trans*-[Cr(hbc)(ONO)₂]BF₄, the hydroxyl-functionality was exploited to increase the absorptivity of the complex by appending 1-pyrenecarboxylic acid through an ester linkage. Much like the anthracyl derivative, the pyryl- appendage adds strong absorption bands in the near UV ($\epsilon > 10^4 \text{ M}^{-1} \text{ cm}^{-1}$). As expected based on the previous phosphorescence

sensitization experiments with the $trans\text{-}[\text{Cr}(\text{L})\text{Cl}_2]^+$ complexes, the modified nitrito- complexes displayed higher efficiencies for NO release upon photolysis into the strongly absorbing $\pi\text{-}\pi^*$ transitions of the appended aromatic groups. Thus, the anthacyl- and pyryl- derivatives produced eight and twelve fold more NO, respectively, than the corresponding equimolar solution of the benzyl- derivative or the simple unmodified cyclam (Figure 1.11).^{47d} The quantum yield for NO release was virtually identical for all of the systems studied ($\Phi_{\text{NO}} = 0.17 - 0.19$ irradiating at 366 nm), consistent with the notion that the appended chromophores function solely as light harvesting antenna, efficiently transferring the photoinduced excitation to the photochemically active ligand field excited states.

Figure 1.11. NO amperogram demonstrating enhanced NO production from appended conjugated organic functionalities. All solutions had equal starting concentrations (990 nM). Reprinted in modified form with permission from (DeRosa, F.; Bu, X.; Ford, P. C. *Inorg. Chem.* **2005**, *44*, 4157-4165. Copyright 2007 American Chemical Society.



The light absorbing properties of the modified cyclam complexes developed by De Rosa *et al* were markedly improved over those of the simple cyclam, especially in the near ultraviolet (near-UV) region where the aromatic appendages contribute strong π - π^* transitions. However, in the context of application as a biomedical drug, near-UV light is less than ideal as it suffers from very poor tissue penetration and can be damaging to biological tissues. To circumvent this De Rosa investigated the ability of the pyryl- derivative, *trans*-[Cr(pbc)(ONO)₂]BF₄, to generate NO upon two photon excitation (TPE). Unfortunately, no net photochemistry was detected from the complex upon excitation with femtosecond (fs) pulses of 800 nm. This was attributed to the weak two photon absorption coefficient for pyrene (0.1 GM; GM = 10⁻⁵⁰ cm⁴·s/photon).^{47g}

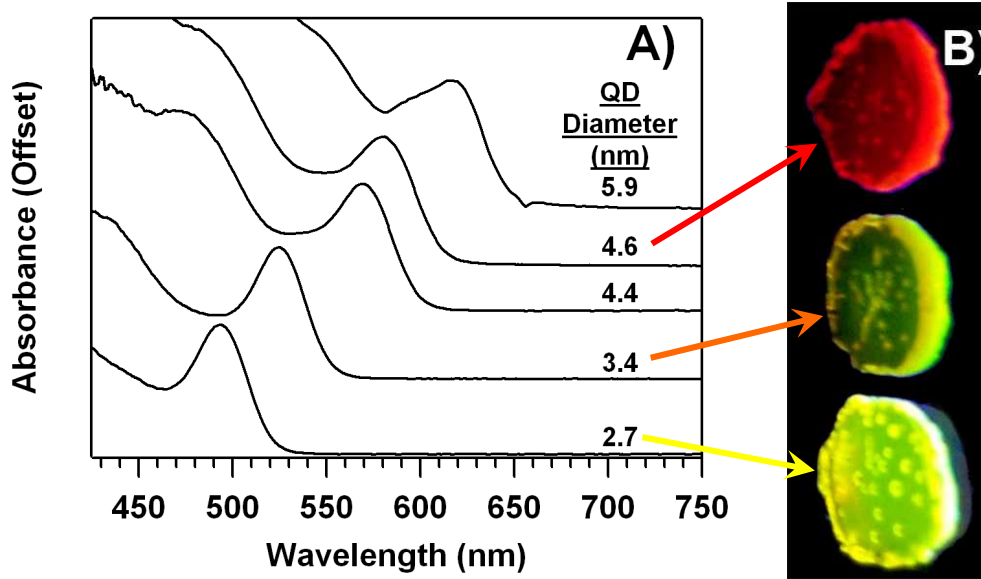
In principle however, the strategy employing a chromophore appended to the cyclam ring having an appreciable two photon absorption coefficient poses exciting possibilities for development of the Cr^{III} nitrito system as red absorbing, photoactive NO donors for biomedical applications. Several chromophores are being investigated by this laboratory for their strong absorbing capabilities in the red via both single and two photon absorption. One such chromophore, semiconductor quantum dots, is a fairly new player in the chemist's tool box of chromophores. The application of these new interesting materials as sensitizers for photochemical NO donors is the focus of this dissertation.

C. Semiconductor Nanoparticles (Quantum Dots)

i. What are Quantum Dots?

One of the highlights of the intensive efforts of nanotechnology was the experimental validation of size and shape tunable properties of materials in the size regime lying between single atoms and the bulk. Throughout the 1970's and early 1980's, the photophysics and electronic properties of semiconductors were investigated for their potential application in solar energy conversion. Several theoretical investigations predicted that in a certain size regime, the optical and electronic properties of semiconductors would become tunable. Work by Dr. Arnim Henglein⁵³ and Dr. R. Rossetti *et al*⁵⁴ confirmed these predictions upon synthesizing colloidal clusters of cadmium sulfide (CdS) having diameters of roughly 2-6 nm by precipitation of Cd²⁺ by sulfide salts in aqueous buffers. Whereas bulk CdS begins absorbing light at $\lambda \leq 515$ nm, the absorption threshold for colloids having diameters smaller than 6 nm shifted to higher energy with decreasing size. This phenomenon was dubbed "quantum confinement", which describes the effect of electronic confinement of the electron and hole pairs (excitons) within the semiconducting material when the dimensions are on the order of the Bohr radius of the bulk material bound-exciton. Much like Schrodinger's treatment of the wavefunction of an electron confined by walls of infinite potential, in so called "quantum dots (QDs)" the wavefunctions representing the exciton are physically confined within the volume of the particle. Dr. Louis Brus solved the Schrodinger equation for a particle in a sphere to give

Figure 1.12. Size tuned optical properties of CdSe QDs A) Absorbance spectra of different sized CdSe QDs in toluene. B) Image showing photoluminescence from solid sol gels embedded with 3 different QD sizes. (Blue background is due to UV hand lamp used to illuminate the sol-gels).



an analytical expression for the energy (E) of the lowest excited state of a semiconductor particle as a function of radius, R (Equation 1.1).⁵⁵ In this equation,

$$E = E_g + \frac{\hbar^2 \pi^2}{2R^2} \left[\frac{1}{m_e} + \frac{1}{m_h} \right] - \frac{1.8e^2}{\epsilon R} + \text{smaller terms} \quad (1.1)$$

E_g is the bulk band gap energy, m_e and m_h are the effective masses of the electron and hole, respectively, e is the charge on an electron, and ϵ is the dielectric coefficient of the semiconductor. Equation 1.1 predicts the energy required to create an exciton within a QD as function of size, and thus describes the widening of the band gap as a function of decreasing particle size. The effect is quite striking in a material such as cadmium selenide (CdSe) in which the energy gap between the valance and conduction bands (band gap) can be tuned across

virtually the entire visible spectrum (Figure 1.12). Due to this attribute, CdSe can be considered the *prototypical* QD.

ii. QD synthesis

A variety of techniques have been described for generation of the nanomaterials that display the effects of quantum confinement, including so called “high energy input” physical methods like molecular-beam-epitaxy (MBE) and metalorganic-chemical-vapor-deposition (MOCVD), high temperature chemical growth of particles in glass matrices, and various wet-chemical methods based on organometallic synthesis. Of these methods, the wet-chemical methods most familiar to a chemist have been shown to be the most effective in generating high quality materials as judged by their narrow size dispersity, crystallinity, well-defined optical properties, and ease of manipulation of their solubility and reactivity via chemical control of their surfaces.

The wet-chemical, or “bottom-up” approach to QD synthesis can be understood in terms of La Mer’s model of nucleation and growth of colloidal particles, wherein the key element for controlled growth is the temporal separation of nucleation and further growth of the particles from remaining monomers in solution. In 1993, based on work conducted in the laboratory of Professor Mounji Bawendi at MIT, Dr. Christopher Murray *et al* published the first wet-chemical approach to nearly monodisperse, high quality CdSe QDs via an organometallic synthesis that could be effectively described according to La Mer’s model.⁵⁶ In this method, a room temperature mixture of dimethylcadmium

(Me₂Cd) and selenium in trioctylphosphine are quickly injected through a large bore needle into a molten mixture of coordinating ligands, trioctylphosphine (TOP) and trioctylphosphine selenide (TOPO) at 350 °C. The rapid injection of precursors results in supersaturation of monomers, which is relieved by nucleation of small CdSe particles. At the same time, the temperature of the mixture falls below the threshold needed for formation of new nuclei. Controlled growth of the nuclei from the remaining monomers in solution is accomplished by careful control of temperature and reaction time. Following this initial “fast” growth phase, the particles can continue to grow via a process known as Ostwald ripening whereby dissolution of the smaller particles suffering from higher-surface-energies fuels the growth of the larger particles. As this latter phase tends to broaden the size distribution, many current synthetic techniques are directed at optimizing reaction conditions that avoid the Ostwald ripening phase of QD growth.⁵⁷

The presence of coordinating ligands stabilizes the growing particles, preventing their aggregation into bulk semiconductor material. A variety of ligands have been used, the vast majority being comprised of alkylphosphines, alkylphosphine oxides, alkylamines, alkylphosphates, alkylphosphites, alkylphosphonic acids, alkylphosphoramides, alkylthiols, fatty acids, and various combinations of these with variable alkyl- chain lengths. In general, the polar head group of the ligands binds the QD surface while the alkyl chain extends out into the solvent medium providing solubility and screening interparticle van der

Waals forces that would otherwise cause the QDs to aggregate. During the synthesis, these stabilizers function as a kinetic barrier against uncontrolled growth, controlling both access of the monomer fuel to QD surface and functioning as a barrier against formation of the thermodynamically favored bulk structure.

The growth of CdSe QDs can easily be monitored by UV-visible absorption spectroscopy of small aliquots removed over the course of the reaction. Depending on particular reaction conditions, the initial nuclei display a discrete absorption feature near ~450 nm. As the particles grow, their absorbance spectrum red shifts due to quantum confinement effects until the particle radii reach roughly 5.6 nm, the Bohr radius in bulk CdSe. For growth beyond this size the absorption spectrum approximates that of the bulk semiconductor with an absorption onset approaching 710 nm (1.751 eV) which is the band gap energy of bulk CdSe.

Over the last decade or so, a variety of variations of the preparation reported by Murray *et al* have appeared including the replacement of the pyrophoric Me_2Cd with cadmium oxide⁵⁸ or the use of so called single-source-precursors⁵⁹ for the metal and chalcogenide species which removes the need for a high temperature nucleation step. Furthermore, high quality QD synthesis is no longer limited to CdSe, and rather has been expanded to materials with optical properties that can be size-tuned throughout a wide range of the electromagnetic spectrum including ZnSe and PbS which emit in the UV-blue and infrared regions, respectively.

iii. QD Optical Properties

The strong photoluminescence (PL) of quantum dots is one of their most coveted properties. Excitation across the band gap leads to fast thermal relaxation of the electron and hole to the “band-edge” which can radiatively recombine, releasing a photon of energy equal to the band gap (“band-edge” or BE emission). Extensive research has demonstrated the crucial role of the surface composition and passivation in determining the quantum yields for QDs.⁶⁰ Unsaturated surface atoms, so-called “dangling bonds”, provide traps for the photo-excited carriers. Population of these “surface traps” can lead to a broad PL feature on the low energy side of the BE emission due to radiative recombination of the trapped carriers sometimes referred to as “deep-trap” emission. By carefully tuning the reaction conditions, including coordinating ligand identities and ratios, metal to chalcogenide ratio, and reaction temperature, it has been shown that the participation of these surface traps can be minimized by conditions that favor highly crystalline surface reconstruction and maximized surface atom passivation. This has led to CdSe QDs with PL quantum yields as high as 70–80%.

Another method to maximize PL quantum yields that has become fairly ubiquitous is the growth of an inorganic shell of a wider band-gap material around the preformed cores.⁶¹ For CdSe, the most common choice is ZnS, yielding CdSe/ZnS “core/shell” QDs which were first demonstrated via a wet-chemical approach by Dr. Margaret Hines *et al.*^{61a} Growth of a shell of ZnS around CdSe leads to electronic passivation of the core surface, which effectively confines the

excited carriers within the core due to the large band offset between CdSe and ZnS. As with the cores, a final layer of organic ligands bound to the outer ZnS shell imparts solubility of the core/shell QDs. Increases in PL quantum yields of an order of magnitude are common following growth of 1–2 monolayers of ZnS. For thicker shells, the quantum yields begin to fall back down, presumably due to strain-induced formation of defects at the core/shell interface caused by the mismatch between the lattice constants of the two materials.^{61b} However, shells thicker than 1 monolayer also impart enhanced chemical stability of the QDs in terms of surface oxidation and resistance to photo-degradation. The enhanced quantum yields and stability are major factors that make core/shell CdSe/ZnS QDs the materials of choice for researchers using QDs in complex chemical environments such as biomedical luminescent tags, or in applications requiring extensive material processing such as in QD driven opto-electronics.

Even with the improvements in particle quality and electronic passivation, the photoluminescent properties of the QDs are observed to be highly sensitive and vary from report to report. A large number of investigations have shown both photoenhancement and quenching in solid thin films and in dispersions of semiconductor QDs. The changes observed can be divided into two main categories, 1) reversible, and 2) irreversible. In the latter case, continuous irradiation with above band-gap light of thin films in the presence of air⁶² or moisture⁶³, or in solution in the presence of methanol⁶⁴ or air⁶⁵ leads to an increase in the photoluminescence intensity. In this case, the observed effect is

attributed to permanent photo-induced changes in the surface structure, either by rearrangement and/or loss of surface passivants, or by oxidation to form CdO and SeO₂. Both of these mechanisms are supported by X-ray photoelectron spectroscopy (XPS) and time-of-flight secondary ion mass spectrometry (ToF-SIMS) studies in which the surface structure was investigated at different stages of photolysis.⁶⁶ Additionally, purely chemical treatments either with sodium borohydride⁶⁷ or dissolved oxygen⁶⁸ have been shown to have similar photo-enhancement effects attributed to oxidation of the surface of the nanoparticles.

Only a few reports have shown examples of reversible type photo-enhancement behavior. Dr. Marcus Jones *et al* found that the photoluminescence of previously irradiated solutions of CdSe and excess stabilizer (trioctylphosphine oxide, TOPO) dropped in intensity, eventually falling below the original, “pre-brightened”, level.⁶⁴ This process was observed to be extremely slow. A similar “darkening” following irradiation was observed by Dr. Zhivko Zhelev *et al*, whom additionally found no changes in the corresponding optical absorbance spectra during either the photo-enhancement or darkening periods.⁶⁹ These examples are indicative of generating a photostationary state, which clearly does not involve the permanent photo-chemistry typified by experiments described previously.

Single particle photoluminescence experiments have shown that particles exhibit luminescence intermittency or blinking.⁷⁰ The widely accepted explanation for the on/off behavior is Auger ionization of the particles due to the generation of multiple excitons within a single particle. This leads to trapping of

carriers at or near the particle surface, generating trap states that, following another photo-excitation, decay nonradiatively. Additionally, correlated atomic force microscopy and single-particle fluorescence microscopy have shown that a significant portion of the particles in a sample (sometimes exceeding 50% of the ensemble) are dark.⁷¹ Yet, until recently there has been no experimental evidence linking the distribution of bright and dark particles seen in single-particle work with the photo-enhancement effects observed for ensembles. A recent report by Dr. J. Müller *et al* shows that when the environment of a sample of CdSe is quickly purged with air, particles that were originally dark under vacuum are turned on, while those that were already emissive become brighter.⁷³ This suggests that the effects described for ensemble measurements are due, at least partially, to tuning of the relative population of bright and dark particles in the ensemble.

iv. QD Surface Functionalization

As discussed above, the passivating layer of surface ligands provides a point of interface between the QDs and the environment around them. Careful choice of these ligands allows one to control whether the QDs are soluble in organic or aqueous environments, how they self-assemble into higher ordered structures, whether they can be embedded in polymer or glass matrices, and whether they can be further functionalized through the attachment of other chromophores, biologically relevant molecules, or even other nanostructures.

Using a technique commonly referred to as “surface exchange”, the original hydrophobic coating of QDs can be exchanged with a variety of Lewis base type ligands simply by mild heating in an excess of new ligand. For instance, a common strategy to make water-soluble QDs, and thus render them biologically compatible, is to exchange the alkyl-chain type ligands with bifunctional mercaptocarboxylic acids. In a process governed by the laws of mass action, the thiol- head groups displace the original organic coating and bind to the QD surface. Deprotonation of the carboxyl- tail group gives an anionic species which is soluble in mildly basic aqueous solutions ($\text{pH} > 7$). Another important attribute of this strategy is that the carboxyl- tail groups act as a further point of functionalization via condensation reactions with amines or alcohols using well established carbodiimide activation chemistries. In the first demonstration of its kind, Drs. Warren Chan and Shuming Nie exploited this strategy by conjugating core/shell CdSe/ZnS QDs coated with mercaptoacetic acid to the free amine functionalities on both the protein transferrin and the immunomolecule IgG using the water soluble cross-linker, ethyl-3-(dimethylaminopropyl)carbodiimide (EDC).⁷³ Transferrin labeled QDs were observed to undergo receptor mediated endocytosis into cultured HeLa cells, a result that played a key role in making QDs a compelling new tool for biologists in the area of tissue specific fluorescent labeling and imaging.

In more recent work by Dr. Hedi Mattoussi and coworkers at the Naval Research Laboratory (NRL), dihydrolipoic acid (DHLA) replaces the monodentate

mercaptocarboxylic acids used previously in order to increase the stability of the QDs in solution.⁷⁴ Whereas QD preparations utilizing mercaptoacetic- or mercaptopropionic acids as surface stabilizer are only stable in most cases for several days⁷⁴, the DHLA coated materials were shown to remain stable in aqueous solutions for periods exceeding one year. Because the covalent interaction between the QD surface and the stabilizing ligand has been demonstrated to be fairly weak, the ligands have a tendency to diffuse away upon dilution^{60b}, ultimately leading to destabilization and aggregation of the QDs. The bidentate nature of DHLA is expected to enhance its binding affinity to the QD surface, allowing long term stability of QD dispersions in water.

In the studies by Mattoussi *et al*, mixtures of DHLA coated QDs and proteins carrying long cationic side chains were observed to form stable electrostatic assemblies. When otherwise identical proteins covalently labeled with cyanine dye (Cy3) were used, efficient energy transfer from the central QD to the proximal protein bound dye was observed. In related work, Dr. Aaron Clapp *et al* demonstrated that the efficiency of energy transfer from the QDs to the dyes could be enhanced both by tuning the QD size and by increasing the dye/QD stoichiometry.^{74b} The former property is associated with the ability to size tune the PL spectrum of the QDs to maximize spectral overlap with the acceptor absorbance. According to the formalism described by Förster to quantify non-radiative energy transfer between two weakly coupled dipoles, the efficiency for transfer is highest when the spectral overlap between donor emission and acceptor

absorbance is highest.⁷⁵ This study has led to the development of this QD based technology for sensing and biological imaging.⁷⁶

Recently, a number of studies have investigated non-radiative energy transfer from QDs to a variety of acceptors such as other QDs⁷⁷, quantum wires^{77d}, phthalocyanines⁷⁸ and metalloproteins⁷⁹ to name a few. Several models, including the Förster mechanism outlined above, have been inferred to account for the observed photophysics, with varied degrees of effectiveness.^{79,80}

This field is still in its infancy and requires much more careful investigation especially with respect to the way QDs and other molecular, biological, or nanostructured species interact with each other both physically and electronically. Yet, it is clear that the ability to tune the electronic coupling between the QD donors and the acceptors by varying their size makes QDs a powerful new class of photochemical sensitizers. In the current studies, the exceptional photophysical characteristics of QDs highlighted above are exploited with the goal of using optically excited QDs to sensitize release of nitric oxide from the previously studied dinitritio chromium(III) cyclam complexes.

D. Current Studies

i. New Quantum Dot Based Supramolecular Structures for Photochemical Nitric Oxide Delivery

The studies on chromium (III) dinitrito system initiated by De Leo indicate that complexes of this type have a high potential for application as photochemical

NO-donors. De Rosa showed that the cyclam periphery can be covalently modified with dye molecules which efficiently sensitize the photochemically active chromium (III) excited state there-by providing a strong framework for improving the light-absorbing properties of these materials. In this work, the ability of QDs to sensitize the excited states of molecules of the type $[\text{Cr}(\text{L})\text{X}_2]^+$, where L = cyclam or a modified cyclam, and X = Cl^- or ONO^- , is investigated.

a) Coupling of $\text{Cr}(\text{L})\text{X}_2^+$ (L = cyclam or modified cyclam) to QD Surfaces.

First, a general methodology is described where-by transition metal complexes can be covalently coupled to the surface of QDs to form modified QDs (mQDs).

In the first strategy complexes of the form $\text{Cr}(\text{L})\text{Cl}_2^+$, where L = functionalized cyclam carrying either a hydroxyl- or amine appendage, were covalently coupled to QDs having carboxyl- functional groups using a carbodiimide as a cross-linker. This complex was chosen because it exhibits the characteristic Cr(III) doublet phosphorescence at 77 K. As demonstrated by DeRosa *et al*, the Cr(III) doublet phosphorescence can be used to probe energy transfer from appended dyes to the metal center.

In the preliminary work, CdSe QDs coated with mercaptopropionic acid (MPA) were reacted with the free hydroxyl- functionalized cyclam, hbc (hbc = 5,7-dimethyl-6-(*p*-hydroxymethylbenzyl)-1,4,8,11-tetraazacyclotetradecane). Although the conjugates were found to be insoluble, solid state nuclear magnetic resonance (NMR) spectroscopy (^1H and ^{13}C) and Fourier-transform infrared

(FTIR) spectroscopy were used to quantify the surface ligand composition of the new mQD and to verify formation of an ester bond between the QD surface bound MPA and hbc molecules. Because of the negligible PL from “core-only” type CdSe QDs passivated with thiol ligands and the insolubility of these materials in aqueous solutions, a photophysical investigation of the conjugates was not attempted.

Following the synthesis of water-soluble CdSe/ZnS core/shell QDs coated with DHLA having appreciable PL quantum yields in aqueous solution, a more detailed investigation for conjugating various chromium(III) cyclam complexes to the QD surface was conducted. In this case, the successful conjugation to Cr(L)Cl_2^+ (L = functionalized cyclam with amine (-NH₂) appendage) was accomplished via amide linkages to the QD surface bound DHLA. The QDs were found to be rather unstable towards activation by EDC, which often caused aggregation of the mQDs and precipitation from solution. However with careful choice of reagent concentrations and with the addition of a high molecular weight amine modified polyethylene glycol (mPEG-NH₂), mQDs that were stable to the reaction conditions and to the post-preparative purification steps were obtained. Stable mQDs were investigated using gel electrophoresis and photoluminescence spectroscopy. Although electrophoresis showed evidence of successful formation of mQDs based on surface charge neutralization, attempts to detect sensitized phosphorescence from the appended Cr^{III} centers proved unsuccessful. Yet, mQDs with one or more surface bound Cr(L)Cl_2^+ had quenched PL spectra when

compared to the control, consistent with energy transfer from the optically excited QD to the appended chromium(III) complexes.

An alternative strategy amenable to covalent conjugation of cyclam-type complexes to the QD surface was via the addition of a thiol functionality to the cyclam periphery. Several new derivatized chromium(III) cyclam derivatives were synthesized and characterized by mass spectroscopy and UV-visible spectroscopy, however synthetic challenges precluded attempts to use them in QD surface conjugation.

b) Bimolecular Interaction of Aqueous Mixtures of QDs and $\text{Cr}(\text{cyclam})\text{X}_2^+$ (X = Cl or ONO).

In collaboration with Alexis D. Ostrowski, dilute mixtures of CdSe/ZnS core/shell QDs coated with DHLA and various concentrations of both the dichloro- and dinitrito- analogues of *trans*-chromium(III) cyclam were investigated in aqueous media. Both steady state and time-resolved optical techniques (absorbance and photoluminescence) were used to investigate the effect of the added complexes on the QD PL intensity. Furthermore, a NO sensitive electrode was used to detect the sensitized release of NO via both single photon excitation (SPE) and two photon excitation (TPE).

Concentration dependent PL quenching is observed consistent with energy transfer from the optically excited QDs to the added metal complexes. The observed quenching behavior is consistent with the formation of electrostatic assemblies between the cationic chromium (III) cyclam complexes and the anionic

QD surface. These assemblies are stable in mildly basic buffered solution and have enhanced light absorbing capabilities when compared to the chromium(III) complexes alone due to the extremely large extinction coefficients of the QDs.

As discussed above, the nitrito- analogue *trans*-[Cr(cyclam)(ONO)₂]BF₄ was shown in this laboratory to release NO with very high quantum yields (up to 50%) upon visible light excitation. Due to the enhanced light absorption imparted by the QDs in the mixtures, the ability of the QDs to sensitize NO release was also probed using an electrochemical NO detector. Depending on the experimental conditions, irradiated mixtures of QDs and *trans*-Cr(cyclam)(ONO)₂⁺ showed a 5-75 fold enhancement in NO production in comparison to solutions containing *trans*-Cr(cyclam)(ONO)₂⁺ alone.

Based on the promising results for QD sensitized NO release using single photon excitation (SPE), two photon excitation (TPE) experiments were conducted to determine if wavelengths more amenable to tissue penetration could also sensitize NO release due to the high two photon absorption (TPA) cross sections observed for semiconductor QDs. Consistent with theoretical predictions⁸¹ and the experimental measurements by Dr. Daniel Larson *et al*⁸², the CdSe/ZnS core/shell QDs used here displayed a TPA cross section of ~10,000 GM at 800 nm, where 1 GM = 10⁻⁵⁰ cm⁴·s·photon⁻¹. This value is >200x higher than the TPA cross section of fluorescein (36 GM⁸³), a common laser dye used as a TPA standard that was recently demonstrated by Dr. Stephen R. Weckler from this laboratory to sensitize NO release via TPE from a Roussin's salt derivative.^{48b}

PL of the QDs generated by TPE at 800 nm was quenched in a concentration dependent manner by added *trans*-Cr(cyclam)(ONO)₂⁺, similar to observations using SPE, consistent with transfer of the NIR excitation to the electrostatically surface assembled NO-donors.

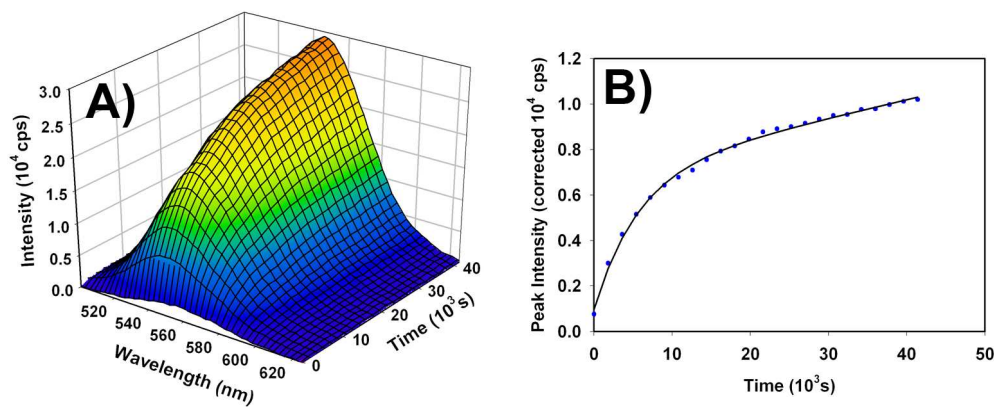
These recent results demonstrate that the strong light absorbing capabilities of QDs, both in the SPE and TPE regimes, makes them highly amenable towards use as light harvesting antenna for photochemical reactions. Specifically in the case of the results with the proto-typical NO-donor *trans*-Cr(cyclam)(ONO)₂⁺, the ability to sensitize this complex using NIR wavelengths via TPE of the QDs has broad implications for its use, and the use of other related photochemical NO donors, as potential photochemotherapeutics. For these supramolecular systems, TPE of the QDs allows activation by longer wavelength light which is required to incur enhanced tissue penetration. Although attempts so far to detect sensitized NO release via TPE of the QDs have proven challenging, a more systematic study of this system is currently underway in this laboratory. Because of the extensive work in development of QDs for tissue/cell specific labeling for bio-medical imaging, the potential use of QDs in combined drug-delivery/NO-donor drug activation strategies is a much anticipated outcome of the current effort highlighted in this work.

ii. Photoenhancement of QDs in the Presence of Nitric Oxide

Appendix I will be dedicated to a discussion of the photophysical/photochemical effects of small molecules, including NO, on the

photoluminescence (PL) properties of CdSe QDs. This discussion and the experimental work described stems largely from an observation made by Dr. Leroy Laverman in studies with Professor Geoffery Strouse. Dr. Laverman observed that a sample of CdSe QDs imbedded in a solidified sol-gel matrix (an example of which is shown in Figure 1.12B) was observed to undergo photoluminescence (PL) enhancement (or brightening) when subjected to continuous laser irradiation in the presence of a NO atmosphere (Figure 1.13). The initial premise was to investigate the possibility for use of the QDs as PL “turn-on” type sensors for NO, technology of considerable interest to the biomedical community. This project quickly proceeded to a general investigation of the varied photophysical processes observed in QDs under various experimental conditions and in the presence of various gases including NO. The results from these studies will be discussed in terms of photochemical effects governed by tuning between sub-populations of QDs within an ensemble.

Figure 1.13. CdSe QD photoluminescence brightening data obtained by Dr. Leroy Laverman upon continuous laser irradiation of a sol gel doped with CdSe QDs in the presence of a nitric oxide atmosphere.



E. References

1. Kawasaki, E. S.; Player, A. *Nanomed.* **2005**, *1*, 101-109.
2. Lincoln, J; Hoyle, C. H. V.; Burnstock, G. *Nitric Oxide in Health and Disease* Cambridge University Press: New York, **1997**.
3. Culotta, E.; Koshland Jr., D. E. *Science* **1992**, *258*, 1862-1865.
4. Fye, W. B. *Circulation* **1986**, *74*, 222-229 and references therein.
5. Ignarro, L. J; Lipton, H.; Edwards, J. C.; Baricos, W. H.; Hyman, A. L.; Kadawitz, P. J.; Gruetter C. A. *J. Pharm. Exp. Ther.* **1981**, *218*, 739-749.
6. (a) Diamond, J.; Blisard, K. *Mol. Pharm.* **1976**, *12*, 688-692. (b) Katsuki, S.; Ferid, M. *Mol. Pharm.* **1977**, *13*, 330-341. (c) Schultz, K. D.; Schultz, K.; Schultz, G. *Nature* **1977**, *265*, 750-751. (d) Arnold, W.; Mittal, C. K.; Katsuki, S.; Murad, F. *Proc. Nat. Acad. Sci.* **1977**, *74*, 3203-3207.
7. (a) Furchgott, R. F.; Zawadzki, J. V. *Nature* **1980**, *288*, 373-376. (b) Furchgott, R. F. *Trend. Pharm. Sci.* **1981**, *10*, 173-176. Furchgott, R. F.; Zawadzki, J. V.; Cherry, P. D. in *Vasodilatation*, ed. Vanhoutte, P. M.; Leusen, I. Raven Press: New York, **1981**, 49-66.
8. Furchgott, R. F.; Jothianandan, D.; Freay, A. D. in *NITRIC OXIDE FROM L-ARGININE: A bioregulatory system*, ed. Moncada, S; Higgs, E. A. Elsevier Science Publishers: Amsterdam, **1990**, 5-18 and references therein.
9. Gruetter, C. A.; Gruetter, D. Y.; Lyon, J. E.; Kadowitz, P. J.; Ignarro, L. J. *J. Pharmacol. Exp. Ther.* **1981**, *219*, 181-186.
10. Rapoport R. M.; Murad, F. *Circ. Res.* **1983**, *52*, 352-357.
11. (a) Gibson, Q. H.; Roughton, F. J. W. *J. Physiol.* **1957**, *136*, 507-526. (b) Martin, W.; Smith, J. A.; White, D. G. *Br. J. Pharmacol.* **1986**, *89*, 563-571.
12. (a) Gryglewski, R. J.; Palmer, R. M. J.; Moncada, S. *Nature* **1986**, *320*, 454-456. (b) Rubanyi, G. M.; Vanhoutte, P. M. *Am. J. Physiol* **1986**, *250*, H822-H827
13. Furchgott, R. F. in *Vasodilatation*, ed. Vanhoutte, P. M. Raven Press: New York, **1988**, 401-414.

14. Downes, M. J.; Edwards, M. W.; Elsey, T. S.; Walters, C. L. *Analyst*, **1976**, *101*, 742-748.
15. Palmer, R. M. J.; Ferrige, A. G.; Moncada, S. *Nature* **1987**, *327*, 524-526.
16. Moncada, S.; Palmer, R. M. J.; Higgs, E. A. *Pharmac. Rev.* **1991**, *43*, 109-142 and references therein.
17. (a) Palmer, R. M. J.; Ashton, D. S.; Moncada, S. *Nature* **1988**, *333*, 664-666. (b) Moncada, S.; Palmer, R. M. J.; Higgs, A. *Biochem. Pharm.* **1989**, *38*, 1709-1715.
18. Brecht, D. S.; Snyder, S. H. *Proc. Natl. Acad. Sci. USA* **1990**, *87*, 682-685.
19. Knowles, R. G.; Moncada, S. *Biochem. J.*, **1994**, *298*, 249-258 and references therein.
20. Murad, F. *Angew. Chem. Int. Ed.* **1999**, *38*, 1856-1868 and references therein.
21. (a) Ignarro, L. J.; Adams, J. B.; Horwitz, P. M.; Wood, K. S. *J. Biol. Chem.* **1986**, *261*, 4997-5002. (b) Ignarro, L. J. *Angew. Chem. Int. Ed.* **1999**, *38*, 1882-1892 and references therein.
22. Mitchell, H. H.; Shonle, H. A.; Grindley, H. S. *J. Biol. Chem.* **1916**, *24*, 461-490.
23. (a) Tannenbaum, S. R.; Fett, D.; Young, V. R.; Land, P. D.; Bruce, W. R. *Science* **1978**, *200*, 1487-1489. (b) Green, L. C.; Ruiz De Luzuriaga, K.; Wagner, D. A.; Rand, W.; Istfan, N.; Young, V. R.; Tannenbaum, S. R. *Proc. Natl. Acad. Sci. USA* **1981**, *78*, 7764-7768.
24. Stuehr, D. J.; Marletta, M. A. *Proc. Natl. Acad. Sci. USA* **1985**, *82*, 7738-7742.
25. Hibbs, J. B., Jr.; Taintor, R. R.; Vavrin, A.; Granger, D. L.; Drapier, J. C.; Amber, I. J.; Lancaster, J. R., Jr. in *NITRIC OXIDE FROM L-ARGININE: A bioregulatory system*, ed. Moncada, S; Higgs, E. A. Elsevier Science Publishers: Amsterdam, **1990**, 189-224 and references therein.
26. Hibbs, J. B., Jr.; Taintor, R. R.; Vavrin, Z. *Science* **1987**, *235*, 473-476.
27. Iyengar, R.; Stuehr, D. J.; Marletta, M. A. *Proc. Natl. Acad. Sci. USA* **1987**, *84*, 6369-6373.

28. Hibbs, J. B., Jr.; Taintor, R. R.; Vavrin, Z.; Rachlin, E. M. *Biochem. Biophys. Res. Comm.* **1988**, *157*, 87-94.
29. Stuehr, D. J.; Nathan, C. F. *J. Exp. Med.* **1989**, *169*, 1543-1555.
30. Lancaster, J. R., Jr.; Hibbs, J. B., Jr. *Proc. Natl. Acad. Sci. USA*, **1990**, *87*, 1223-1227.
31. (a) Wink, D. A.; Vodovotz, Y.; Laval, J.; Laval, F.; Dewhirst, M. W.; Mitchell, J. B. *Carcinogenesis* **1998**, *19*, 711-721. (b) Wink, D. A.; Mitchell, J. B. *Free Rad. Biol. Med.* **2003**, *34*, 951-954 and references therein. (c) Fukumura, Dai, Kashiwagi, S.; Jain, R. K. *Nat. Rev. Cancer* **2006**, *6*, 521-534 and references therein.
32. Wink, D. A.; Grisham, M. B.; Mitchell, J. B.; Ford, P. C. *Method Enzymol.* **1996**, *268*, 12-31.
33. von Sonntag, C. *The Chemical Basis of Radiation Biology* Taylor and Francis, Ltd: London, **1987**.
34. a) Howard-Flanders, P. *Nature*, **1960**, *186*, 485-487. (b) Dewey, D. L. *Nature*, **1960**, *186*, 780-782. (c) Powers, W. E.; Tolmach L. J. *Nature*, **1963**, *197*, 710-711.
35. (a) Thomlinson, R. H.; Gray, L. H. *Br. J. Cancer* **1955**, *9*, 539-549. (b) Gatenby, R. A.; Kessler, H. B.; Rosenblum, J. S.; Coia, L. L.; Moldofsky, P. J.; Hartz, W. H.; Broder, G. J. *Int. J. Radiat. Oncol. Biol. Phys.* **1988**, *14*, 831-838. (c) Krishna, M. C.; English, S.; Yamada, k.; Yoo, J.; Murugesan, R.; Devasahayam, N.; Cook, J. A.; Golman, K.; Ardenkjaer-Larsen, J. H.; Subramanian, S.; Mitchell, J. B. *Proc. Natl. Acad. Sci. USA* **2002**, *99*, 2216-2221.
36. Howard-Flanders, P. *Nature* **1957**, *180*, 1191-1192.
37. Mitchell, J. B.; Wink, D. A.; DeGraff, W.; Gamson, J.; Keefer, L. K.; Krishna, M. C. *Cancer Res.* **1993**, *53*, 5845-5848.
38. (a) Griffin, R. J.; Makepeace, C.m.; Hur, W. J.; Song, C. W. *Int. J. Rad. Oncol. Biol. Phys.* **1996**, *36*, 377-383. (b) Kurimoto, M.; Endo, S.; Hirashima, Y.; Hamada, H.; Ogiichi, T.; Takaku, A. *J. Neuro-Oncol.* **1999**, *42*, 35-44.
39. Cook, T.; Wang, Z.; Alber, S.; Liu, K. ; Watkins, S. C.; Vodovotz, Y.; Billiar, T. R.; Blumberg, D. *Cancer Res.* **2004**, *64*, 8015-8021.

40. Ridder, M. D.; Verobski, V. N.; Darville, M. I.; Van Den Berge, D. L.; Monsaert, C.; Eizirik, D. L.; Storme, G. A. *Int. J. Rad. Oncol. Biol. Phys.* **2004**, *60*, 598-606.
41. examples: (a) Ford, P. C.; Bourassa, J.; Miranda, K.; Lee, B.; Lorkovic, I.; Boggs, S.; Kudo S.; Laverman L. *Coord. Chem. Rev.* **1998**, *171*, 185-202. (b) Tfouni, E.; Krieger, M.; McGarvey, B. R.; Franco, D. W. *Coord. Chem. Rev.* **2003**, *236*, 57-69. (c) Pavlos, C. M.; Xu, H.; Toscano, J. P. *Cur. Topics Med. Chem.* **2005**, *5*, 635-645. (d) Eroy-Reveles, A A.; Leung, Y.; Mascharak, P. K. *J. Am. Chem. Soc.* **2006**, *128*, 7166-7167.
42. Dolmans, D. E. J. G. J.; Fukumura, D.; Jain, R. *Nat. Rev. Cancer* **2003**, *3*, 380-387 and references therein
43. (a) Wan, S.; Parrish, J.A.; Anderson, R. R.; Madden, M. *Photochem. Photobiol.* **1981**, *34*, 679-681. (b) Svaasand, L. O.; Ellingsen, R. *Photochem. Photobiol.* **1985**, *41*, 73-76.
44. Dougherty, T. J.; Marcus, S. L. *Eur. J. Cancer* **1992**, *28A*, 1734-1742.
45. (a) Works, C. F.; Ford, P. C. *J. Am. Chem. Soc.* **2000**, *122*, 7592-7593. (b) Works, C. F.; Jocher, C. J.; Bart, G. D.; Bu, X.; Ford, P. C. *Inorg. Chem.* **2002**, *4*, 3728.
46. (a) Bourassa, J.; DeGraff, W.; Kudo, S.; Wink, D. A.; Mitchell, J. B.; Ford, P. C. *J. Am. Chem. Soc.* **1997**, *119*, 2853-2860. (b) Bourassa, J.; Lee, B.; Bernard, S.; Schoonover, J.; Ford, P. C. *Inorg. Chem.* **1999**, *38*, 2947-2952. (c) Bourassa, J.; Ford, P. C., *Coord. Chem. Rev.* **2000**, *200-202*, 887-900. (d) Conrado, C.; Bourassa, J.; Egler, C.; Wecksler, S.; Ford, P.C. *Inorg. Chem.* **2003**, *42*, 2288-2293. (e) Conrado, C. L.; Wecksler, S.; Egler, C.; Magde, D.; Ford, P. C., *Inorg. Chem.* **2004**, *43*, 5543-5549. (f) Wecksler, S. R.; Hutchinson, J.; Ford, P. C. *Inorg. Chem.* **2006**, *45*, 1192-1200. (g) Bourassa, J. L., Ph.D. Dissertation, U.C. Santa Barbara, Santa Barbara, CA (**1998**). (h) Conrado, C., Ph.D. Dissertation, U.C. Santa Barbara, Santa Barbara, CA (**2002**). (i) Wecksler, S. R., Ph.D. Dissertaion, U.C. Santa Barbara, Santa Barbara, CA (**2006**).
47. (a) De Leo, M. A., Ph.D. Dissertation, U.C. Santa Barbara, Santa Barbara, CA (**1998**). (b) De Leo, M.; Ford, P. C. *J. Am. Chem. Soc.* **1999**, *121*, 1980-1981. (c) DeLeo, M. A.; Ford, P. C. *Coord. Chem. Rev.* **2000**, *208*, 47-59. (d) DeRosa, F.; Bu, X.; Ford, P.C. *Inorg. Chem.* **2005**, *44*, 4157-4165. (e) DeRosa, F.; Bu, X.; Pohaku, K.; Ford, P.C. *Inorg. Chem.* **2005**, *44*, 4166-4174. (f) DeRosa, F.; Bu, X.; Ford, P.C., *Inorg. Chem.* **2003**, *42*, 4171-4178. (g) DeRosa, F., Ph.D. Dissertation, U.C. Santa Barbara, Santa Barbara, CA (**2003**).

48. (a) Wecksler, S. R.; Mikhailovsky, A.; Ford, P. C. *J. Am. Chem. Soc.* **2004**, *126*, 13566-13567. (b) Wecksler, S. R.; Mikhailovsky, A.; Korystov, D.; Ford, P. C. *J. Am. Chem. Soc.* **2006**, *128*, 3831-3837.
49. examples: (a) Adamson, A. W. *J. Phys. Chem.* **1967**, *71*, 798-808. (b) Adamson, A. W. *Pure Appl. Chem.* **1969**, *20*, 25-52 and references therein. (c) Forster, L. S. *Chem. Rev.* **1990**, *90*, 331-353 and references therein. (d) Forster, L. S. *Coord. Chem. Rev.* **2002**, *227*, 59-92 and references therein.
50. (a) Suslick, K. S.; Watson, R. A. *Inorg. Chem.* **1991**, *30*, 912-919. (b) Suslick, K. S.; Bautista, J. F.; Watson, R. A. *J. Am. Chem. Soc.* **1991**, *113*, 6111-6114.
51. Yamaji, M.; Hama, Y.; Miyazaki, Y.; Hoshino, M. *Inorg. Chem.* **1992**, *31*, 932-934.
52. Hoshino, M.; Nagashima, Y.; Seki, H.; De Leo, M.; Ford, P. C. *Inorg. Chem.* **1998**, *37*, 2464-2469.
53. Henglein, A. *Chem. Rev.* **1989**, *89*, 1861-1873 and references therein
54. Rossetti, R.; Ellison, J. L.; Gibson, J. M.; Brus, L. E. *J. Chem. Phys.* **1984**, *80*, 4464-4469.
55. Brus, L. *J. Phys. Chem.* **1986**, *90*, 2555-2560.
56. Murray, C. B.; Norris, D. J.; Bawendi, M. G. *J. Am. Chem. Soc.* **1993**, *115*, 8706-8715.
57. de Mello Donegá, C.; Liljeroth, P.; Vanmaekelbergh, D. *Small* **2005**, *1*, 1152-1162 and references therein.
58. (a) Peng, Z. A.; Peng, X. *J. Am. Chem. Soc.* **2001**, *123*, 183-184. (b) Peng, X. *Chem. Eur. J.* **2002**, *8*, 334-339.
59. Cumberland, S. L.; Hanif, K. M.; Javier, A.; Khitrov, G. A.; Strouse, G. F.; Woessner, S. M.; Yun, C. S. *Chem. Mater.* **2002**, *14*, 1576-1584.
60. examples: (a) Qu, L.; Peng, X. *J. Am. Chem. Soc.* **2002**, *124*, 2049-2055. (b) Kalyuzhny, G.; Murray, R. W. *J. Phys. Chem. B* **2005**, *109*, 7012-7021. (c) de Mello Donegá, C.; Hickey, S. G.; Wuister, S. F.; Vanmaekelbergh, D.; Meijerink, A. *J. Phys. Chem. B* **2003**, *107*, 489-496.

61. (a) Hines, M. A.; Guyot-Sionnest, P. *J. Phys. Chem.* **1996**, *100*, 468-473. (b) Dabbousi, B. O.; Rodriguez-Viejo, J.; Mikulec, F. V.; Heine, J. R.; Mattoussi, H.; Ober, R.; Jensen, K. F.; Bawendi, M. G. *J. Phys. Chem. B*, **1997**, *101*, 9463-9475. (c) Peng, X.; Schlamp, M. C.; Kadavanich, A. V.; Alivisatos, A. P. *J. Am. Chem. Soc.* **1997**, *119*, 7019-7029.
62. Nazzal, A. Y.; Wang, X.; Qu, L.; Yu, W.; Wang, Y.; Peng, X.; Xiao, M. *J. Phys. Chem. B*. **2004**, *108*, 5507-5515.
63. Cordero, S. R.; Carson, P. J.; Estabrook, R. A.; Strouse, G. F.; Buratto, S. K. *J. Phys. Chem. B*. **2000**, *104*, 12137-12142.
64. Jones, M.; Nedeljkovic, J.; Ellingson, R. J.; Nozik, A. J.; Rumbles, G. *J. Phys. Chem. B*. **2003**, *107*, 11346-11352.
65. Wang, Y.; Tang, Z.; Correa-Duarte, M. A.; Pastoriza-Santos, I.; Giersig, M.; Kotov, N. A.; Liz-Marzán, L. M. *J. Phys. Chem. B*. **2004**, *108*, 15461-15469.
66. Asami, H.; Abe, Y.; Ohtsu, T.; Kamiya, I.; Hara, M. *J. Phys. Chem. B*, **2003**, *107*, 12566-12568.
67. Jang, E.; Jun, S.; Chung, Y.; Pu, L. *J. Phys. Chem. B*, **2004**, *108*, 4597-4600.
68. Myung, N.; Bae, Y.; Bard, A. J. *Nano. Lett.*, **2003**, *3*, 747-749.
69. Zhelev, Z.; Jose, R.; Nagase, T.; Ohba, H.; Bakalova, R.; Ishikawa, M.; Baba, Y. *J. Photochem. Photobio. B*, **2004**, *75*, 99-105.
70. Nirmal, M.; Dabbousi, B. O.; Bawendi, M. G.; Macklin, J. J.; Trautman, J. K.; Harris, T. D.; Brus, L. E. *Nature* **1996**, *383*, 802-804.
71. Ebenstein, Y.; Maokari, T.; Banin, U. *Appl. Phys. Lett.*, **2002**, *80*, 4033-4035.
72. Muller, J.; Lupton, J. M.; Rogach, A. L.; Feldmann, J.; Talapin, D. V.; Weller, H. *Appl. Phys. Lett.*, **2004**, *85*, 381-383.
73. Chan, W. C. W.; Nie, S. *Science* **1998**, *281*, 2016-2018.
74. (a) Mattoussi, H.; Mauro, J. M.; Goldman, E. R.; Anderson, G. P.; Sundar, V.C.; Mikulec, F. V.; Bawendi, M. G. *J. Am. Chem. Soc.*, **2000**, *122*, 12142-12150. (b) Clapp, A. R.; Medintz, I. L.; Mauro, J. M.; Fisher, B. R.; Bawendi, M. G.; Mattoussi, H. *J. Am. Chem. Soc.*, **2004**, *126*, 301-310.

75. (a) Förster, T. *Discuss. Faraday Soc.*, **1959**, 27, 7-17. (b) Lakowicz, J. R. *Principles of Fluorescence Spectroscopy*, 2nd Ed., Kluwer Academic: New York, **1999**.
76. Medintz, I. L.; Uyeda, H. T.; Goldman, E. R.; Mattoussi, H. *Nat. Mater.* **2005**, 4, 435-446 and references therein.
77. (a) Kagan, C. R.; Murray, C. B.; Bawendi, M. G. *Phys. Rev. B* **1996**, 54, 8633-8643. (b) Crooker, S. A.; Hollingsworth, J. A.; Tretiak, S.; Klimov, V. I. *Phys. Rev. Lett.* **2002**, 89, 186802-1 – 186802-4. (c) Achermann, M.; Petruska, M. A.; Crooker, S.A.; Klimov, V. I. *J. Phys. Chem. B* **2003**, 107, 13782-13787. (d) Lee, J.; Govorov, A. O.; Kotov, N. A. *Nano Lett.* **2005**, 5, 2063-2069. (e) Wargnier, R.; Baranov, A. V.; Maslov, V. G.; Stsiapura, V.; Artemyev, M.; Pluot, M.; Sukhanova, A.; Nabiev, I. *Nano Lett.* **2004**, 4, 451-457.
78. (a) Dayal, S.; Lou, Y.; Samia, A. C. S.; Berlin, J. C.; Kenney, M. E.; Burda, C. *J. Am. Chem. Soc.* **2006**, 128, 13974-13975. (b) Dayal, S.; Królicki, R.; Lou, Y.; Qiu, X.; Berlin, J. C.; Kenney, M. E.; Burda, C. *Appl. Phys. B* **2006**, 84, 309-315.
79. Ipe, B. I.; Niemeyer, C. M. *Angew. Chemie, Int. Ed.* **2006**, 45, 504-507.
80. Clapp, A. R.; Medintz, I. L.; Mattoussi, H. *ChemPhysChem*, **2006**, 7, 47-57 and references therein.
81. Blanton, S. A.; Hines, M. A.; Schmidt, M. E.; Guyot-Sionnest, P. *J. Luminescence* **1996**, 70, 253-268 and references therein.
82. Larson, D. R.; Zipfel, W. R.; Williams, R. M.; Stephen, W. C.; Bruchez, M. P.; Wise, F. W.; Webb, W. W. *Science*, **2003**, 300, 1434-1436.
83. Webb, W.W.; Xu, C., *J. Opt. Soc. Am. B* **1996**, 13, 481-491.

2. Chapter II. Experimental

A. Reagents and Instrumentation

i. Reagents

Cadmium(II) nitrate tetrahydrate ($\text{CdNO}_3 \cdot 4\text{H}_2\text{O}$, 98%) and dimethylcadmium ($\text{Cd}(\text{CH}_3)_2$, 97% min.) were purchased from Strem. Selenium powder (99.5+%, 200 mesh), thiophenol (99+%), straight chained 1-hexadecylamine (technical grade, 90%), 1-octadecene (technical grade, 90%), tetramethylammonium hydroxide (99%), 3-mercaptopropionic acid (99+%), DL-thioctic acid (98+%), N,N'-bis(2-aminoethyl)-1,3-propanediamine (97%), and 48% hydrogen bromide were purchased from Acros Organics. 1-Hexadecylamine was further purified by vacuum distillation. Zinc Oxide (technical grade, $\geq 99.0\%$), diethylzinc, trioctylphosphine (technical grade, 90%), trioctylphosphine oxide (technical grade, 90%), hexamethyldisilathiane, nickel(II) chloride hexahydrate ($\text{NiCl}_2 \cdot 6\text{H}_2\text{O}$), chromium(III) chloride tetrahydrofuran complex ($\text{CrCl}_3 \cdot 3\text{THF}$, 97%), 2,4-pentanedione (99+%), dicyclohexylcarbodiimide (DCC, 99%), 4-dimethylaminopyridine (DMAP, 99%), 1-hydroxybenzotriazole, 3-aminopropyltrimethoxysilane (APS), (sodium hydroxide (50% w/w), concentrated ammonium hydroxide, and sodium bicarbonate were all purchased from Aldrich and used without further purification. Elemental sulfur, oleic acid, and triethylamine were purchased from Fisher and used without further purification.

p-Xylylene glycol was purchased from TCI chemical corp. and used without further purification. Methoxy- poly(ethylene glycol) amine, average M.W. 5,000 (mPEG-NH₂-5000) was purchased from Nektar and used as received. 1-Ethyl-3-(3-dimethylaminopropyl) carbodiimide (EDC) and *N*-hydroxysuccinimide (NHS) were purchased from Pierce.

Air sensitive compounds were manipulated under an argon atmosphere in an inert atmosphere dry box (Vacuum Atmospheres Company, Model # HE-493) or on a dedicated Schlenk line. High-grade argon for Schlenk line work was first passed through a drying column loaded with Drierite/molecular sieve (4Å).

ii. Solvents

Toluene for spectroscopic studies was obtained from Burdick and Jackson (spectroscopic grade) and was further purified by distillation under dinitrogen over sodium metal. Acetonitrile, methanol, and methylene chloride were all distilled under dinitrogen from calcium hydride (CaH₂). Sure-seal bottles of anhydrous dimethylformamide were purchased from Aldrich and used without purification. All other solvents used were reagent grade and used without purification unless otherwise stated. Nanopure water, used for all buffered solutions and spectroscopic studies, was obtained from a Millipore water purification system. Phosphate buffers (15 mM) were prepared in nanopure water and their pH was adjusted using an Orion Research (model 701 A) digital ionalyzer equipped with a Corning Deep Vessel electrode (model 476306).

iii. Gases

All gases were purchased from PRAXAIR Inc. and used as received unless further specified. High grade argon used for inert atmosphere preparation was passed through a Drierite/molecular Sieve (4 Å) column to remove any remaining water. De-oxygenated solutions were prepared by sparging solutions with dinitrogen or argon for approximately one minute per milliliter or via three freeze-pump-thaw (3 f-p-t) cycles.

Nitric Oxide (99%, Aire Liquide) was purified by passage through a stainless steel column filled with Ascarite II (Thomas Scientific) to remove higher nitrogen oxide impurities. All manipulations with NO gas were performed on a dedicated Schlenk-type manifold using greaseless stainless steel tubing and fittings and Teflon/glass stopcocks.

iv. Instrumentation and Methods

a) UV-vis Absorption Spectroscopy

UV-vis absorption spectra were measured using either a diode array spectrophotometer (Hewlett Packard P8572) or dual beam spectrophotometer (Shimadzu UV-2401 PC). All spectra were recorded in high quality UV-vis quartz cells (Starna Cells) having a 1 cm pathlength.

b) Infrared Spectroscopy

All infrared spectra were obtained on a FTIR spectrometer (BioRad FTS 60 SPC 3200). Solution infrared spectra were recorded in sealed cells (International

Crystal Labs) with a fixed path length of 0.1 cm, having CaF₂ windows and a Teflon spacer and stoppers. For solid samples, IR-grade KBr was used to prepare solid KBr pellets.

c) NMR

Solution phase ¹H and ¹³C NMR spectra were performed at room temperature in grade 7 U-P NMR tubes (Kontes Glass Company) on a 200 MHz spectrometer (Varian Mercury Vx) in deuterated chloroform, (Cambridge Isotope laboratories, Inc.) and referenced to the solvent peak (CHCl₃, $\delta = 7.27$ (1) ppm relative to TMS).

Solid state cross polarization magic angle spinning (CP MAS) ¹³C NMR spectra were performed at room temperature on a 300 MHz spectrometer (Bruker Advance) in collaboration with Dr. Jerry Hu of the Materials Research Laboratory spectroscopy facility at UCSB. The instrument was equipped with a 4-mm broadband MAS probe double tuned to ¹H (300.1 MHz) and the X channel to ¹³C (75.5 MHz). A sample spinning speed of 9 kHz was used. Chemical shifts were referenced to TMS.

d) Mass Spectrometry

All mass spectra were obtained on a single quadrupole mass spectrometer (PE Sciex QStar) with an electrospray ionization source run with a Fisons Masslinks data system. Automatic injections were achieved using a Harvard apparatus infusion pump 22 equipped with a Hamilton 250 μ L syringe at a flow rate of 10

μL per minute. Sample solutions were prepared in various solvents (acetonitrile, water, methanol, etc.) and diluted to a concentration between 10-100 μM .

e) Electrochemical Detection of Nitric Oxide

Real time detection of nitric oxide was accomplished using a nitric oxide sensitive electrode (amiNO-700, Innovative Instruments, Inc. Tampa, FL.). The amiNO-700 is capable of detecting nanomolar concentrations of NO in aqueous solution. The electrode was calibrated from 50 to 400 nM in [NO] via injections of known quantities of KNO_2 into acidified solutions ($\sim 0.1 \text{ M H}_2\text{SO}_4$) containing KI as a reducing agent. The concentration of NO determined experimentally was then extrapolated from the calibration curve.

f) Gel electrophoresis

Gel electrophoresis of water soluble quantum dots and modified quantum dots was conducted in 1.5 % agarose gels with 0.5x Tris-Borate-EDTA (TBE) buffer medium. The voltage was held at 100 V for ~ 1 h. 6 nm gold nanoparticles were used as a real-time imaging standard during the electrophoretic run. Gel staining was accomplished by treatment of the gels following electrophoresis with “Silver Initiator” and “Silver Enhancer” solutions (Nanoprobes, Catalogue # 2013). The developing gels were imaged with a conventional desktop scanner.

g) Steady State Photoluminescence Luminescence Experiments and Quantum Yield Measurements.

Steady state photoluminescence (PL) measurements were performed on a Fluorolog-2 fluorimeter (Jobin Yvon/SPEX, Edison, New Jersey). Samples were excited with a 300 W xenon arc lamp, and the corresponding PL was collected at a 90° from the excitation source, except in the case of PL from solids or low temperature glasses which was collected in front-face configuration. The excitation and emission beams were passed through SPEX 1681 Singlemate monochromators in order to isolate the appropriate wavelengths. The slits were varied depending on the particular experiment, resulting in a band pass of 1-4 nm. The emitted light collected from the monochromator was then focused onto a red sensitive Hamamatsu R928-A water cooled photomultiplier tube (PMT) configured for single photon counting and interfaced with a computer running SPEX DM3000f software. The PL spectra were corrected for PMT response and deviations in lamp intensity by the ratio method using Rhodamine-B as a standard. Solution phase samples were prepared in high quality, four sided quartz cuvettes (Starna cells) such that the absorbance at the excitation wavelength was less than 0.1. PL from low temperature glasses was obtained in high quality quartz tubes. Photoluminescence quantum yields of dilute solutions were determined by the relative method outlined by Demas and Crosby.¹ Briefly, the integrated PL intensity of two dilute solutions, one of the compound of interest and the other

of a standard compound with a known PL quantum yield having a spectrum with similar shape and at similar energy to that of the compound being studied, is recorded under *identical* experimental conditions (sample orientation, sampling geometry, band pass, etc). The quantum yield (ϕ_x) of the unknown is then calculated using the following equation:

$$\phi_x = \phi_{ref} \left(\frac{A_{ref}(\lambda_{ref})}{A_x(\lambda_x)} \right) \left(\frac{I(\lambda_{ref})}{I(\lambda_x)} \right) \left(\frac{n_x^2}{n_{ref}^2} \right) \left(\frac{D_x}{D_{ref}} \right) \quad (2.1)$$

In this equation, $I(\lambda)$ is the relative intensity of the exciting light (if identical experimental conditions and wavelength are used, then this term cancels out), $A(\lambda)$ is the absorbance of each sample at the excitation wavelength, n is the refractive index of the solvent(s), and D is the integrated intensity (area under the curve) of the corrected PL spectra. Parameters for the reference compound in Eq. 2.1 are indicated by the index '*ref*'. In these studies, $[\text{Ru}(\text{bpy})_3](\text{PF}_6)_2$ (bpy = 2,2'-bipyridine) in degassed acetonitrile ($\phi_r = 0.062$)² is used as the quantum yield standard.

h) Laser Photolysis Set-Up for Photoenhancement Studies

Photolysis was conducted using a water cooled cw Ar⁺ laser (Spectraphysics Beamlok 2065-8) (488nm, spot size 1mm, average power 200-3000mW). Emission was collected at right angle and detected by focusing into a 0.5 m monochromator (Acton Research SP-500) and dispersing the signal onto a charge coupled device (CCD) camera (Roper Scientific SPEC:10). A

holographic notch filter was used to filter out residual laser scatter. For a typical experiment, 1 s acquisitions were collected every 5 s for 1000 scans, under constant laser photolysis. Alternatively, a pulsed Nd:YAG laser (Continuum NY-61) was used to excite the sample of interest using the third harmonic (355 nm) of the fundamental operating at 3–3000 mW (8 ns pulse width {FWHM}, 20 Hz repetition rate). For the pulsed experiments the excited emission was collected via a fiber optic coupled to a spectrometer (Acton Research SpectraPro-275) and spectrally imaged with a liquid nitrogen cooled charge coupled device (CCD) camera (Princeton Scientific).

i) Photoluminescence Lifetime Measurements

Fluorescence lifetime measurements were performed with Dr. Alexander A. Mikhailovsky in the UCSB optical characterization facility using a time-correlated single-photon-counting technique (TCSPC).³ The sample was excited by 460 nm laser pulses with a duration of about 120 fs produced via the second harmonic generation process from the output of an Ti:sapphire laser (Spectra Physics Tsunami). In order to avoid saturation of the chromophore, the repetition rate of the excitation pulses was reduced to 2 MHz by a custom-built acousto-optical pulse picker. The luminescence was dispersed in a monochromator (Acton Research SPC-300) and detected by a micro channel-plate photomultiplier tube (MCP PMT; Hamamatsu R3809U-51). The triggering signal for the correlator board was generated by a fast photodiode illuminated via a beam-splitter introduced into the excitation beam. The MCP PMT output and triggering signal

were connected to a SPC-630 time correlated single photon counting board (TCSPC; Becker & Hickl) which performed statistical analysis of the photon flux and restored the fluorescence transients. The instrument response function has a full width at half maximum (FWHM) of ~55 ps and is determined by the speed of MCP PMT response.

j) Femtosecond Transient Absorbance (TA) Experiments

Femtosecond (fs) photolysis experiments were performed in collaboration with Dr. Alexander A. Mikhailovsky in the UCSB optical characterization facility on a femtosecond transient absorption spectrometer similar to the one described previously by Klimov and McBranch.⁴ The system utilizes the output of a Ti:Sapphire regenerative amplifier (Spectraphysics Spitfire) producing 100 fs optical pulses with 1 kHz repetition rate, central wavelength of 800 nm, and pulse energy <1 mJ. The sample was excited by ultra-short pulses with central wavelength of 400 nm, generated in 1 mm thick β -BBO crystal via the second harmonic generation process. The excitation pulse energy was adjusted by calibrated neutral density filter wheel. Photoinduced absorption changes were monitored by broadband fs continuum pulses. The continuum was generated by focusing low energy (< 2 μ J) 800 nm pulses onto a 2 mm thick crystalline sapphire plate. The delay between pump and probe pulses was varied by a translation stage with a corner cube reflector inserted into the pump beam. An optical chopper synchronized with the fs laser repetition frequency was employed to modulate the excitation beam and provided a synchronization signal for the

lock-in amplifier (SRS SR830). Samples were placed in 1 mm pathlength quartz cuvettes and sparged with argon to remove oxygen. The pump and probe beams were focused on the sample in a near-collinear geometry using a lens and a parabolic mirror, respectively. The probe light was dispersed by a monochromator (Acton SpectraPro 300) and detected by a Si photodiode connected to the lock-in amplifier via a transimpedance amplifier. The operation of the setup was controlled by a LabView program running on a PC.

k) Two Photon Excitation Photoluminescence Measurements

Two photon excitation photoluminescence (TPE PL) measurements were done in collaboration with Dr. Alexander Mikhailovsky at the UCSB optical characterization facility. Samples were excited with a tightly collimated ($\sim 120 \mu\text{m}$) high intensity laser beam, and the corresponding up-converted fluorescence was detected at a 90° angle. TPE was achieved using a mode-locked Ti:Sapphire laser (Spectraphysics Tsunami) with excitation pulses of ~ 100 fs and energy of ~ 6 nanoJoules (nJ) operating with a repetition rate of 80 MHz. The emitted light from the sample was collected onto a high numerical aperture lens and focused onto the spectrometer's entrance. The radiation dispersed from the spectrometer was then detected by a thermoelectrically cooled charged coupled device (CCD) camera (Roper Scientific Spec 10:100B/TE). Solutions were irradiated for approximately 30 s with a central wavelength of $\lambda_{\text{exc}} = 800$ nm and the corresponding TPE induced fluorescence was monitored from $\lambda_{\text{mon}} = 480\text{-}750$ nm.

I) Two Photon Absorption Cross Section (δ) Measurements

The TPE photoluminescence (TPE PL) technique was employed for determining two photon absorption cross sections.⁵ These measurements were done in collaboration with Dr. Alexander Mikhailovsky at the UCSB optical characterization facility. In this technique, a sample is excited with a tightly collimated high-intensity laser beam ($\sim 120 \mu\text{m}$), the emission is collected at a 90° angle and focused onto the spectrophotometer. The light collected from the spectrophotometer is then detected using a thermoelectrically cooled charged coupled device (CCD) camera (Roper Scientific Spec10:100B/TE). The laser used for excitation is a tunable mode locked Ti:Sapphire (Spectraphysics Tsunami) which is capable of generating ~ 100 fs pulses with an energy of ~ 6 nJ and a repetition rate of 80 MHz between the wavelengths of $\lambda_{\text{exc}} = 690\text{-}1000$ nm. The fluorescence detected from two photon excitation is then monitored from $\lambda_{\text{mon}} = 480$ to 750 nm, and the integrated TPE fluorescence intensity is utilized to determine the TPA cross section as described below.

According to previous work by Xu and Webb,⁵ the integrated PL intensity (I) due to TPE can be described in terms of the equation below:

$$I = A\phi \int_{-\infty}^{+\infty} \frac{I_0^2(t)\delta cl}{1 + I_0^2(t)\delta cl} dt. \quad (2.2)$$

In the above equation, the sample contributes the following parameters: δ is the TPA cross section, c is the concentration, l is the pathlength, and ϕ is the photoluminescence (PL) quantum yield. The term A accounts for all of the

experimental variables associated with collection of TPE induced photon emission from the sample (geometric factors, spectrometer and detector efficiencies, etc.). The function $I_0(t)$ describes the temporal profile of the excitation pulse. When operating in the limit of low light intensity and a highly diluted sample, the denominator in Eq. 2.2 becomes infinitely small, leaving the following expression for I :

$$I = A\phi\delta c l \int_{-\infty}^{+\infty} I_0^2(t) dt, \quad (2.3)$$

or more simply,

$$I = B\phi\delta c l P^2. \quad (2.4)$$

In Eq. 2.4, the function $I_0(t)$ is reduced to the experimental excitation power, P , and B is a constant.

The experimental factors defining B are difficult to measure and in practice, relative measurements (similar to the steady state PL quantum yields described above) are employed in which the signal, I_{ref} , obtained from a reference compound with a known TPA spectrum and TPA cross section is compared to that observed for the sample of interest. As long as all other experimental parameters remain *identical*, one can simply take the ratio of the integrated PL intensities:

$$\frac{I}{I_{ref}} = \frac{\phi\delta c}{\phi_{ref}\delta_{ref}c_{ref}} \frac{P^2}{P_{ref}^2} K^{-1}. \quad (2.5)$$

For the terms in the denominator, the index '*ref*' refers to the reference compound used for the comparison. K is a correction factor that accounts for differences in the refractive indices of the two samples determined mainly by their respective

solvents. In the case of nearly-collimated beams used here, $K = n^2 / n_{ref}^2$, and reduces to 1 for the case where the reference and the sample of interest are in the same solvent. Eq. 2.5 can be rearranged as follows to obtain the TPE cross section (δ) of the unknown sample:

$$\delta = \frac{\phi_{ref} \delta_{ref} c_{ref} P_{ref}^2}{\phi c P^2} \frac{I}{I_{ref}} K. \quad (2.6)$$

B. Synthesis

i. Cadmium Selenide (CdSe) Nanocrystal Quantum Dots (QDs)

a) Single Source Precursor Method using $\text{Li}_4[\text{Cd}_{10}\text{Se}_4(\text{SPh})_{16}]$

◆ $\text{Li}_2[\text{Cd}_4(\text{SPh})_{10}]$, (SPh = Thiophenol)

This complex was prepared based on a literature method⁶ using Li^+ in place of tetramethylammonium as the counter-ion. Thiophenol (37.28 mL, 0.363 mol) was dissolved in methanol (120 mL) and triethylamine (50.96 mL, 0.366 mol) was added. To the vigorously stirred mixture, a solution of $\text{Cd}(\text{NO}_3)_2 \cdot 4\text{H}_2\text{O}$ (42.0 g, 0.136 mol) in methanol (120 mL) was *slowly* added allowing for complete dissolution. Finally, a solution of LiNO_3 (10.6 g, 0.154 mol) in methanol (80 mL) was quickly added and stirring was discontinued after ~1 min. The mixture was allowed to sit at room temperature for ~1 h and then stored in a refrigerator (5-10

°C) for several more hours allowing the product to crystallize. The white solid was filtered, washed with ice cold methanol, and air dried. Yield: 51.0 g (96 %).

◆ **Li₄[Cd₁₀Se₄(SPh)₁₆]**

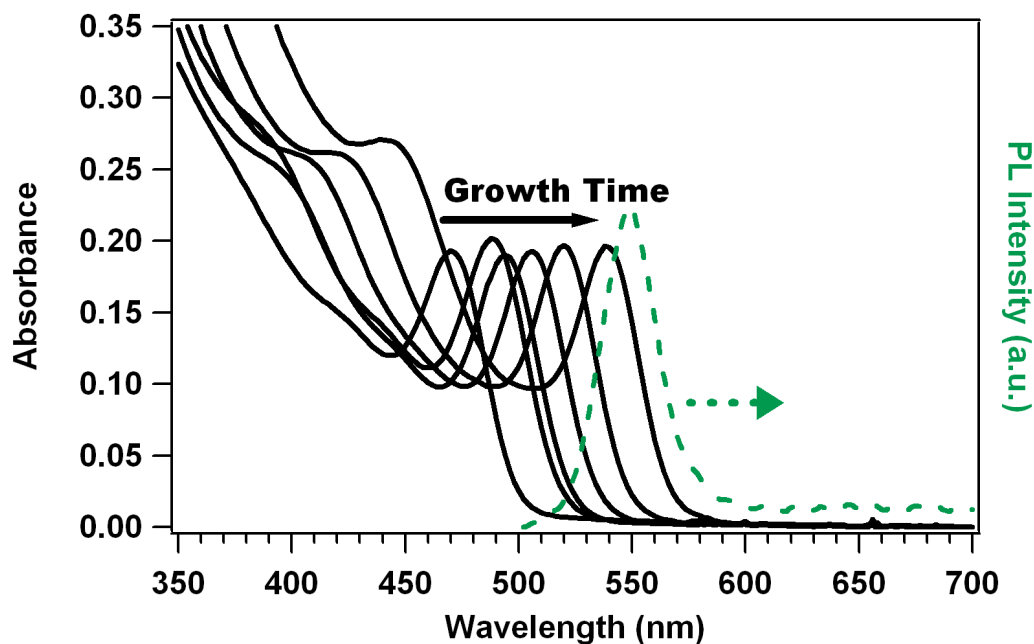
This complex was prepared based on a literature method⁶ using the lithium salt of [Cd₄(SPh)₁₀]²⁻. Li₂[Cd₄(SPh)₁₀] (17.0 g, 10.9 mmol) was dissolved in acetonitrile (20 mL) with gentle heating. The head space of the flask was flushed with argon and elemental selenium (0.863 g, 10.9 mmol) was added. The mixture was stirred overnight under argon atmosphere, during which time the initial black color of the elemental selenium gave way to milky white indicating product formation. The white mixture was transferred to a 500 mL Erlenmeyer flask and heated to ~75 °C. Under constant stirring, acetonitrile (~400 mL) was added to the heated mixture until the white product just dissolved. The solution was then filtered hot and allowed to cool and slowly crystallize undisturbed at room temperature for several hours and then in a refrigerator overnight, in the dark. The product was obtained as a white crystalline solid following filtration and air drying. Yield 7.5 g (13 %). This product is stable for several months when stored in the dark in argon flushed vials. Recrystallization can be effected from hot acetonitrile.

◆ **CdSe QDs using Li₄[Cd₁₀Se₄(SPh)₁₆] as a Single Source Precursor.**

This material was synthesized based on a previously reported procedure.⁷ 1-Hexadecylamine (HDA) (60g) was degassed under reduced pressure at 120 °C for

1 h in a 3 neck round bottom flask equipped with a condenser, a thermometer, and a stir bar. The flask was periodically back-filled with argon during the degassing procedure. The temperature was then reduced to 60 °C and $\text{Li}_4[\text{Cd}_{10}\text{Se}_4(\text{SC}_6\text{H}_5)_{16}]$ (2.00 g, 0.6350 mmol) was added to the molten HDA under argon flow resulting in a bright yellow solution. The temperature of the vigorously stirred reaction mixture was raised to 190-240 °C to allow growth of the CdSe QDs. The progress of the reaction was followed by *quickly* (to avoid solidification of the aliquot prior to transfer) removing ~100 μL aliquots via glass syringe from the reaction mixture at regular intervals using a wide bore needle, diluting in chloroform or toluene, and monitoring the absorbance spectra (Figure 2.1). When the desired particle diameter was reached as determined from the

Figure 2.1. Example of use of absorbance to monitor the CdSe-HDA QD growth. Also shown (green dashed line) is the PL spectrum of the last aliquot (~3.7 nm QDs).



position of the 1S ([1S(*e*)-1S_{3/2}(*h*)] transition⁸) (typical reaction times are <30 min. for very small QDs, e.g. <3 nm, to several hours for the largest QDs, e.g. >5 nm, and are strongly dependent upon the concentration of the precursor and reaction temperature⁵), the temperature was dropped to ~180 °C and the particles were annealed for ~24 h. The temperature was decreased to 60 °C and anhydrous methanol (200 mL) was added to flocculate the QDs. Following centrifugation, the colorless supernatant was discarded. The QDs were dissolved in minimal CHCl₃ and then re-flocculated with methanol and the process was repeated once more to remove elementals, other reaction by-products, and excess HDA. The CdSe QDs coated with HDA (CdSe-HDA) were dried under reduced pressure to obtain a free flowing powder that is soluble in a variety of organic solvents (e.g. chloroform, hexanes, and toluene). QDs isolated as powders were stored under argon in the dark. Alternatively, isolated QDs can be dissolved in a ~0.1 M solution of HDA in hexanes or toluene and stored under argon in the dark. Maintaining the QDs in an environment of excess surface ligand ensures that the surface coating remains complete.

For long term storage (months to years), the reaction mixture is allowed to cool to room temperature and solidify without addition of methanol and the unpurified QDs are stored in the protective plug of HDA. QDs stored in this way can be isolated by dissolving in minimal chloroform and flocculating with methanol as described above. This procedure routinely gives CdSe-HDA QDs with PL quantum yields of 1-10 %.

The size and concentration of the QDs was estimated based on the peak position and intensity of the 1S absorbance transition, and correlation with reported QD sizing curves⁹ and the size dependent extinction coefficient¹⁰ of this transition.

b) “Hot Injection” Route for CdSe QDs

The CdSe QDs coated with a mixture of hexadecylamine (HDA), trioctylphosphine (TOP), and trioctylphosphine oxide (TOPO) ligands were synthesized and isolated according to published procedures based on the decomposition of dimethylcadmium (Me_2Cd) and trioctylphosphine selenide (TOP-Se) precursors.¹¹ One detailed preparation is described here.

The ratio of coordinating ligands was 20-40-40 mol % TOP-TOPO-HDA. TOPO (9.01 g, 23.3 mmol) was heated at 180 °C under reduced pressure for 2 h in a 50 mL 3 neck round bottom flask. After cooling to ~60 °C under argon flow, HDA (5.63 g, 23.3 mmol) was added and the mixture was heated at 120 °C under reduced pressure for 1 h more to remove traces of $\text{O}_2/\text{H}_2\text{O}$. The mixture was then returned to argon flow and heated slowly to 330 °C at which point, the heating mantle was removed. When the temperature reached 300 °C, a mixture of Me_2Cd (0.172 g, 1.2 mmol) and TOP-Se (3 mL, 2.0 M) diluted with TOP (2 mL, 4.5 mmol) was quickly injected from a gas-tight syringe with high speed stirring. Once the temperature stabilized (~150 °C), the heating was restored and the temperature of the vigorously stirred mixture was raised to ~225 °C. The reaction was monitored over the course of the growth by periodically removing a small

aliquot (~100 μL) and following changes in the absorbance spectrum. After 25 min., the mixture was cooled to ~60 °C and the CdSe cores were flocculated by addition of 2 volume equivalents of methanol. Following centrifugation and removal of the supernatant, the CdSe cores were dissolved in minimal hexanes (~20 mL) and centrifuged to remove insoluble by-products of the reaction. After re-flocculating with methanol, the CdSe cores were washed with another equivalent of methanol and then dried under reduced pressure. Purified QDs are dissolved in a solution of ~0.1 M HDA in hexanes and stored under argon in the dark. Based on the known parameters, this preparation gave ~2.4 μmol^{10} of CdSe cores with a narrow PL (FWHM = 29 nm) centered at 555 nm. Based on previous studies⁹ this indicates that these CdSe core quantum dots have diameters of ~3.8 nm. The photoluminescence quantum yield for these QDs was determined to be 11 %.

ii. Growth of a Zinc Sulfide (ZnS) shell to give CdSe/ZnS Core/Shell QDs

a) Slow Addition Method using Diethylzinc and Hexamethyldisilathiane

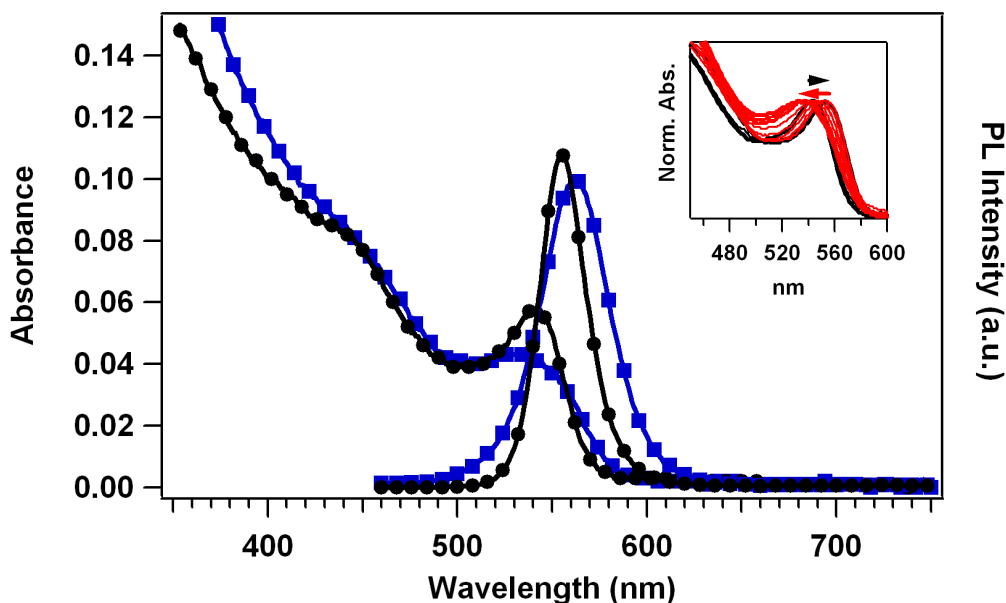
A zinc sulfide (ZnS) shell was grown around the CdSe cores using established procedures described briefly here.¹² The amounts of zinc and sulfur precursors necessary to obtain a shell of 6 monolayers were calculated based on the volume ratio of a spherical shell and a spherical core using the bulk lattice parameters of

CdSe and ZnS. What follows is a preparation for growth of a shell of 6 monolayers of ZnS over the 3.8 nm CdSe cores obtained from the “hot injection” procedure described above.

TOPO (12.5 g, 32.3 mmol) was heated at 190 °C under reduced pressure for 2 h. After cooling to 60 °C, TOP (1.22 mL, 2.7 mmol) and the CdSe cores described in the previous section dissolved in hexanes (5 mL, 0.12 mM) were added under argon flow. The mixture was carefully returned to vacuum and heated at 100 °C under reduced pressure for 1 h to remove volatiles and residual O₂/H₂O. Following this procedure, the mixture was returned to argon flow and heated to 170 °C for the shell growth. Meanwhile, a mixture of diethyl zinc (355 μL, 3.5 mmol) and hexamethyldisilathiane (730 μL, 3.5 mmol) in TOP (7 mL, 15.7 mmol) was loaded into a gas tight syringe and transferred to a syringe pump. When the core mixture temperature had stabilized, the shell precursor solution was added drop-wise under vigorous stirring over the course of ~10 min.. Once the injection was complete, the temperature was lowered to ~90 °C and the core/shell QDs were allowed to anneal for 2 h. The temperature was then lowered to 70 °C and 10 mL of argon-sparged 1-butanol was added to prevent solidification of the TOPO upon further cooling. These core/shell QDs were stored in the dark in their growth mixture. Isolation/purification was affected by flocculation of the QDs with four volume equivalents of methanol. Following removal of the colorless supernatant, the QDs were washed (2x) with methanol and dried under reduced pressure. This synthesis gives core/shell QDs with a

photoluminescence band centered at 561 nm (FWHM = 45 nm) and a quantum yield of ~15 % (Figure 2.2).

Figure 2.2. Comparison of the optical properties (absorbance and PL) of 3.8 nm core CdSe QDs (black circles) grown by the hot injection route and the corresponding CdSe/ZnS core/shell QDs (blue squares) grown via the slow addition of organometallic shell precursors. Inset: Absorbance of “out-of-batch” aliquots diluted in hexanes removed during shell growth to monitor progression of the 1S transition.



Typically, as a shell of ZnS is grown over the CdSe cores, the absorption of the 1S transition is observed to red shift at first, consistent with the increase in particle size. This is due to incomplete confinement of the exciton wavefunction within the core by the initial thin ZnS shell.¹² For thicker layers, the shift becomes negligible. In addition, the spectra typically broaden due to heterogeneous shell growth resulting in an increase in the particle size distribution.¹² However, somewhat unusual behavior was observed during the above described 6 ML shell growth. Namely, although an initial red shift (~10 nm) is observed for the growth of the first ~2 ML (black curves in the inset of

Figure 2.2), the growth of the remaining shell results in a blue shift accompanied by a large broadening of the 1S transition. It is unclear what caused the latter effect. The observed changes could be caused a large increase in polydispersity of the QDs that favors smaller particles with higher energy transitions. Alternatively, some alloying between the ZnS and CdSe may occur, a scenario which would also result in blue shifting due to the higher band gap of the added ZnS material; this phenomenon was not further investigated.

b) Growth of ZnS shell via Successive Ion Layer Adsorption and Reaction (SILAR)

This synthetic method is based on previously published procedures with slight modifications.¹³

◆ Zinc and Sulfur Precursor Solutions

Zinc and sulfur precursor solutions were made based on a literature protocol.^{13b} Briefly, for a 0.1 M zinc solution, ZnO (0.2034 g, 2.500 mmol) was mixed with oleic acid (6.18 g) in 1-octadecene (18.0 mL) and heated to ~300 °C under argon until the solution became homogeneous. A 0.1 M sulfur solution was prepared by dissolving elemental sulfur (0.0802 g, 2.501 mmol) in 1-octadecene (25.0 mL) at ~180 °C under argon. The zinc solution was cooled to 80 °C and the sulfur solution was cooled to room temperature. Both solutions were prepared immediately prior to the ZnS shell growth.

◆ Growth of ZnS shells via SILAR

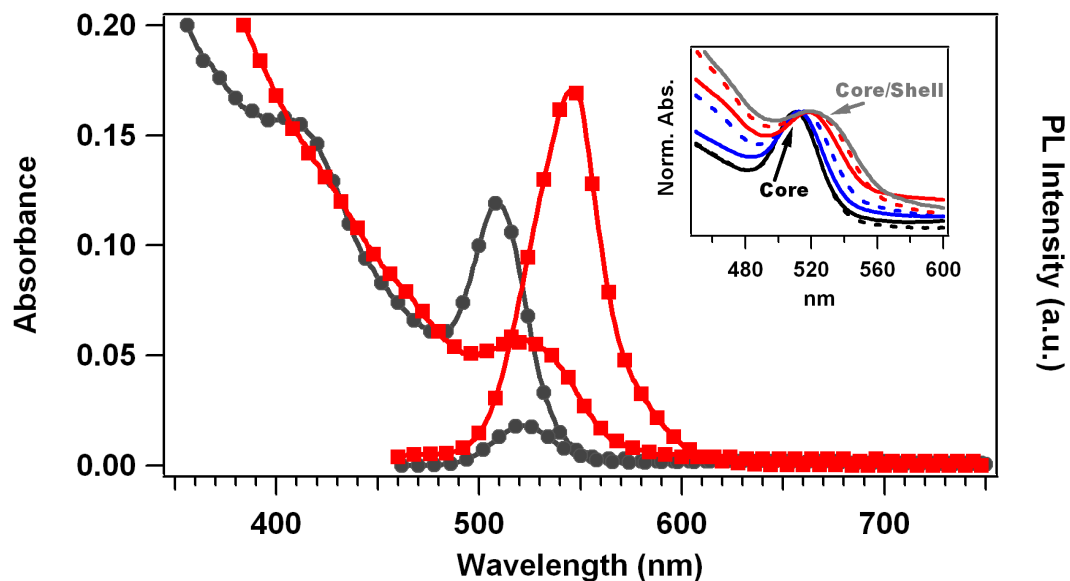
The following is a detailed method for use of the SILAR technique to grow 2 monolayers (ML) of ZnS shells over 3.0 nm CdSe-HDA cores obtained using the single source precursor route described above.

1-Octadecene (3.0 mL) and hexadecylamine (HDA) (1.00 g) were mixed together in a 3 neck round bottom flask and heated under vacuum at 100 °C for one hour to remove water and oxygen and then cooled to room temperature. A solution of 3.0 nm CdSe-HDA cores (1.83 nmol) in hexanes was added and the mixture was evacuated carefully first at room temperature, and then at 100 °C for 30 min. more to remove hexanes and any other low boiling impurities. The mixture was returned to argon flow and heated to 240 °C for the shell growth. Shell precursor injection amounts were determined for quantitative growth of 2 monolayers of ZnS over 3 nm cores based on the known lattice parameters of ZnS. Fast injections (< 1 s) were made under argon in the order Zn followed by S, repeat, for a total of 4 injections. The solution is allowed to stir for 10 min. in between injections and an aliquot (~100 µL) to monitor the absorbance spectrum. The injection amounts are as follows: 220 µL each zinc and sulfur precursors for 1st ML, 260 µL for the 2nd ML. After the last injection, the solution is allowed to stir for another 30 min. at 240 °C, and then cooled to room temperature. The core/shell QDs are purified following the extraction method of Li *et al.*^{13a} Hexanes (5 mL) was added and the diluted reaction mixture was extracted with methanol (10 mL, 2x). The QDs remained in the hexanes layer. Acetone (10 mL) was added to precipitate the QDs and remove excess amine. After centrifugation

and removal of the colorless supernatant, the purified product was dried under argon flow. The dry powder was dissolved in hexanes and any insoluble materials were removed by centrifugation, followed by passing the solution through a 0.4 μm syringe filter. The CdSe/ZnS QDs were stored in hexanes in the dark for future use. The PL quantum yield for these QDs was 80%.

Large scale shell growth. The above synthesis was scaled up for shell growth on 1.72 μmol of 3.0 nm CdSe-HDA cores with similar results.

Figure 2.3. Optical properties (absorbance and PL) of 3.0 nm CdSe-HDA cores (grey circles) and corresponding CdSe/ZnS core/shell QDs (red squares) shelled via SILAR. Inset: Absorbance of “out-of-batch” aliquots diluted in hexanes following each injection and following sample annealing, demonstrating red shift and broadening of 1S transition (red tail in the later injections is due to a scattering edge from particulates in the samples.)



iii. QD Surface Ligand Exchange to Give Water Soluble QDs

a) Mercaptopropionic Acid Coated CdSe (CdSe-MPA)

CdSe-HDA QDs (0.540 g) was suspended in dimethylformamide (10 mL) with light sonication. To this suspension, an excess of mercaptopropionic acid (10 mL) was added and the mixture is heated with stirring at 70 °C for 1 hour under argon, during which time the mixture becomes homogeneous indicating surface exchange of the HDA for the thiol group has occurred. The solvent is reduced by approx. 2/3 under reduced pressure during which time the mixture becomes cloudy. Methanol (5 mL) was added to induce complete precipitation. Following centrifugation and disposal of the colorless supernatant, the procedure was repeated a second time to ensure complete recapping of the surface. The solid was washed with methanol (~5x) to remove liberated HDA and excess mercaptopropionic acid. The orange powder was dried *in vacuo*. Yield 0.465 g.

The CdSe-MPA QDs can then be dissolved in water following deprotonation of the carboxylic acid tail groups. This was accomplished by suspending the CdSe-MPA in DI H₂O and raising the pH to above 11 with tetramethylammonium hydroxide. Following this step, the CdSe-MPA QDs are soluble in mildly basic (pH > 7) aqueous solution. Although negligible changes were seen in the absorbance spectrum following surface exchange with MPA, the PL was almost completely quenched. ¹³C CPMAS Solid State NMR { δ in ppm}: 27 (1C, α -C), 40 (1C, β -C), 129 (*m,p*-thiophenol), 134 (*o*-thiophenol), 182 (COO⁻). IR (KBr) {cm⁻¹}: 1710 (C=O).

b) Dihydrolipoic Acid coated CdSe/ZnS core/shell QDs

◆ Preparation of Dihydrolipoic Acid (DHLA).

This compound was synthesized based on previously reported procedures.¹⁴ A solution of DL-thioctic acid (also known as lipoic acid) (1.000 g, 4.85 mmol) in NaHCO₃ (0.25 M, 20.0 mL) was cooled to 0 °C. To this vigorously stirred solution was added 4 equivalents of sodium borohydride (0.7340 g, 19.4 mmol) in small portions over the course of 30 min.. The solution was then sparged with argon (ca. 10 min) and allowed to stir at 0 °C for a total of 4 h. The solution was then acidified to pH = 1 with HCl (6M), and extracted with toluene (3 x 6 mL). The combined organic fractions were dried over MgSO₄, and filtered. Removal of the solvent under reduced pressure yielded the product as a colorless oil. Yield 0.88 g (87%).

◆ DHLA coated CdSe/ZnS QDs

The initial HDA/TOP/TOPO capping groups can be exchanged for DHLA (freshly prepared by the reduction of lipoic acid with sodium borohydride)¹⁴ according to published procedures with slight modifications.¹⁵ In order to accomplish this, DHLA (20 mg, 96 μmoles) was dissolved in methanol (15 mL) and the pH was adjusted to ~12 with tetramethylammonium hydroxide in order to deprotonate the carboxylic acid functionality. The solution was sparged with argon to remove O₂ and dried CdSe/ZnS QDs (10 mg, 16 nmol) were added under subdued light to form a suspension. The mixture was then stirred at reflux under

argon overnight during which time, the mixture became homogeneous indicating that the DHLA thiol-groups had displaced the original hydrophobic capping groups and solubility in the methanol was imparted by the new anionic DHLA coating. After cooling to room temperature, the QDs were flocculated using four volume equivalents of diethyl ether and centrifuged. The QDs were re-dissolved in minimal methanol and flocculated once more with diethyl ether and centrifuged. After drying under reduced pressure, the QDs were dissolved in phosphate buffer (15 mM, pH 8.2) and purified using 3 cycles of concentration/dilution (10:1) with phosphate buffer (15 mM, pH 8.2) in a centrifugal filtration device (Millipore, M_w cutoff $\sim 10,000$ daltons) to give a final concentrated stock solution. Following purification, the DHLA capped core/shell QDs had a PL quantum yield of 2-10 % in phosphate buffered solution (15 mM, pH 8.2). Again, the absorbance spectrum of the core/shell QDs remained unchanged following surface exchange with DHLA. Although the PL was quenched somewhat, these DHLA coated core/shell QDs typically had PL quantum yields of ~ 2 % in phosphate buffered solution (15 mM, pH 8.2). Furthermore, concentrated aqueous solutions (2- 50 μM) of DHLA coated core/shell QDs were stable for at least several months.

iv. Preparation of Silica based Sol-Gels Embedded with CdSe-HDA.

a) A general preparation follows for CdSe-HDA (2.5-6.5 nm).

CdSe-HDA (0.005g; ~30 nmol) was suspended in 3-aminopropyltrimethoxysilane (APS) (5 mL; 30 mmol). The mixture was sonicated for 15 min. to affect complete dissolution of the particles. Any undissolved material was removed by centrifugation. Deionized H₂O (0.6 mL; 30 mmol) was added to initiate hydrolysis and the mixture was sonicated for 25 min.. The viscous solution was cast into a 1" diameter Teflon mold. The sol-gel was allowed to form over the course of 3-4 days on the benchtop. The partially dried samples were carefully removed from the molds and transferred to a vacuum oven. Evacuation of the sols at room temperature for 6 days removed virtually all residual moisture and alcohol by-products as assessed by thermogravimetric analysis (TGA). The resultant dried circular (~1" diameter, ~3 mm thick) sols are optically transparent and maintain the optical spectra (absorbance and PL) observed for the embedded CdSe-HDA in solution. TGA (% mass loss): prior to vacuum treatment – 20%, after 6 days dynamic vacuum - <2%.

v. *Simple Chromium(III) Cyclam Complexes*

a) ***Trans*-[Chromium(III) (1,4,8,11-tetraazacyclotetradecane)Cl₂]Cl,
trans-[Cr(cyclam)Cl₂]Cl (1)**

The *trans*-[Cr(cyclam)Cl₂]Cl was supplied by Ryan O. Absalonson whom prepared it by a procedure reported by Bakac and Espenson.¹⁶ Yield: 74 %. UV-Vis (H₂O) { λ_{\max} in nm (ϵ in M⁻¹ cm⁻¹)}: 368 (27.1), 404sh (24.3), 570 (16.9).

b) ***Trans*-[Chromium(III) (1,4,8,11-tetraazacyclotetradecane)(ONO)₂]BF₄,
[Cr(cyclam)(ONO)₂]BF₄ (2) *trans*-**

The *trans*-[Cr(cyclam)(ONO)₂]BF₄ was supplied by Ryan O. Absalonson whom prepared it by a procedure that has been reported by DeLeo *et al.*¹⁷ Yield: 60%. UV-Vis (H₂O) { λ_{\max} in nm (ϵ in M⁻¹ cm⁻¹)}: 340 (245.5), 476 (32).

vi. *C-Substituted Cyclam Complexes*

a) **Nickel (II) Complexes and Free Ligand**

◆ **α -bromo- α' -hydroxy-p-dimethyl benzene**

This compound was synthesized following a previously reported synthesis based on similar complexes.¹⁸ A solution of *p*-xylylene glycol (5.000 g, 36.2 mmol) in benzene (100 mL) was treated with 48 % hydrogen bromide (6.25 mL, 54.9 mmol). The resulting pale yellow mixture was heated at reflux for 30 h

using a Dean-Stark apparatus to trap water formed during the reaction. The reaction mixture was then cooled to room temperature and washed with sodium hydroxide (6 N, 50 mL), hydrochloric acid (10%, 50 mL), water (2 x 100 mL), and finally brine solution (75 mL). The organic fraction was dried with magnesium sulfate and the solvent was removed under reduced pressure, yielding a white power that was used without further purification. Yield 6.86 g (94.2 %). MS (ESI): 200 (M^+) (calcd); found 200.

♦ **[5,7-Dimethyl-1,4,8,11-tetraazacyclotetradeca-4,7-dienato-nickel(II)]NO₃, [Ni(dienato)]NO₃ (3)**

This compound was synthesized according to a previously reported procedure using NiCl₂·6H₂O in place of Ni(OAc)₂·4H₂O.^{18a,19} NiCl₂·6H₂O (5.000 g, 21.0 mmol) was dissolved in water (100 mL). To this solution was added N,N'-Bis(2-aminoethyl)-1,3-propanediamine (3.371 g, 21.0 mmol) and the mixture was heated for 15 min during which time the color changes from green to deep red-violet. 2,4-Pentanedione (4.205 g, 42.0 mmol) was added and the solution was heated at reflux for 5 h. A saturated solution of sodium nitrate is added and the pH of the solution was adjusted to ~10 by adding 6N sodium hydroxide dropwise. The solution was refrigerated following concentration to give large red platelets. Further concentration and refrigeration of the mother liquor gave more red, microcrystalline powder. The solid was washed with diethyl ether and dried under vacuum. Yield 2.950 g (42.3%). MS (ESI): 281 (M^+) (calcd), 281 (found). IR (KBr) {cm⁻¹}: 1557 (C=C), 1541 (C=N).

◆ **[5,7-Dimethyl-6-(1'-methyl-4'-(1''-hydroxymethyl)-benzyl)-1,4,8,11-tetraazacyclotetradeca-4,7-diene-nickel(II)]NO₃,Br,
[Ni(hydroxybenzylidene)]NO₃,Br (4)**

This complex was made using a previously reported procedure.^{18a, 20, 21} **3** (1.269 g, 3.69 mmol) was dispersed in absolute ethanol (25 mL). α -bromo- α' -hydroxy-p-dimethyl benzene (0.965 g, 4.80 mmol) was added and the mixture was heated at reflux for 4 h during which time a fine, yellow precipitate formed. After cooling to room temperature, the mixture was filtered and the solid was washed with ice cold absolute ethanol, followed by diethyl ether. The solid was then dried under vacuum. Yield 1.749 g (86.9%). MS (ESI); 401 ($M^{2+}-H^+$) (calcd), 401 (found). IR (KBr) {cm⁻¹}: 1668 (C=N).

◆ **[5,7-Dimethyl-6-(1'-methyl-4'-(1''-hydroxymethyl)-benzyl)-1,4,8,11-tetraazacyclotetradecane-nickel(II)](ClO₄)₂,
[Ni(hydroxybenzylcyclam)](ClO₄)₂ ([Ni(hbc)](ClO₄)₂, 5)**

This complex was made using a previously reported procedure.^{18a, 20,21} **4** (1.749 g, 3.21 mmol) was suspended in methanol (15 mL). A 15 fold excess of sodium borohydride (1.820 g, 48.2 mmol) was added to the mixture with vigorous stirring, resulting in an immediate color change of the suspension from yellow to grey/white to pink/purple with the concomitant evolution of heat and H₂ (g). The mixture was stirred for 2 h at room temperature during which time small amounts of methanol were added to counter evaporation. The methanol was removed under vacuum and the pink/purple solid was dissolved in hot water (120 mL).

The mixture was heated to boiling and filtered to remove any insoluble material. To the dark brown filtrate, a saturated solution of sodium perchlorate was added dropwise causing the precipitation of orange solid. Upon refrigeration, more orange powder precipitated. The mixture was filtered, and the orange powder was washed with ice cold water followed by diethyl ether. Yield 1.428 g (73.4%). MS (ESI): 203 (M^{2+}) (calcd), 405 ($M^{2+}-H^+$) (calcd), 203, 405 (found). IR (KBr) $\{cm^{-1}\}$: 3438 (O-H), 3210 (N-H). *Caution: Due to their potential explosion, compounds containing perchlorate must be handled with extreme care!!*

◆ **5,7-Dimethyl-6-(1'-methyl-4'-(1''-hydroxymethyl)-benzyl)-1,4,8,11-tetraazacyclotetradecane (hbc, 6)**

This compound was prepared following a previously reported procedure.^{18a, 21,22} **5** (1.378 g, 2.27 mmol) was dispersed in 75 mL water and the solution was heated to ensure homogeneity. A 30 fold excess of sodium cyanide (3.342 g, 68.1 mmol) was added yielding a cloudy white mixture. The mixture was heated at reflux for 2 h during which time, the solution slowly became a homogeneous yellow color, signaling the production of the $Ni(CN)_4^{2-}$ complex. After cooling to room temperature, the pH was adjusted to >12 with 6 M sodium hydroxide. The mixture was then extracted with chloroform (6 x 50 mL). The organic fractions were collected and dried with magnesium sulfate and the solvent was removed under reduced pressure yielding a viscous oil. Subjecting the oil to prolonged vacuum resulted in a very hygroscopic, white powder. Yield 0.595 g (75.2%). MS (ESI): 349 ($M + H^+$) (calcd), 349 (found). 1H NMR ($CDCl_3$) $\{\delta$ in ppm $\}$: 0.938 (d,

6H), 1.703 (t, 2H), 1.856 (t, 2H), 2.303-2.925 (m, 15H), 4.613 (s, 2H), 7.223 (d, 4H). ^{13}C NMR (CDCl_3) $\{\delta$ in ppm $\}$: 20.27 (2C, $-\text{CH}_3$), 29.26 (2C, β -C), 47.46 (1C, α -C), 50.06 (2C, α -C), 51.29 (2C, α -C), 52.14 (2C, α -C), 61.11 (2C, α -C), 64.77 (1C, CH_2OH), 127.10 (2C, Arom), 129.07 (2C, Arom), 138.92 (1C, Arom), 143.04 (1C, Arom). ^{13}C CPMAS (Solid State) $\{\delta$ in ppm $\}$: 21.12 (2C, $-\text{CH}_3$), 29.96 (2C, β -C), 47.50 (sh) (1C, α -C), 50.976 (2C, α -C), 54.54 (4C, α -C), 62.83 (2C, α -C), 64.51 (1C, CH_2OH), 120-135 (4C, Arom), 139.29 (1C, Arom), 144.74 (1C, Arom).

b) Chromium(III) Complexes

- ◆ **Trans-[Chromium(III) (5,7-Dimethyl-6-(1'-methyl-4'-(1''-hydroxymethyl)-benzyl)-1,4,8,11-tetraazacyclotetradecane) Cl_2] Cl , [Cr(hbc) Cl_2] Cl , 7)**

This compound was prepared according to a previously reported procedure.^{18a,21} Solid 97% $\text{CrCl}_3 \cdot 3\text{THF}$ (0.200 g, 0.518 mmol) and **6** (0.181 g, 0.519 mmol) were dissolved together in anhydrous dimethylformamide (15 mL). The purple mixture was heated at reflux for 40 min. The condenser was removed and the volume was allowed to reduce to approximately 1-2 mL. During this time, a light colored precipitate was observed to form. After cooling to room temperature, the residue was suspended in acetone and filtered. The purple solid was washed with more acetone followed by diethyl ether and the resultant powder

was dried under vacuum. Yield: 0.117 g (44.6 %). MS (ESI): 470 (M^+) (calcd), 470 (found). UV-vis (H_2O) $\{\lambda_{max}, nm\}$: 360, 430(sh), 568.

- ◆ **Trans-[Chromium(III) (5,7-Dimethyl-6-(1'-methyl-4'-(1'')-bromomethyl)-benzyl)-1,4,8,11-tetraazacyclotetradecane)Cl₂]Br, [Cr(bromobenzylcyclam)Cl₂]Cl ([Cr(bbc)Cl₂]Cl, 8)**

This compound was prepared according to a previously reported procedure.^{18a,21} **7** (0.251 g, 0.495 mmol) was suspended in 48 % HBr (10 mL) and stirred for 6 hours. The suspension was filtered through a "M" glass frit and the solid product was washed with ice cold water, followed by acetone, and finally diethyl ether. The resultant greyish-blue powder was dried under vacuum. Yield 0.254 g (84 %). MS (ESI) : 534 (M^+) (calcd), 534 (found).

- ◆ **Trans-[Chromium(III) (5,7-Dimethyl-6-(1'-methyl-4'-(1'')-aminomethyl)-benzyl)-1,4,8,11-tetraazacyclotetradecane)Cl₂]Br, [Cr(aminobenzylcyclam)Cl₂]Br ([Cr(abc)Cl₂]Br, 9) and the dimer *N*-[Bis-(Chromium(III) (5,7-Dimethyl-6-(1'-methyl-4'-(1'')methyl)-benzyl)-1,4,8,11-tetraazacyclotetradecane))amine)Cl₄]Br₂, *N*-[(Cr(benzylcyclam)Cl₂)₂NH]Br₂ (*N*-[(Cr(bc)Cl₂)₂NH]Br₂, 9a)**

Compound **9** was prepared according to a previously reported procedure^{18a,21} with slight modifications in order to separate compound **9a**. **9a** is a *previously uncharacterized* reaction by-product produced during the synthesis of **9**. **8** (0.254 g, 0.414 mmol) was suspended in degassed anhydrous acetonitrile (15 mL) under

argon yielding a bluish-pink suspension. ~30 drops of concentrated NH₄OH was added slowly to the stirring suspension. The mixture was stirred overnight under argon, during which time the blue color disappeared giving way to a pink suspension. The pink suspension is filtered through a plug of celite on filter paper yielding a purple filtrate and leaving behind a purplish colored celite plug. The solvent of the purple filtrate was removed under reduced pressure yielding mainly **9** as a pink-purple powder. Yield 0.125 g (55 %). MS (ESI) : 469 (M⁺) (calcd), found 469. UV-vis (Methanol) {λ_{max}, nm}: 383, 430(sh), 562. The purple solid trapped on the celite plug was dissolved with methanol. Removal of the solvent yielded mainly **9a** as a blue-grey powder. Yield 0.105 g (47 %). MS (ESI): 461 (M²⁺/2) (calcd), found 461. UV-vis (Methanol) {λ_{max}, nm}: 383, 430(sh), 562. *Note that 9 produced in this way always has some remaining impurity due to incomplete removal of 9a. However, 9 was used without any further purification.*

♦ **Trans-[Chromium(III) (5,7-Dimethyl-6-(1'-methyl-4'-(1''-aminomethyl)-benzyl)-1,4,8,11-tetraazacyclotetradecane)(CN)₂]ClO₄, [Cr(aminobenzylcyclam)Cl₂]ClO₄ ([Cr(abc)(CN)₂]ClO₄, 10)**

This compound was prepared based on a literature procedure for the simple cyclam analogue with several modifications.²³ A portion of **9** (0.112 g, 0.202 mmol) was dissolved in anhydrous degassed dimethylformamide (5 mL) under argon. The purple solution was heated to ~65 °C and 8 equivalents of NaCN (0.079 g, 1.616 mmol) were added. The mixture was stirred with heating for 30 min during which time the color changed from purple to peachy orange. After

cooling to room temperature, the mixture was filtered and the solvent was removed under reduced pressure. The solid was dissolved in minimal hot water to give a yellow solution and several scoops of solid NaClO₄ were added. The mixture was placed in the refrigerator overnight. The resulting yellow solid was washed with ice cold water, followed by a few drops of acetone, and finally diethyl ether. Yield 0.15 g (13 %). MS (ESI): 451 (M⁺) (calcd), found 451. UV-vis (H₂O) {λ_{max}, nm}: 332, 419. *Caution: Due to their potential explosion, compounds containing perchlorate must be handled with extreme care!!*

◆ **Trans-[Chromium (III)(5,7-Dimethyl-6-(1'-methyl-4'-(1''-(amido-6,8-dithiooctane)methyl)-benzyl)-1,4,8,11-tetraazacyclotetradecane)(Cl)₂]Br, [Cr(lipoicbenzylcyclam)Cl₂]Br ([Cr(lbc)Cl₂]Br, 11)**

A portion of **9** (0.0224 g, 0.0407 mmol) was mixed with lipoic acid (0.0084 g, 0.0407 mmol) and dimethylaminopyridine (0.0015 g, 0.01221 mmol) in anhydrous methylene chloride (8.0 mL). The resultant suspension was sparged with argon (ca. 5 min) and cooled to 0 °C. A solution of dicyclohexylcarbodiimide (0.0092, 0.0448 mmol) in anhydrous methylene chloride (2.0 mL) was slowly added and the mixture was stirred for 1 h at 0 °C, and 18 h at room temperature. The mixture was filtered and the purple solid was washed with dichloromethane and ether. *Crude product* yield 0.012 g (40%). MS (ESI): 657 (M⁺) (calcd.), found 657. UV-vis (MeOH) {λ_{max}, nm (ε, M⁻¹cm⁻¹)}: 334(sh) (38.8), 378 (53.1), 430(sh) (31.0), 560 (21.8), 578(sh) (21.1).

- ◆ **Trans-[Chromium (III)(5,7-Dimethyl-6-(1'-methyl-4'-(1''-(amido-6,8-dimercaptooctane)methyl)-benzyl)-1,4,8,11-tetraazacyclotetradecane)(Cl)₂]Br,**
[Cr(dihydrolipoicbenzylcyclam)Cl₂]Br ([Cr(dhlbc)Cl₂]Br, 12)

A portion of **9** (0.0449 g, 0.082 mmol) was mixed with dihydrolipoic acid (0.017 g, 0.082 mmol) and dimethylaminopyradine (0.003 g, 0.025 mmol) in anhydrous methylene chloride (16.0 mL). The resultant suspension was sparged with argon (ca. 8 min) and cooled to 0 °C. A solution of dicyclohexylcarbodiimide (0.0186 g, 0.090 mmol) in anhydrous, argon sparged (ca. 5 min) methylene chloride (4.0 mL) was slowly added and the mixture was stirred for 1 h at 0 °C, and 18 h at room temperature. The mixture was filtered and the blue-purple solid was washed with dichloromethane and ether. Crude product yield 0.0348 g (57%). MS (ESI): 659 (M⁺) (calcd.), 659 (found).

vii. Coupling Reactions of QDs and Various Cyclam Complexes

a) Reactions of CdSe-MPA with Compounds 6 and 7

- ◆ **Coupling of hbc (6) to CdSe-MPA**

CdSe-MPA (0.100 g, 8.16×10^{-7} mol) was suspended in anhydrous degassed dimethylformamide (10 mL) under argon. To this suspension, a catalytic amount of dimethylaminopyridine (0.005g, 4.09×10^{-5} mol), and 200 equivalents of hydroxybenzotriazole (0.022 g, 1.63×10^{-4} mol) were added, and the mixture was cooled to 0 °C in subdued light. Dicyclohexylcarbodiimide (0.034g, 1.63×10^{-4}

mol) was added and the mixture was stirred for 10 min.. **6** (0.057g, 1.63×10^{-4} mol) was then added and the solution was stirred for 3 h at 0 °C, and then stirred for 40 h at room temperature in subdued light. Centrifugation of the mixture gives a pale yellow supernatant and an orange powder. The powder was washed with dichloromethane followed by chloroform and then dried *in vacuo*. ¹³C CPMAS Solid State NMR { δ in ppm}: 18.12 (α -C, Free thiol), 27.01 (α -C, surface bound thiol), 35-55 (β -C), 58-65 (β -C), 120-138 (Arom), 139-145 (Arom), 173 {sh} (-COO- ester), 181.24 (-COO⁻).

◆ **Coupling of [Cr(hbc)Cl₂]Cl, (7) to CdSe-MPA**

CdSe-MPA (0.100 g, 8.16×10^{-7} mol) was suspended in anhydrous dimethylformamide (10 mL) under argon. To this suspension, a catalytic amount of dimethylaminopyridine (0.005g, 4.09×10^{-5} mol), and 200 equivalents of hydroxybenzyltriazole (0.022 g, 1.63×10^{-4} mol) were added, and the mixture was cooled to 0 °C in subdued light. Dicyclohexylcarbodiimide (0.034g, 1.63×10^{-4} mol) was added and the mixture was stirred for 10 min. **7** (0.083g, 1.63×10^{-4} mol) was then added and the solution was stirred for 3 h at 0 °C, and then stirred for 5 days at room temperature in subdued light. Centrifugation of the mixture gives a pale purple supernatant and an orange powder. The powder was washed with dichloromethane followed by water and then dried *in vacuo*.

◆ **Conjugation of DHLA coated CdSe/ZnS QDs with Cr(abc)Cl₂⁺**

General Procedure for Coupling DHLA Coated QDs to R-NH₂

QDs were diluted in phosphate buffered solution (15 mM, pH 7.4) to various final concentrations (0.01 to 1.0 μM) at room temperature under subdued light conditions. An excess of primary amine containing compound (R-NH_2) was then added to the QD solution. A concentrated stock solution of 1-ethyl-3-(3-dimethylaminopropyl) carbodiimide (EDC) in water was freshly prepared and an aliquot of this was immediately injected into the QD/ R-NH_2 reaction mixture to give a final large excess of EDC with respect to the number of QD surface carboxyl- groups. The reaction mixture was then gently stirred in the dark for typically 1-2 h. At this point, any sedimented material was removed by centrifugation and/or filtration through a 0.2 μm syringe filter, and the soluble fraction was purified by 2-3 cycles of concentration/dilution (10:1) with phosphate buffer (15mM, pH 8.2) in a centrifugal filtration device (Millipore, M_w cutoff \sim 10,000 daltons). *See Chapter III for experimental details and analysis.*

C. References

1. Demas, J. N.; Crosby, G. A. *J. Phys. Chem.* **1971**, *75*, 991-1024.
2. Caspar, J. V.; Meyer, T. J. *J. Am. Chem. Soc.* **1983**, *105*, 5583-5590.
3. O'Connor, D. V.; Phillips, D. *Time Correlated Single Photon Counting*; Academic Press, London, U. K., **1984**.
4. Klimov, V.I.; McBranch, D.W. *Optics Letters* **1998**, *23*, 277-279
5. Webb, W.W.; Xu, C., *J. Opt. Soc. Am. B* **1996**, *13*, 481-491.
6. Dance, I. G.; Choy, A.; Scudder, M. *J. Am. Chem. Soc.* **1983**, *106*, 6285-6295.
7. Cumberland, S. L.; Hanif, K. M.; Javier, A.; Khitrov, G. A.; Strouse, G. F.; Woessner, S. M.; Yun, C. S. *Chem. Mater.* **2002**, *14*, 1576-1584.
8. Klimov, V. I.; McBranch, D. W.; Leatherdale, C. A.; Bawendi, M. G. *Phys. Rev. B* **1999**, *60*, 13740-13749.
9. Mikulec, F. V.; Kuno, M.; Bennati, M.; Hall, D. A.; Griffin, R. G.; Bawendi, M. G. *J. Am. Chem. Soc.* **2000**, *122*, 2532-2540.
10. Yu, W. W.; Qu, L.; Guo, W.; Peng, X. *Chem. Mater.* **2003**, *15*, 2854-2860.
11. (a) Murray, C. B.; Norris, D. J.; Bawendi, M. G. *J. Am. Chem. Soc.* **1993**, *115*, 8706-8715. (b) Talapin, D. V.; Rogach, a. L.; Kornowski, A.; Haase, M.; Weller, H. *Nano Lett.* **2001**, *1*, 207-211. (c) de Mello Donega, C.; Hickey, S. G.; Wuister, S.; Vanmaekelbergh, D.; Meijerink, A. *J. Phys. Chem. B* **2003**, *107*, 489-496.
12. Dabbousi, B. O.; Rodriguez-Viejo, J.; Mikulec, F. V.; Heine, J. R.; Mattoussi, H.; Ober, R.; Jensen, K. F.; Bawendi, M. G. *J. Phys. Chem. B* **1997**, *101*, 9463-9475.
13. (a) Li, J. J.; Wang, Y. A.; Guo, W.; Keay, J. C.; Mishima, T. D.; Johnson, M. B.; Peng, X. *J. Am. Chem. Soc.*, **2003**, *125*, 12567-12575. (b) Xie, R.; Kolb, U.; Li, J.; Basché, T.; Mews, A. *J. Am. Chem. Soc.*, **2005**, *127*, 7480-7488.
14. (a) Uyeda, H. T.; Medintz, I. L.; Jaiswal, J. K.; Simon, S. M.; Mattoussi, H. *J. Am. Chem. Soc.* **2005**, *127*, 3870-3878. (b) Gunsalus, I. C.; Barton, L. S.; Gruber, W. *J. Am. Chem. Soc.* **1956**, *78*, 1763-1768.
15. (a) Mattoussi, H.; Mauro, J. M.; Goldman, E. R.; Anderson, G. P.; Sundar, V. C.; Mikulec, F. V.; Bawendi, M. G. *J. Am. Chem. Soc.* **2000**, *122*, 12142-12150. (b) Cheng, C. – T.; Chen, C. – Y.; Lai, C. – W.; Liu, W. –

- H.; Pu, S. – C.; Chou, P. – T.; Chou, Y. – H.; Chiu, H. – T. *J. Mater. Chem.* **2005**, *15*, 3409 – 3414.
16. Bakac, A.; Espenson, J.H. *Inorg. Chem.* **1992**, *31*, 1108-1109.
17. De Leo; M. A.; Bu, X.; Bentow, J.; Ford, P. C. *Inorg. Chim. Acta* **2000**, *300-302*, 944-950.
18. (a) DeRosa, F., Ph.D. Dissertation, U.C. Santa Barbara, Santa Barbara, CA (**2003**). (b) Kang, S. K.; Kim, W. S.; Moon, B. H. *Synthesis* **1985**, 1161-1162.
19. Martin, J. G.; Cummings, S. C. *Inorg. Chem.* **1973**, *12*, 1477-1482.
20. De Santis, G.; Fabbrizzi, L.; Iacopino, D.; Pallavicini, P.; Perotti, A.; Poggi, A. *Inorg. Chem.* **1997**, *36*, 827-832.
21. DeRosa, F.; Bu, X.; Pohaku, K.; Ford, P.C. *Inorg. Chem.* **2005**, *44*, 4166-4174.
22. Barefield, K. *Inorg. Chem.* **1972**, *11*, 2273-2274.
23. Kane-Maguire, N. A. P.; Bennet, J. A.; Miller, P. K. *Inorg. Chim. Acta* **1983**, *76*, L123-L125.

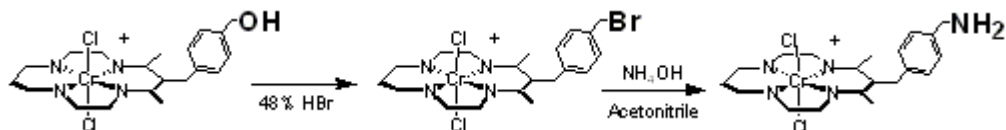
3. Chapter III. Conjugation of Various Cyclam Analogues to Quantum Dot Surfaces.

A. Introduction

As has been described elsewhere by Dr. Frank DeRosa¹, a recent graduate of the Ford Group, the “C-substituted” *trans*-chromium (III) cyclam system (cyclam is the 5,7-dimethyl-6-R-1,4,8,11-tetraazacyclotetradecane ligand, where R is a substituent on the macrocycle ring) is a versatile building block for constructing bichromophoric donor/acceptor systems. By exploiting facile Schiff base condensations, the 6 position of the cyclam ring can be modified with a variety of functional groups including *p*-hydroxymethylbenzene and anthracene (Figure 1.9). In the *trans*-chromium(III) complexes, the anthracenyl- appendage is shown to facilitate efficient non-radiative energy transfer to the metal center. This results in doublet phosphorescence from the chromium(III) at 77 K (*dichloro* analogue)^{1a} or release of nitric oxide (*dinitrito* analogue)^{1b}. Alternatively, the *p*-hydroxymethylbenzyl- derivative (hbc, **6**) provides a means to further functionalize the *trans*-chromium(III) cyclam core with molecules having potential to serve as light absorbing antenna.¹ One example is the conversion of the free hydroxyl- (-OH) group to an amino- (-NH₂) group, as in [Cr(abc)Cl₂]Br (**9**), via the bromo-intermediate (Figure 3.1). Both the hydroxyl- and amine-groups can be condensed with molecules having available carboxylic acid functionalities via carbodiimide coupling methodologies. In this way, DeRosa

was able to bind the red absorbing dye galloxyanine to the $trans$ -[Cr(abc)Cl₂]⁺ derivative, and pyrene to the $trans$ -[Cr(hbc)(ONO)₂]⁺ derivative.

Figure 3.1. Functionalized C-substituted $trans$ -chromium(III) cyclam complexes.



In this chapter, several strategies for covalent attachment of the photoactive chromium(III) cyclam complex to a QD surface are described.

B. Thiol Functionalized Cyclams for Binding to QD

Surfaces

One strategy that has been used extensively to bind molecules of interest to QD surfaces is by use of a thiol (-SH) containing linker.² The use of thiols as a linker to bind to QD surfaces has been widely exploited, resulting in the construction of a variety of QD based functional nanostructures including QDs bound to DNA^{2h,j}, a CdSe homodimer^{2a}, CdSe and gold nanoparticle assemblies^{2b}, and CdSe/molecular wire heterostructures^{2d}. In the case of CdSe QDs, the choice of thiols over other typical QD coating agents including amines is presumably due to the higher affinity of sulfur for Cd(II).^{2b,c} In fact, NMR studies by Dr. Mia Berrettini and coworkers at UCSB showed that surface exchange of amine coated CdSe with the bifunctional 2-aminoethanethiol (AET) linker resulted in preferential binding of the CdSe surface through the thiol end of AET.^{2b}

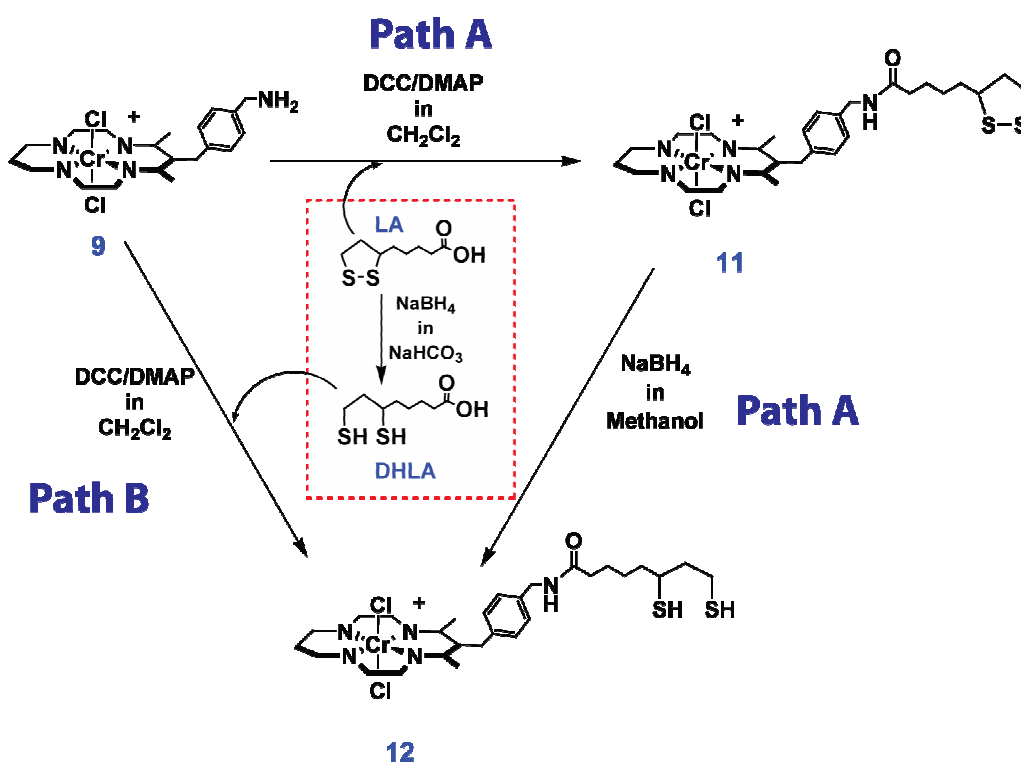
Dihydrolipoic acid (DHLA), a molecule bearing two thiol groups on one end and a carboxylic acid on the other, was chosen as the chromium (III) cyclam/QD linker based on substantial literature showing its versatility in passivation/stabilization and functionalization of nanoparticle surfaces.³ Dr. Hedi Mattoussi at the U.S. Naval Research Laboratory first reported the use of DHLA as a surface coating for CdSe/ZnS core/shell QDs in 2000.^{3a} The rationale for use of DHLA rather than other short chain mercaptocarboxylic acids was the perceived increased interaction of the dithiol with the QD surface due to the chelating effect.^{3a} In fact, Mattoussi *et al* have reported that aqueous solutions of the DHLA coated QDs are stable for periods of 1-2 years a substantial improvement over the QDs coated with unidentate thiols which are typically stable for less than a week under comparable conditions.⁴ Several other reports have demonstrated stable QD dispersions using other bidentate thiol coating ligands besides DHLA.^{2e, 6}

i. Functionalization of Chromium(III) Cyclam with Lipoic Acid

In the current study, the demonstrated ability to modify the hydroxyl- or amino- functionality of *trans*-[Cr(hbc)Cl₂]Cl (**7**) and *trans*-[Cr(abc)Cl₂]Br (**9**), respectively, via carbodiimide mediated condensation reactions with molecules bearing carboxyl (-COOH) functionalities was exploited. Carbodiimides have been popular reagents for coupling amines to carboxylic acid groups since the mid-50's.⁷ They function by reacting first with a carboxylic acid to create an activated *o*-acylisourea intermediate. The unstable intermediate is then attacked

by a nucleophile such as a primary amine, forming an amide bond and an isourea by-product. Dicyclohexylcarbodiimide (DCC) is the most popular, water insoluble cross-linking agent, and was first used in 1955 by Sheehan and Hess for peptide synthesis. It is referred to as a “zero-length cross-linker”⁷ because it does not add any atoms to the coupled product, and rather joins the two species via an amide bond. Although they are weaker nucleophiles, alcohols have also been demonstrated to undergo nucleophilic attack of activated *o*-acylisourea intermediates, leading to the analogous ester products.^{3b,8}

Figure 3.2. Potential reactions for the generation of a DHLA functionalized *trans*-chromium cyclam complex.



Recently, Dr. Harry T. Uyeda and coworkers at the NRL demonstrated that DHLA can be modified at the carboxylic acid position with a polyethylene glycol

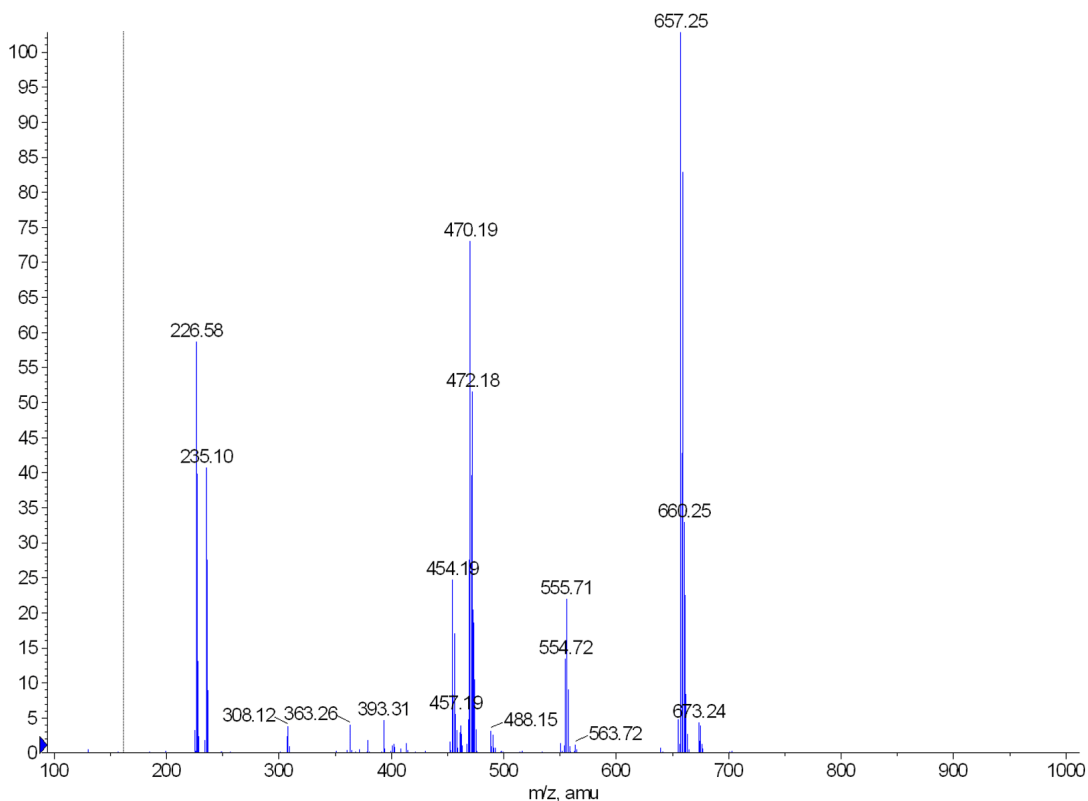
(PEG) chain via DCC mediated coupling to the terminal hydroxyl- group of PEG. QDs could then be coated with these new PEG-modified DHLA molecules or with mixtures of these and DHLA. This allows for a general methodology of modifying pendant groups in order to link various molecules to the surface of QDs using DHLA as a linker (Figure 3.2).

Based on the work by Uyeda *et al*, there are two pathways amenable to modification of the chromium(III) cyclam complexes with a DHLA molecule (Figure 3.2).^{3b} The first involves conjugation of lipoic acid (LA) (also called DL thioctic acid) to the metal complex via condensation with the hydroxyl- or amino-groups of **7** or **9** respectively. This is followed by reduction of the disulfide to yield the dithiol modified complex (Figure 3.2, Path A). The alternative pathway of initial reduction of the disulfide followed by condensation to the metal complex would also be possible (Figure 3.2, Path B), but due to the large propensity for re-oxidation of the free thiols and to the potential for side-reactions of the unprotected thiol group, the former pathway was attempted first.

Although considerable precedent exists for carbodiimide assisted condensation of carboxylic acids with hydroxyl- groups, reaction of LA with **7** using DCC as the cross-linker resulted in only partial conversion to the ester, and only over extended reaction times (>72 h). However, in the case of reaction of **9** with LA, the reaction was nearly complete within 18 h. The reaction was monitored by mass spectrometry for loss of the starting material ($M^+ = 469$) and the concomitant increase in the peak at 657 for the cation of the amide product

(Figure 3.3). When the reaction was done as a suspension of **9** in anhydrous methylene chloride, isolation of the solid product was achieved easily by filtration, with all the organic material being removed by successive washes with methylene chloride.

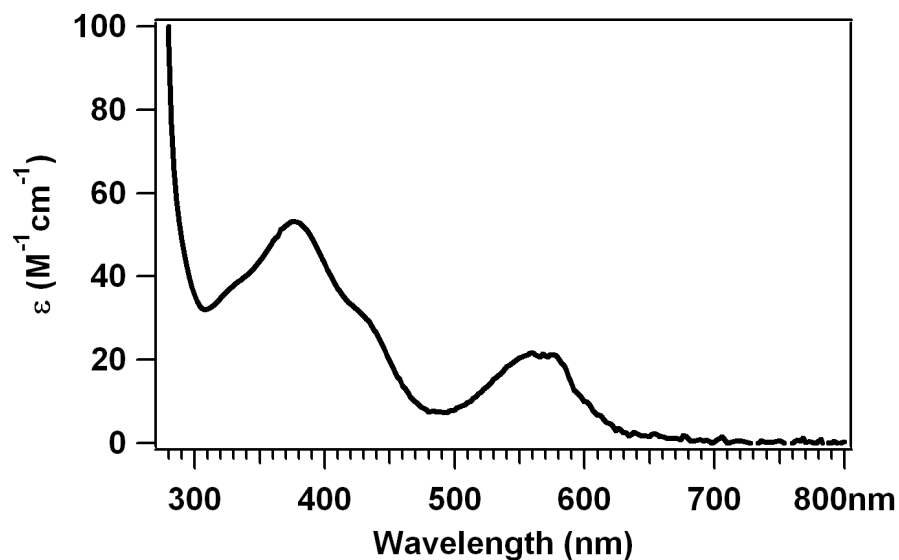
Figure 3.3. ESI (+) mass spectrum of **11**.



The UV-visible absorption spectrum of an argon sparged methanolic solution of the crude product, *trans*-[Cr(lbc)Cl₂]Br (~2 mM) (**11**), is shown Figure 3.4. The spectrum of **11** is similar, in shape, peak position and peak intensities, to that of all of its *trans*-Cr(cyclam)Cl₂ predecessors.^{1a} DeRosa demonstrated that substituents on the cyclam periphery exhibit only limited changes (with the exception of strongly absorbing organic dyes) on the ligand field transitions that

dominate the UV-visible absorbance of these complexes. This results supports the assignment of the product observed here as a *trans*- dichloro chromium(III) cyclam complex. Notably, a shoulder centered at 334 nm ($\epsilon = 38.8 \text{ M}^{-1} \text{ cm}^{-1}$) is observed that is not familiar to this family of complexes. This feature is assigned to the absorbance of the disulfide present on the newly coupled lipoic acid substituent. Indeed, the broad absorbance band in this region is frequently used to characterize disulfides,⁹ and its disappearance is often monitored during reductions to the corresponding thiols.¹⁰

Figure 3.4. UV-vis extinction spectrum of **11** in methanol.

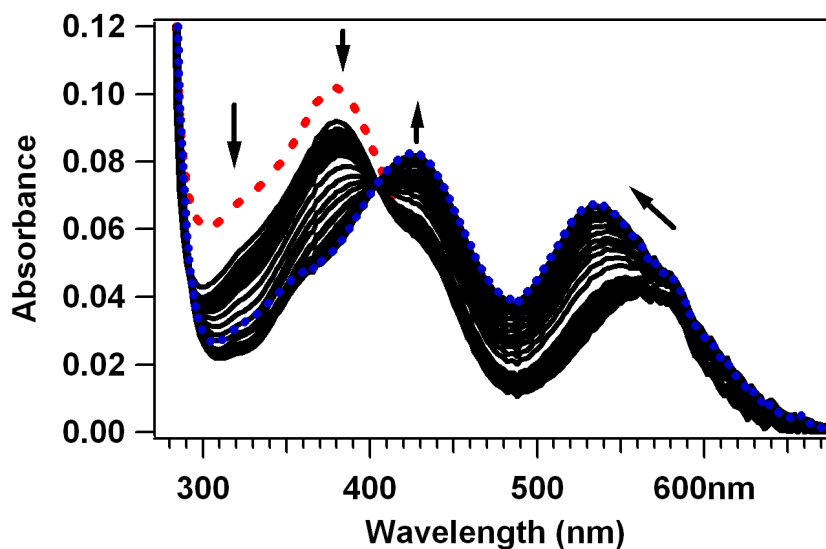


In an independent measurement, the UV-visible absorbance spectrum for a methanolic solution of α -lipoic acid was recorded. The extinction coefficient for the peak centered at 334 nm was determined to be $192 \text{ M}^{-1} \text{ cm}^{-1}$, in close agreement with that observed by others.^{9b,c} One point that should be discussed

here concerns the purity of **11**. Clearly, the intensity of the shoulder at 334 nm in the absorbance spectrum of **11** was much lower (nearly 5 fold) than what was expected for a similar concentration of lipoic acid. One possibility is that the product studied here was actually a mixture of *trans*-dichloro chromium (III) cyclam complexes, of which **11** was only one component. In fact, a close inspection of the mass spectrum of the product (Figure 3.3) indicates the presence of a cation with mass at 470, consistent with the presence of *trans*-[Cr(hbc)Cl₂]⁺. This suggests that the starting material **9** itself was still impure (Figure 3.1.). The prevalence of Cr(hbc)Cl₂⁺, residual starting material **9**, and possibly other *trans*-dichloro chromium(III) cyclam adducts would account for the observed “inflation” of the ε values for the ligand field transitions with respect to that attributed to the disulfide appendage in Figure 3.4. Although considerable effort has been undertaken in this laboratory to synthesize **9** with a higher purity, so far this goal has proven rather elusive.

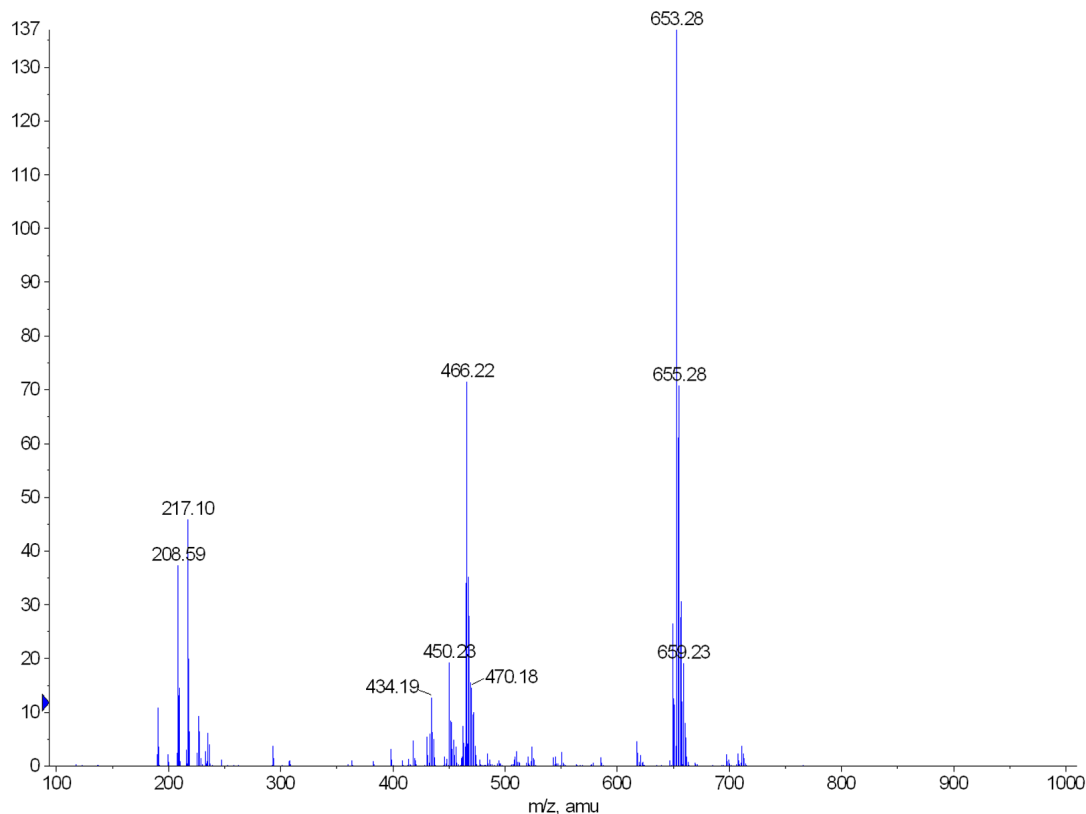
Lipoic acid is typically converted to dihydrolipoic acid via sodium borohydride reduction.¹¹ As mentioned above, this conversion can be followed by the disappearance of the transition centered at 334 nm in the UV-vis spectrum.¹⁰ In this context, the sodium borohydride reduction of **11** to generate the dithiol appended analogue was investigated using UV-visible spectroscopy as well as mass spectrometry. Figure 3.5 demonstrates the UV-vis changes that occur when the solution having the absorbance spectrum shown in Figure 3.4 was reacted with ~3.6 molar equivalents of sodium borohydride. Substantial changes in the

Figure 3.5. Absorbance spectra over the course of 170 min. reaction of **11** with 3.6 equiv. of NaBH₄ in methanol.



strength and positions of the metal centered transitions were observed consistent with a scrambling of the ligands bound to the Cr(III) center. No clear isosbestic point was evident suggesting that this was not a simple $A \rightarrow B$ reaction. The shift of the 1st quartet band (Q_1) at 560 nm to ~534 nm over the course of 140 min was consistent with an increase in ligand field strength. The Q_2 band also shifts, albeit in the reverse direction, from 378 nm to 428 nm. For comparison, in *trans*-[Cr(cyclam)(OH₂)₂]³⁺, the Q_1 and Q_2 bands were positioned at 510 nm and 408 nm, respectively.¹² Mass spectrometry analysis of aliquots over the course of the reaction showed conversion of both the parent ($M^+ = 657$) and the main impurities ([Cr(abc)Cl₂]⁺ = 469 and [Cr(hbc)Cl₂]⁺ = 470) to other chromium containing species that have lost one or more chlorides. The peaks likely associated with breakdown of the impurities were identified as [Cr^{III}(abc)Cl]²⁺ ($M^{2+}/2 = 217$) and

Figure 3.6. ESI (+) mass spectrum of an aliquot removed following 170 min. during the reduction of **11** with NaBH₄ in methanol.



[Cr^{III}(hbc)(OH)] ($M^{2+}/2 = 208.5$) (Figure 3.6). The analogous species resulting from the decomposition of the [Cr(lbc)Cl₂]⁺ cation were not observed (i.e. [Cr(lbc)Cl]²⁺ ($M^{2+}/2 = 311$) and [Cr(lbc)(OH)]²⁺ ($M^{2+}/2 = 302$)), suggesting that the fate of this complex in the presence of sodium borohydride was more complicated. Still, it was apparent that rather than only reducing the disulfide bridge which would give a cationic product with a peak at 659, sodium borohydride also affected the reduction of the Cr^{III} metal center to the more labile Cr^{II} species (Cr^{III}/Cr^{II} $E_{\text{redox}} = -0.985$ V vs. SCE¹³). The Cr^{II} quickly re-oxidizes to

Cr^{III}, likely due to residual air in the system, but not before the chloride ligands exchange with the ubiquitous solvent and residual water in the solvent.

Unfortunately sodium borohydride appears to be too strong a reductant for this system. Attempts to use other disulfide reduction reagents, such as dithiothreitol were unsuccessful. A study by Howie from the Sawyer group at UC Riverside demonstrated that lipoic acid cannot be reduced electrochemically in water.¹⁴ It can be reduced in acetonitrile, but only at very negative potentials (-1.92 V vs SCE). The electrochemical data of Howie *et al* combined with the experimental observations discussed above suggest that this protocol for construction of the thiol appended Cr(III) cyclam complex may not be compatible with the energetics of the Cr^{III}/Cr^{II} redox couple.

ii. Functionalization of Chromium Cyclam with DHLA: Surface Exchange of QDs

Based on the problems described above, the second pathway outlined by Uyeda *et al.* for preparing compounds functionalized with DHLA, namely conversion of LA to DHLA via sodium borohydride reduction followed by condensation with **9**, was pursued (Figure 3.2 Path B). Under virtually identical reaction conditions to those described above for LA, **9** can be coupled directly with DHLA using DCC as the coupling agent. After ~24 h, the mass spectrum of the reaction mixture (Figure 3.3) indicated complete disappearance of the starting material with the major product having a peak at 659, consistent with the cation of *trans*-[Cr(dhlbc)Cl₂]Br (**12**).

Before attempting to optimize the above reaction or completely purify and characterize **12**, the possibility of binding **12** to the surface of CdSe/ZnS QDs via its dithiol linker was investigated. In analogy to literature reports for surface exchange of QDs with DHLA¹⁴ or DHLA modified iridium complexes^{3e}, basic methanolic solutions of **12** alone or 1:1 molar ratio of **12** and DHLA were refluxed with CdSe/ZnS QDs coated with hydrophobic ligands. Normally, in the case of QD surface exchange with DHLA alone, the QDs are initially insoluble due to their hydrophobic coatings but dissolve over the course of the reaction indicating surface exchange with the deprotonated DHLA ligands. In either reaction conducted with **12**, even after 12 h of reflux, the QDs did not dissolve in the methanol mixture. After the solid was isolated by centrifugation, attempts to re-dissolve it in a polar solvent such as DMSO or DMF failed.

It would appear that *under the conditions used* for the surface modification of the QDs with **12** or mixtures of **12** and DHLA, the exchange was ineffective or the exchange occurred but led to modified QDs (mQDs) with poor solubility properties. There are several potential problems with the conditions used here. First of all, it is unclear whether under the highly basic conditions (pH ~12) used for the reactions, **12** retains its integrity. No controls have been conducted to date to ascertain whether the *trans*-dichloro chromium cyclams are generally stable under highly basic conditions. However, UV-vis data on the filtrates isolated from the QD surface exchange reactions described above, which are expected to contain a large excess of **12** even if exchange does take place, appear to suggest

the contrary, where the Q_1 ligand field band is red shifted from its original position at ~560 nm toward 500 nm.

Another problem is solubility. QD solubility is dictated by the solubility properties of the ligand surface coating. It is unclear what solubility, if any, mQDs having a complete coating of complexes like **12** would have. In fact data that will be presented in a later section of this chapter suggests that only a relatively low percentage of the total surface composition can be comprised of chromium complexes while still retaining mQD solubility in polar solvents. In those studies it was found that, even under low surface loading conditions, a solubility modifier such as polyethylene glycol (PEG) must be bound to the QD surface as well to maintain the solubility of mQDs. mQDs with PEG modified surfaces have been demonstrated to exhibit enhanced solubility properties in polar solvents when compared to those QDs whose solubility is governed only by the anionic component of their surface coating.^{3b} It is possible that tuning the ratio of **12** and DHLA in the surface exchange reaction may result in a final surface composition that allows the QDs to be dispersed in water, or perhaps other polar solvents. Alternatively, a mixture of **12** and the DHLA modified polyethylene glycol chains described by Uyeda *et al*^{3b} could be used. To this end, the synthesis of DHLA modified with polyethylene glycol is currently being pursued in this laboratory.

C. Surface Conjugation Reactions Between Water

Soluble QDs and Chromium (III) Cyclam Complexes

Considerable evidence shows that carbodiimide assisted condensation reactions are amenable to *direct* QD surface modification.^{2f,h 16} By *direct* is meant that one of the active molecules is already bound to the QD surface, and one performs the condensation reaction to these surface bound linkers. Indeed, QDs have been linked to a variety of biomolecules, redox active complexes and chromophores including the proteins transferrin^{2f} and lectin¹⁶ⁱ, ferrocene^{16k}, and a fluorescein derivative^{16k}, all using this simple peptide coupling chemistry. Typically a bifunctional linker such as a mercaptocarboxylic acid (HS-----COOH) is used in which the thiol end of the molecule binds directly to the surface of the QDs and the carboxyl-group imparts solubility in polar solvents such as water, and can then be further coupled with an amine or alcohol containing molecule via the standard carbodiimide assisted methodology. In this context, the following sections describe reactions of the hydroxyl- (**6** and **7**) and amine (**9** and **10**) functionalized cyclams with QDs coated with the bifunctional linkers mercaptopropionic acid (MPA) and dihydrolipoic acid (DHLA).

i. CdSe-MPA Conjugated with hbc (6) or Cr(hbc)Cl₂⁺ (7)

There have been relatively few quantitative studies so far that monitor the surface structure of QDs during ligand exchange or coupling reaction. Most commonly, changes in the optical properties and/or changes in the solubility

properties have been taken as benchmarks for a successful reaction.¹⁷ However, it is also important to characterize the nature of the coupling interaction in order to optimize the chemistry and understand the observed photochemical properties.

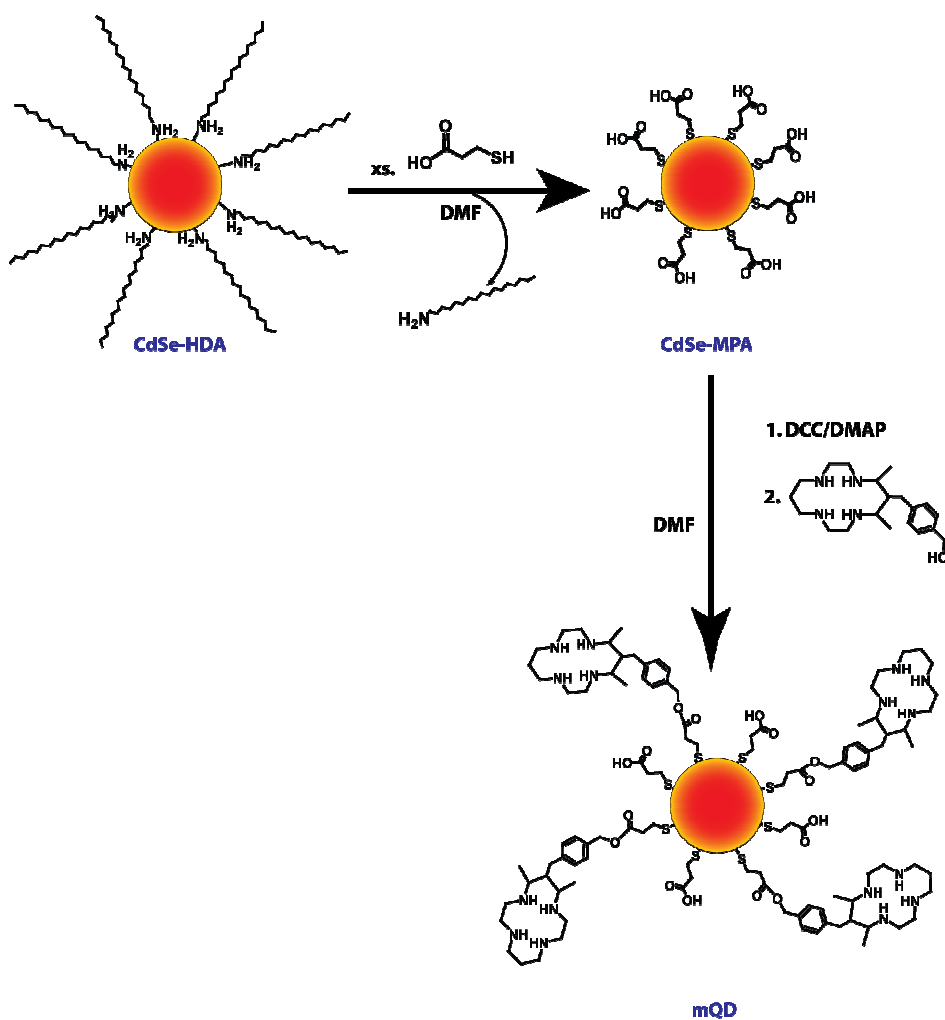
A few independent studies have shown the power of FT-NMR and FT-IR in identifying species on the surface of QDs, determining the extent of recapping procedures, and monitoring coupling reactions with functionalities on the surface. Veinot and coworkers used solution phase NMR and solid-state IR to monitor both the recapping of CdS quantum dots with 4-mercaptoaniline, and subsequent cross-coupling reactions where amide linkages were formed between the aniline amine and the carboxylic acid group of a variety of molecules.^{16k} In that study, formation of the amide bond was characterized both by the appearance of the C(O)NH resonance in the ¹H NMR spectrum, as well as by the appearance of the amide carbonyl and amide C-N stretching vibrations. More recently Berrettini *et al* demonstrated the power of solid-state NMR in a detailed study of small (~2.1 nm) CdSe quantum dots.^{2c} Using a combination of cross polarization magic angle spinning (CPMAS) and HETCOR analysis, independent study of the nanomaterial core, surface, and surface/ligand interface was possible in unprecedented detail.^{2c}

18

In the present study, solid-state IR (KBr) and solid-state NMR methods were chosen to characterize CdSe-MPA QDs and the mQDs resulting from conjugation of the CdSe-MPA QDs with **6** or **7** (Figure 3.7). It should be noted that because **7** is paramagnetic, a detailed NMR investigation of that complex is not possible.

For this reason, mQDs formed from reaction of QDs and **6**, the free cyclam analogue of **7**, were used as models.

Figure 3.7. Surface exchange and surface conjugation of CdSe QDs to form mQDs.



a) Infrared Analysis of CdSe-MPA and its Conjugates

Surface exchange of the original hydrophobic coating of CdSe-HDA with MPA gives QDs with a very strong IR band at 1710 cm^{-1} due to the carbonyl- (C=O) stretch of the carboxyl-tails of the new surface coating (Figure 3.7). The

intensity of this band was used to monitor the conjugation of **6** and **7** to the CdSe-MPA because the carboxyl- (C=O) stretch is highly sensitive to conversion of a carboxylic acid (-COOH) to an ester (-C(O)O-).

Figure 3.8. Infrared absorbance spectra of starting materials and surface conjugated mQDs in KBr. Line indicates ν_{CO} at 1710 cm^{-1} .

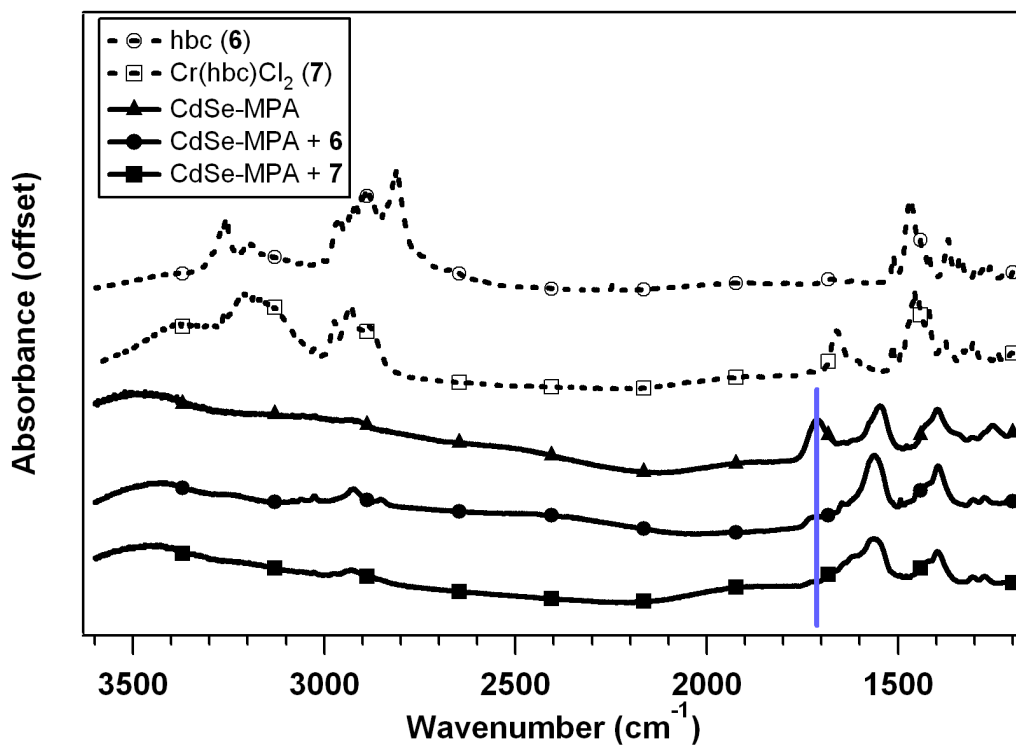


Figure 3.8 compares the IR spectra of the CdSe-MPA, **6**, and **7** starting materials with the new corresponding mQD coupling products, all prepared as concentrated KBr pellets. Prior to the IR experiment, the products were washed with dichloromethane to remove the dicyclohexylurea coupling by-product, followed by chloroform to remove any unreacted **6** and DI water to remove unreacted **7**. Clearly, a large change occurs in the ν_{CO} region for the mQD, where the strong band originally centered at 1710 cm^{-1} for the CdSe-MPA has all but

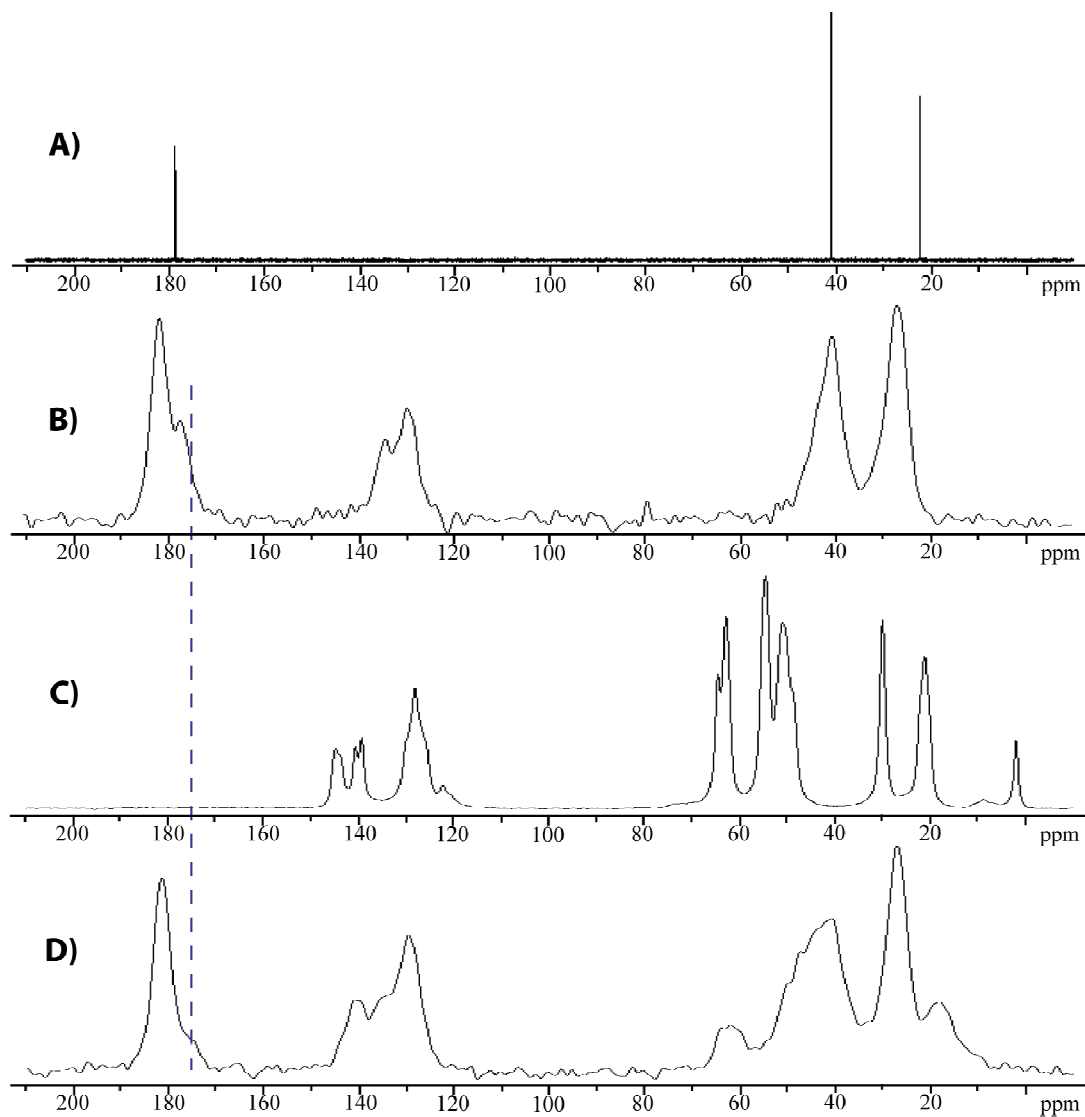
disappeared, leaving behind a shoulder shifted to higher frequency ($\sim 1725\text{ cm}^{-1}$). An ester linkage is expected to shift ν_{CO} to lower frequency if resonance is taken in to account.¹⁹ However there may be other subtle electronic and/or steric effects that effect the ν_{CO} frequency. The large drop in intensity of the original band is strong evidence of coupling in itself.

b) Solid State CPMAS NMR Analysis of CdSe-MPA and its Conjugates

NMR spectroscopy was used in order to gain further insight into the surface ligand composition of the mQD formed from the reaction of CdSe-MPA with **6**. Although CdSe-MPA is soluble in mildly basic aqueous solution, the solubility of the mQDs produced in this study is limited. Since a large signal-to-noise ratio is needed to evaluate small changes in the surface composition of mQD vs the parent QDs, solid state CPMAS ^{13}C NMR was chosen due to its proven track record in evaluating the ligand/surface interface in CdSe QD nanomaterials.^{2c} In CPMAS ^{13}C NMR, very high sensitivity and signal amplification is possible because the proton's of the sample are pulsed first, followed by polarization transfer to the near-by carbon atoms.²⁰ In addition, this technique is *non-destructive* in nature, retaining the integrity of the sample without any modification. This work was done in collaboration with Dr. Jerry G. Hu at the spectroscopy facility in the Materials Research Laboratory at UCSB.

The CPMAS ^{13}C NMR spectrum of CdSe-MPA is shown in Figure 3.9B. The spectrum shown for CdSe-MPA is that obtained for the material following

Figure 3.9. Solid state CPMAS ^{13}C NMR spectra of B) CdSe-MPA, C) hbc (**6**), and D) mQD coupling product of CdSe-MPA and **6**. Dashed line indicates shoulder at 170-175 ppm assigned to the ester product in D). The spectrum in A) is a ^{13}C NMR of the QD ligand MPA in CDCl_3 .



successive washes with dichloromethane (15x), chloroform (15x), and distilled water (4x). The peak observed at 27 ppm for the α -carbon of surface bound mercaptopropionic acid was consistent with data obtained previously for thiols bound to CdSe QDs. The shift from that of the α -carbon of free MPA (22 ppm) (A in Figure 3.9) was indicative of a relatively strong binding interaction between

the thiol and the QD surface, presumably via backbonding to a cadmium atom.^{2b,c} The β -carbon (~40 ppm) appeared in the same place in both bound and unbound moieties and the carboxyl carbon (C=O) appeared at 181 ppm. Unfortunately, an unknown impurity was observed at 177 ppm in the CdSe-MPA starting material. An obvious impurity that would have a carbon whose chemical shift lies in this region would be the carbonyl- carbon of free (unbound) MPA. The absence of any peak (sharp or otherwise) below 27 ppm for CdSe-MPA precluded the assignment of the impurity to free MPA. One possibility was residual dimethylformamide (DMF) from the synthesis, although the carbonyl- carbon peak lies ~15 ppm upfield at 162 ppm in solution. Unfortunately, the inability to remove (by purification) or assign the peak at 177 ppm hampered the later analysis of the mQD product.

Rather unexpectedly, a broad feature between 120-140 ppm was clearly resolved in the spectrum of CdSe-MPA. This feature was assigned to surface bound thiophenol. Previous NMR studies of CdSe QDs synthesized using the $\text{Li}_4[\text{Cd}_{10}\text{Se}_4(\text{SPh})_{16}]$ “single-source” precursor demonstrated that although HDA outnumbered the thiophenol (-SPh) by a molar ratio of roughly 30:1 in a typical synthesis, analysis of these QDs *post-synthesis* indicated a considerable amount of surface bound thiophenol located at special binding sites associated with selenium vacancies.^{2c, 18} Interestingly, where-as *post-synthesis* surface ligand exchange with excess HDA or pyridine were unsuccessful at removing the thiophenol, exchange with AET proceeded to completion.^{2b, 19} Apparently, under the

conditions used here for ligand exchange with MPA, only the HDA was completely replaced, with at least some portion of original thiophenol remaining.

The NMR spectrum of the mQD conjugates of CdSe-MPA and **6** is shown in Figure 3.9D. A qualitative conclusion is that the spectrum of the coupled product is simply a superposition of the carbon signatures of the two reactants (B and C). Similar to IR study described above, a washing procedure (dichloromethane, chloroform, and DI water) was used for this sample prior to analysis. Based on mass spectroscopy data obtained for the final washes in each solvent, no residual **6** remained in this sample, and the signatures from **6** in Figure 3.9 represent cyclam bound to the QD surface. Notably there no longer was a peak at 177 ppm (presumably, the impurity did not carry over through the steps of cross-linking and further washing) and a shoulder was clearly resolved at 170-175 ppm. Typically, carbonyl carbons of ester groups display a peak at 173 ppm.¹⁹ Depending on the extent of substitution, a new peak was expected to grow in this region. Thus, the signals attributed to carbons on **6**, combined with the significant signal at 170-175 ppm, demonstrated the effective conjugation of the free cyclam, **6**, to the QD surface via condensation and ester-bond formation with the surface bound MPA carboxylic acid group. Based on this result and the similarity in the IR spectra for the mQDs with **6** and **7**, an analogous conclusion was drawn for the reaction of CdSe-MPA and **7**.

c) Conclusions/Summary

The NMR and IR data presented above for mQDs with **6** and **7** suggested that the carbodiimide assisted conjugation of chromium(III) cyclam derivatives to the QD surface is possible. However, based on the literature reports of the potential instability of related materials, it became clear that a new strategy would be necessary. As mentioned earlier, a variety of reports document the instability of QDs coated with monodentate thiols.^{2e, 4, 5} Recent work has shown that the interaction between monodentate ligands in general and CdSe QD surfaces is dynamic. Two independent studies showed that high percentages (in some cases >70%) thioglycerol²¹ and pyridine²² ligands are lost during drying of thin films made up of CdSe QDs coated with these ligands. Gregory Kahlyuzhny and Royce W. Murray at UNC used NMR methods to measure the amount and identity of free ligand and other monomeric species in solution as a function of purification and dilution of small (2.0-2.3 nm) CdSe QDs passivated with trioctylphosphine (TOP) and trioctylphosphine oxide (TOPO).²³ Their findings indicate that continued removal of excess ligand from the environment of dissolved QDs, either by purification or dilution, results in continued loss of surface ligands. This effect is clearly indicated by large increases in surface defect photoluminescence.

An additional disadvantage exists specifically in the use of thiol ligands for core only CdSe QDs, especially with the intention of conducting photochemical studies as is proposed in this dissertation. A study of CdSe QDs passivated with a variety of thiol ligands demonstrated that these materials decompose in the

presence of light because the CdSe QDs catalyze the photo-oxidation of the surface bound thiols, leading to eventual ligand loss and particle precipitation.²⁴

The function of the CdSe in this process is to accept an electron from the surface thiol upon photoexcitation of an electron into the conduction band, a process also termed *hole transfer* to the thiol (referring to the electronic vacancy of the valence band which lies energetically below the thiol oxidation potential).^{24, 25}

The ultimate goal of this work requires a system that allows electronic interaction between the QDs and the photo-chemically active chromium complexes, but at the same time remains stable on the time-scale of the proposed sensitization process. In research described in the following section, the QD system was modified to address the concerns expressed in the preceding paragraphs. Specifically, new core/shell type QDs were synthesized and MPA was replaced with the chelating dithiol DHLA.

ii. Conjugation of $Cr(abc)Cl_2^+$ to the Surface of DHLA Coated

CdSe/ZnS QDs

The most common QD systems used now are CdSe/ZnS, “core/shell”-type materials. The higher band-gap inorganic shell electronically passivates the material, strongly disfavoring the tunneling of photo-excited carriers to the surface of QDs. For this reason, these materials have considerably higher photoluminescence quantum yields and the core/shell QDs are less susceptible to degradation and surface oxidation.²⁶ Moreover, although previous work with thiols as CdSe passivants demonstrates their potential for photooxidation,²⁴ in the

case of CdSe/ZnS shell QDs, the ZnS shell is expected to disfavor ligand trapping of photo-excited carriers at the surface.

CdSe/ZnS QDs having ~3 nm cores were synthesized using the SILAR ZnS overcoating procedure reported in the literature.²⁷ In organic solvent, these QDs had a very high photoluminescence (PL) quantum yield ($\phi_{PL} = 0.8$). Following surface exchange with DHLA, the water soluble QDs still maintained strong PL ($\phi_{PL} = 0.05 - 0.1$), albeit considerably lower than in organic solvents. As will be seen later, evidence suggests that the relatively thin (1 monolayer) ZnS shell used for these particular QDs may incompletely passivate the QD surface, resulting in diminished quantum yield once water solubilized with DHLA.

As discussed previously, *trans*-[Cr(abc)Cl₂]Br (**9**) was chosen as a model complex for conjugation with the QDs because this complex displays phosphorescence from the chromium doublet excited state at low temperature (77 K). In this context it was proposed that, following conjugation of **9** to the QD surface, low temperature PL spectroscopy could be used to probe the ability of the QDs to sensitize the chromium(III) centered excited states.

The conjugation reactions between the DHLA coated CdSe/ZnS QDs and **9** were conducted in phosphate buffered solution using the water soluble cross-linking agent 1-ethyl-3-(3-dimethylaminopropyl) carbodiimide (EDC). In general, initial attempts to conjugate **9** to the QDs resulted in *macroscopic aggregation* of the QDs as evidenced by complete precipitation of the luminescent QDs from the aqueous reaction mixture over the course of the 1-2 hour reaction times. In fact,

reaction with EDC alone gave similar results. The aggregates thus formed could not be redissolved. In hind sight, QD aggregation with **9** was actually not surprising giving that the conjugation with **9** leads to QD surface charge neutralization upon formation of the new amide bond. The effects of EDC alone were somewhat surprising, however several similar reports exist in the literature concerning the instability of QDs in the presence of EDC. Clearly, a variety of factors will play a role in the solubility of the QDs including ligand charge and the total surface charge. At this point a polyethylene glycol polymer containing an amine tail group (mPEG-NH₂, M.W._{avg} = 5000) was enlisted to improve the solubility of the QDs in aqueous solution. This modification was made based on the success observed by others in using polyethylene glycol chains as surface ligands for QDs used for biological studies.^{3b,28} As reported by Dr. Harry Uyeda *et al*, QDs coated with PEG modified DHLA are made soluble in polar solvents by the ethylene glycol units, (-CH₂-CH₂-O-)_n, in the PEG chains. For these systems, solubility is no longer dependent on the charge imparted by the deprotonated carboxyl groups of DHLA.^{3b} With chains having >8 repeat units, the QDs are reported to be soluble in aqueous buffer over a wide pH range (5.8 – 12). Thus, integration of PEG along with **9** during the conjugation reaction was expected to improve the solubility of the final mQDs.

Indeed, use of mPEG-NH₂ greatly improved the solubility of the QDs during and after conjugation reactions with EDC. In a typical reaction, an aliquot of concentrated QD stock solution is diluted to 0.1 μM in phosphate buffer (15 mM,

pH 7.4) and a large excess (1 mM, 10,000 equiv.) of mPEG-NH₂ is added. To this mixture, 20,000 equivalents of EDC from a freshly dissolved stock solution is added. The reaction is stirred in the dark for ~2 h. Stable conjugates were formed between the DHLA coated QDs and mPEG-NH₂ in this way with QD concentrations as high as 0.6 μM with only negligible aggregates. The new PEG modified mQDs were stable throughout the multiple centrifuging (13 k) and concentration/dilution cycles used to purify the conjugates.

Figure 3.10. False color image taken of the electrophoresis gel comparing electrophoretic mobility of the QD-DHLA and the modified QD-PEG conjugates towards the positive electrode (up) in a 1.5% agarose gel. Lane 3 (mQD with mPEG-NH₂), Lane 5 (DHLA coated QD starting material), and Lane 12 (6 nm gold nanoparticles used as an imaging standard).



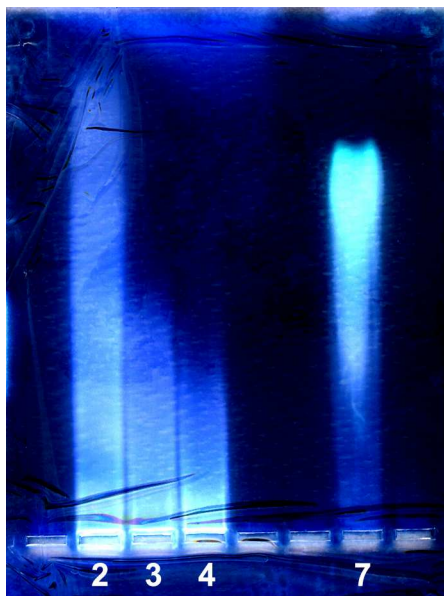
Gel electrophoresis was used to characterize the new purified materials. As stated above, the formation of amide bonds between the surface carboxylic acid groups and the R-NH₂ leads to surface charge neutralization. Because electrophoresis separates materials based on their charge, the PEG modified

mQDs are expected to move more slowly than their highly anionic DHLA coated predecessor. Figure 3.10 shows that this in fact is the case. Similarly, in their studies with PEG modified DHLA, Uyeda *et al* also observed the decreasing electrophoretic mobility of QDs when the ratio of DHLA-PEG/DHLA in the coating was increased.^{3b}

Based on the positive results obtained with mPEG-NH₂ above, it was used as co-reactant along with **9**. However, with **9** the situation is still complicated due to the apparent adverse effects of large surface loading of **9** on the solubility of the QDs. It was found that under conditions similar to those stated above (namely ~0.6 μM QDs and 1 mM total R-NH₂ concentration) an mPEG-NH₂/**9** ratio of at least 20:1 was necessary to avoid aggregation of the QDs. Even with these high PEG ratios, some loss of sample due to aggregation is observed either during the reaction, or during the ensuing purification steps.

Figure 3.11 compares the electrophoretic mobility of mQDs from **3** conjugation mixtures (mPEG-NH₂ only and mPEG-NH₂/**9** 100:1) to the mobility of the unmodified DHLA coated QDs. Clearly, all mQDs have lower mobility than the starting material. Notably, the mQD sample modified with **9** has a lower mobility than those modified with only mPEG-NH₂. This is likely due to the cationic nature of **9**, which neutralizes 2 negative QD surface charges for every one surface bound **9** (one due to the amide bond, and one due to the +1 charge of the complex).

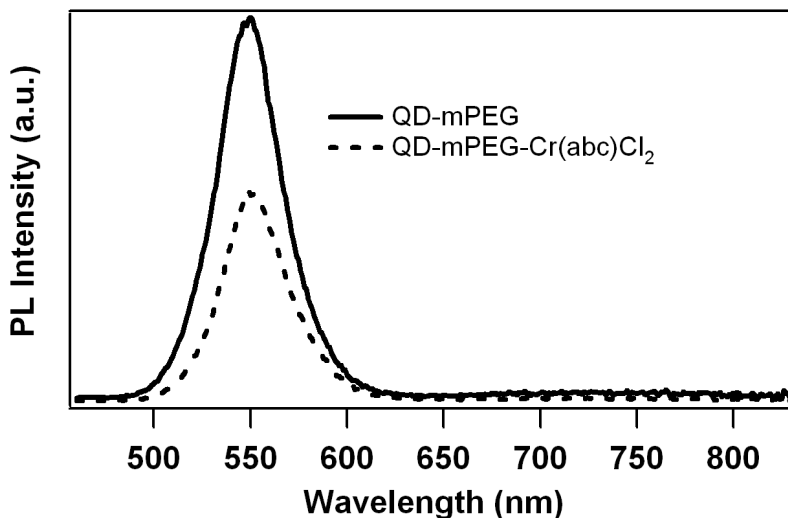
Figure 3.11. False color image comparing electrophoretic mobility of QD-DHLA and indicated purified QD conjugates towards the positive electrode (up) in a 1.5 % agarose gel. Lane 2 (DHLA coated QD starting material), Lane 3 (mQDs modified with mPEG-NH₂), Lane 4 (mQDs modified with a 100:1 mixture of mPEG-NH₂ and **9**), and Lane 7 (6 nm gold nanoparticle standard used for imaging purposes).



This data gives strong evidence for successful surface conjugation. For this system, with a 3 nm CdSe core overcoated with 1 monolayer of ZnS, one can estimate that there are approximately 100 DHLA molecules per QD (assuming 100 % of surface Zn's are bound to a DHLA molecule). Based on the reaction stoichiometry, for a conjugation reaction that is 100% complete (all DHLA's are coupled), this gives a maximum loading of roughly 1 molecule of **9** per QD for the 100:1 reactions. The actual surface loading is apparently considerably less since it is clear from Figures 3.6 and 3.7 that not all DHLA surface sites are coupled (if this were the case, the mPEG-NH₂ only mQDs would be uncharged and immobile in electrophoresis and the mixed samples would migrate in the opposite direction due to the positive (+) charge contributed by **9**). To date, there

have not been any quantitative measurements indicating the number of surface sites that are modified using the EDC coupling strategy for QDs. For the present system, one possible future experiment to address this is to use atomic absorbance/emission analysis on a digested sample of mQDs to quantify the amount of chromium present, and thus the number of **9** per mQD.

Figure 3.12. PL spectra of absorbance matched phosphate buffered solutions (15 mM, pH 8.2) of the two conjugates QD-mPEG and QD-mPEG-Cr(abc)Cl₂. Spectra were excited at 450 nm.



The mQDs obtained via EDC mediated coupling of mPEG-NH₂ or mixtures of mPEG-NH₂ and **9** were studied by PL spectroscopy. Figure 3.12 compares the PL of two mQD samples, one modified with mPEG-NH₂ only and the other with a mixture of mPEG-NH₂ and **9**. These samples were prepared side by side under the same reaction conditions (see above) and purified using the same procedure. The absorbance of the samples at the excitation wavelength (450 nm) was matched. Clearly quenching is observed in the mQD sample reacted with **9** when compared with the mQD contain mPEG-NH₂ only. This result was very enticing,

however it was *not quantitatively* reproducible. Although, *in general* QDs reacted with **9** *typically* displayed weaker PL than that of the PEG only mQDs, the magnitude of this quenching varied from reaction to reaction (<5 %--50 %). In fact, the PEG only mQDs were routinely quenched themselves to varying degrees with respect to the DHLA coated starting materials. Evidently, the photophysics of these materials are *highly* sensitive to the surface morphology and the observed changes in Figure 3.x may not be attributable to the presence of **9** *alone*.

As was discussed at the beginning of this chapter, the reason for using **9** as a model stemmed largely from its phosphorescence at low temperature. DeRosa exploited this to prove that optically exciting the appended chromophores effectively sensitizing the metal centered excited states via internal conversion/intersystem crossing. Although this was the initial strategy proposed with mQD described here, it met with a serious drawback. Unfortunately, although considerably attenuated following overcoating with ZnS, the PL of the QDs used here display a weak broad signal in the red attributed to so called “surface-trap” PL. Surface trap PL presumably originates from a substantial portion of the optically excited QDs decaying radiatively from intergap trap states caused by incomplete *electronic* passivation at the surface of the particles. Although ZnS shells are known to more effectively passivate these trap states, one possibility is that the 1 monolayer shell used here is less than ideal either due to insufficient thickness and/or incomplete surface coverage. It should be noted that even a sample of water soluble CdSe/ZnS QDs obtained from a commercial

source (Ocean Nanotech LLC, Fayetteville, AR) with a reported quantum yield of ~50 % still had residual broad background PL. For most applications such as biomedical imaging and tagging, this weak PL is inconsequential, as it makes up <<1 % of the total PL signal and it cannot be detected in a typical PL spectrum unless one zooms in to the ~700 nm region. However, for the detection of the weak chromium(III) phosphorescence, any background in the 700 nm region, no matter how weak, becomes a problem. Unfortunately, this stymied the efforts to validate energy transfer from the central QD to the bound **9** molecules in the mQDs described above.

D. Future Potential

Although the strategies presented for direct conjugation of chromium(III) cyclam type complexes to QDs has met with only limited success so far, the various results described here present several potentially fruitful avenues for future investigators. For all the strategies presented, the main limitation was the inherent difficulty of retaining solubility of the final mQD products.

Among the plethora of studies using EDC activated QDs for conjugation to a variety of molecules, there are several reports that the QDs are susceptible to aggregation during activation by EDC.^{3a, 29} To the author's knowledge, the recent report by Dr. Kloepper and coworkers at the Jet Propulsion Laboratory in Pasadena, CA is the only one to comment on parameters needed to avoid aggregation during EDC coupling of DHLA coated CdSe/ZnS QDs.^{29a} As not even a decade has spanned since Chan and Nie first reported this technology for

binding of QDs to other species, this field is obviously still in its infancy. A considerable effort is first required to standardize the procedures and conditions used for QD surface conjugation reactions. The data observed here for mQD produced with mPEG-NH₂ and **9** suggests that careful tuning of the reaction conditions allows the production of stable and functional modified QDs. Optimizing this chemistry will pave the way for continued efforts along these lines to conjugate various photoactive transition metal complexes, including the dinitrito-chromium(III) cyclam complexes. The number of ligands used to make QDs water soluble and suitable for attachment to other species grows every year. Although some initial results with DHLA given here show promise, success will likely require new optimized surface ligands. Of the various choices available currently one should consider the various amphiphilic polymers used by many.^{16c-h} Reminiscent of inverse micelles, these materials stabilize QDs by virtue of hydrophobic sub-domains acting on the nascent hydrophobic core, and hydrophilic domains incurring solubility in polar solvents. The hydrophilic domains typically contain reactive functionalities, such as carboxylic acids or amines that can be used to further couple the encapsulated QDs to other molecules or structures of interest. Also, a recent report from the group of Dr. Warren Chan, currently at the University of Toronto, suggests that QD ligands must have lengths exceeding eight carbons (C₈) to have appreciable stability with respect to EDC activation.^{29b} In that work, cross-linked chains of mercaptoundeconoic acid on the surface of CdSe/ZnS QDs are reported to have enhanced stability and

surface functionalities that are amenable to further conjugation. These are only two examples, and many possible avenues for research exist in this field.

The alternate strategy of modifying a molecule with a linker capable of binding to a QD surface first, as in $[\text{Cr}(\text{dhlbc})\text{Cl}_2]\text{Br}$ (**12**) also has considerable potential. At least one recent published report exists for tailoring a metal complex to a QD using a DHLA modified ligand and Uyeda *et al* have demonstrated this strategy's effectiveness for DHLA modified polyethylene glycol. As alluded to earlier, the key for use of a compound like **12** likely lies in use of a mixed QD ligand system in which a solubility enhancer such as PEG is bound to the surface along with **12** to keep the final product from losing its solubility. Alternatively, it maybe possible to design modified cyclams that contain both a QD linker such as DHLA, as well as a solubility modifier like PEG.

E. References

1. (a) DeRosa, F.; Bu, X.; Ford, P.C. *Inorg. Chem.* **2005**, *44*, 4166-4174. (b) DeRosa, F.; Bu, X.; Ford, P.C. *Inorg. Chem.*, **2005**, *44*, 4157-4165. (c) DeRosa, F., Ph.D Dissertation, U.C. Santa Barbara, Santa Barbara, CA (2003).
2. (a) Peng, X. G.; Wilson, T.; Alivisatos, A. P.; Schultz, P. G. *Angew. Chem. Int. Ed. Engl.* **1997**, *36*, 145-147. (b) Cumberland, S. L.; Berrettini, M. G.; Javier, A.; Strouse, G. F. *Chem. Mater.* **2003**, *15*, 1047-1056. (c) Berrettini, M.; Braun, G.; Hu, J. G.; Strouse, G. F. *J. Am. Chem. Soc.* **2004**, *126*, 7063-7070. (d) Javier, A.; Yun, C. S.; Sorena, J.; Strouse, G. F. *J. Phys. Chem. B*, **2003**, *107*, 435-442. (e) Pathak, S.; Choi, S.; Arnheim, N.; Thompson, M. E. *J. Am. Chem. Soc.* **2001**, *123*, 4103-4104. (f) Chan, W. C. W.; Nie, S. *Science* **1998**, *281*, 2016-2018. (g) Bruchez, M.; Moronne, M.; Gin, P.; Weiss, S.; Alivisatos, A. P. *Science* **1998**, *281*, 2013-2016. (h) Mitchell, G. P.; Mirkin, C. A.; Letsinger, R. L. *J. Am. Chem. Soc.* **1999**, *121*, 8122-8123. (i) Wuister, S. F.; Swart, I.; van Driel, F.; Hickey, S. G.; de Mello Donegá, C. *Nano Lett.* **2003**, *3*, 503-507. (j) Zhou, D.; Piper, J. D.; Abell, C.; Klenerman, D.; Kang, D.-J.; Ying, L. *Chem. Comm.* **2005**, 4807-4809.
3. (a) Mattoussi, H.; Mauro, J. M.; Goldman, E. R.; Anderson, G. P.; Sundar, V. C.; Mikulec, F. V.; Bawendi, M. G. *J. Am. Chem. Soc.* **2000**, *122*, 12142-12150. (b) Uyeda, H. T.; Medintz, I. L.; Jaiswal, J. K.; Simon, S. M.; Mattoussi, H. *J. Am. Chem. Soc.* **2005**, *127*, 3870-3878. (c) Roux, S.; Garcia, B.; Bridot, J-L.; Salomé, M.; Marquette, C.; Lemelle, L.; Gillet, P.; Blum, L.; Perriat, P.; Tillement, O. *Langmuir* **2005**, *21*, 2526-2536. (d) Beet, P. D.; Cormode, D. P.; Davis, J. J. *Chem. Comm.* **2004**, *4*, 414-415. (e) Hsieh, J-M.; Ho, M-L.; Wu, P-W.; Cou, P-T.; Tsai, T-T.; Chi, Y. *Chem. Comm.* **2006**, *6*, 615-617.
4. Medintz, I. L.; Uyeda, H. T.; Goldman, E. R.; Mattoussi, H. *Nat. Mater.* **2005**, *4*, 435-446 and references therein.
5. Parak, W. J.; Gerion, D.; Pellegrino, T.; Zanchet, D.; Micheel C.; Williams, S. C.; Boudreau, R.; Le Gros, M. A.; Larabell, C. A.; Alivisatos, A. P. *Nanotech.* **2003**, *14*, R15-R27 and references therein.
6. Querner, C.; Reiss, P.; Bleuse, J.; Pron, A. *J. Am. Chem. Soc.* **2004**, *126*, 11574-11582.

7. Hermanson, G. T. *Bioconjugate Techniques* Academic Press, New York, **1996** and references therein.
8. Conrado, C. L.; Weckler, S.; Egler, C.; Magde, D.; Ford, P. C. *Inorg. Chem.* **2004**, *43*, 5543-5549.
9. (a) Wagner, A. F.; Walton, E. Boxer, G. E.; Pruss, M. P.; Holly, F. W.; Folkers, K. *J. Am. Chem. Soc.* **1956**, *78*, 5079-5081. (b) Barltrop, J. A.; Calvin, M. *J. Am. Chem. Soc.* **1952**, *74*, 6153-6154. (c) Barltrop, J. A.; Hayes, P. M.; Calvin, M. *J. Am. Chem. Soc.* **1954**, *76*, 4348-4367.
10. Eicher, I.; Schmidt, H-L. *Biosensors Bioelectron.* **2001**, *16*, 245-252.
11. Gunsalus, I. C.; Barton, L. S.; Gruber, W. *J. Am. Chem. Soc.*, **1956**, *78*, 1763-1768.
12. Ferguson, J.; Tobe, M. L. *Inorg. Chim. Acta.*, **1970**, *4*, 109-112.
13. Guldi, D.; Wasgestian, F.; Meyerstein, D. *Inorg. Chim. Acta.*, **1992**, *194*, 15-22.
14. Howie, J. K.; Houts, J. J.; Sawyer, D. T. *J. Am. Chem. Soc.* **1977**, *99*, 6323-6326.
15. Cheng, C. – T.; Chen, C. – Y.; Lai, C. – W.; Liu, W. – H.; Pu, S. – C.; Chou, P. – T.; Chou, Y. – H.; Chiu, H. – T. *J. Mater. Chem.* **2005**, *15*, 3409 – 3414.
16. (a) Willard, D. M.; Carillo, L. L.; Jung, J.; Van Orden, A. *Nano. Lett.* **2001**, *1*, 469-474. (b) Hong, R.; Fischer, N. O.; Verma, A.; Goodman, C. M.; Emrick, T.; Rotello, V. M. *J. Am. Chem. Soc.* **2004**, *126*, 739-743. (c) Wu, X.; Liu, H.; Liu, J.; Haley, K. N.; Treadway, J. A.; Larson, J. P.; Ge, N.; Peale, F.; Bruchez, M. P. *Nat. Biotech.* **2003** *21*, 41-46. (d) Ballou, B.; Lagerholm, B. C.; Ernst, L. A.; Brushez, M. P.; Waggoner, A. S. *Bioconj. Chem.* **2004**, *15*, 79-86. (g) Gao, X.; Cui, Y.; Levenson, R. M.; Chung, L. W. K.; Nie, S. *Nat. Biotech.* **2004**, *22*, 969-976. (h) Bakalova, R.; Zhelev, Z.; Ohba, H.; Baba Y. *J. Am. Chem. Soc.* **2005**, *127*, 11328-11335. (i) Zhelev, Z.; Ohba, H.; Bakalova, R.; Jose, R.; Fukuoka, S.; Nagase, T.; Ishikawa, M.; Baba, Y. *Chem. Comm.* **2005**, 1980-1982. (j) Jin, T.; Fujii, F.; Sakata, H.; Tamura, M.; Kinjo, M. *Chem. Comm.*, **2005**, 4300-4302. (k) Veinot, J. G. C.; Galloro, J.; Pugliese, L.; Bell, V.; Pestrin, R.; Pietro, W. J. *Can. J. Chem.* **1998**, *76*, 1530-1539.
17. Schmelz, O.; Mews, A.; Basché, T.; Herrmann, A.; Müllen, K. *Langmuir*, **2001**, *17*, 2861-2865.

18. Berrettini, M. G., Ph.D Dissertation, U.C. Santa Barbara, Santa Barbara, CA (2005)
19. Silverstein, R. M.; Webster, F. X. *Spectrometric Identification of Organic Compounds* John Wiley & Sons, Inc., New York, 1998.
20. Pan, C.; Pelzer, K.; Philippot, K.; Chaudret, B.; Dassenoy, F.; Lecante, P.; Casanove, M. –*J. J. Am. Chem. Soc.* **2001**, *123*, 7584-7593.
21. Kim, D. I.; Islam, M. A.; Avila, L.; Herman, I. P. *J. Phys. Chem. B.* **2003**, *107*, 6318-6323.
22. Kim, B. S.; Islam, M. A.; Brus, L. E.; Herman, I. P. *J. Appl. Phys.* **2001**, *89*, 4022-4026.
23. Kalyuzhny, G.; Murray, R. W. *J. Phys. Chem. B* **2005**, *109*, 7012-7021.
24. Aldana, J.; Wang, Y. A.; Peng, X. *J. Am. Chem. Soc.* **2001**, *123*, 8844-8850.
25. Wuister, S. F.; de Mello Donegá, C.; Meijerink, A. *J. Phys. Chem. B* **2004**, *108*, 17393-17397.
26. (a) Hines, M. A.; Guyot-Sionnest, P. *J. Phys. Chem.* **1996**, *100*, 468-471. (b) Dabbousi, B. O.; Rodriguez-Viejo, J.; Mikulec, F. V.; Heine, J. R.; Mattoussi, H.; Ober, R.; Jensen, K. F.; Bawendi, M. G. *J. Phys. Chem. B* **1997**, *101*, 9463-9475.
27. (a) Li, J. J.; Wang, Y. A.; Guo, W.; Keay, J. C.; Mishima, T. D.; Johnson, M. B.; Peng, X. *J. Am. Chem. Soc.*, **2003**, *125*, 12567-12575. (b) Xie, R.; Kolb, U.; Li, J.; Basché, T.; Mews, A. *J. Am. Chem. Soc.*, **2005**, *127*, 7480-7488.
28. Ballou, B.; Lagerholm, B. C.; Ernst, L. A.; Bruchez, M. P.; Waggoner, A. S. *Bioconj. Chem.* **2004**, *15*, 79-86.
29. (a) Kloepfer, J. A.; Mielke, R. E.; Nadeau, J. L. *App. Environ. Microbiol.* **2005**, *71*, 2548-2557. (b) Jiang, W.; Mardiyani, S.; Fischer, H.; Chan, W. C. W. *Chem. Mater.* **2006**, *18*, 872-878.

4. Chapter IV. Photophysical Investigations of Electrostatic Assemblies Between Quantum Dots and *trans*-Dichloro Chromium(III) Cyclam

A. Introduction

The following two chapters will describe the photoluminescence (PL) quenching of water soluble CdSe/ZnS core/shell QDs co-dissolved with two Cr(III) complexes, [*trans*-Cr(cyclam)Cl₂]Cl (**1**) and [*trans*-Cr(cyclam)(ONO)₂]BF₄ (**2**), in buffered solution. In addition to investigating the effects of **2** on QD PL, chapter V will address the ability of the QDs to sensitize nitric oxide (NO) release from **2**.

As was mentioned earlier, studies in this laboratory have been concerned with the development of transition metal complexes for potential applications as photochemically activated drugs.¹ Dr. Malcolm De Leo from the Ford group at UCSB demonstrated that the dinitrito complex of chromium(III) cyclam, [Cr(cyclam)(ONO)₂]BF₄ (**2**), releases NO with efficiencies as high as 50 % when irradiated into its metal centered transitions.^{1g} To address the problem of the extremely low extinction coefficient of these Laporte forbidden transitions, DeRosa demonstrated how organic dyes can be appended to the cyclam backbone of such complexes.^{1h,2} The dye-derivatized complexes demonstrated efficient energy transfer from the appended chromophore to the metal center, while leaving the photophysics and photochemistry of the metal center unchanged. The net

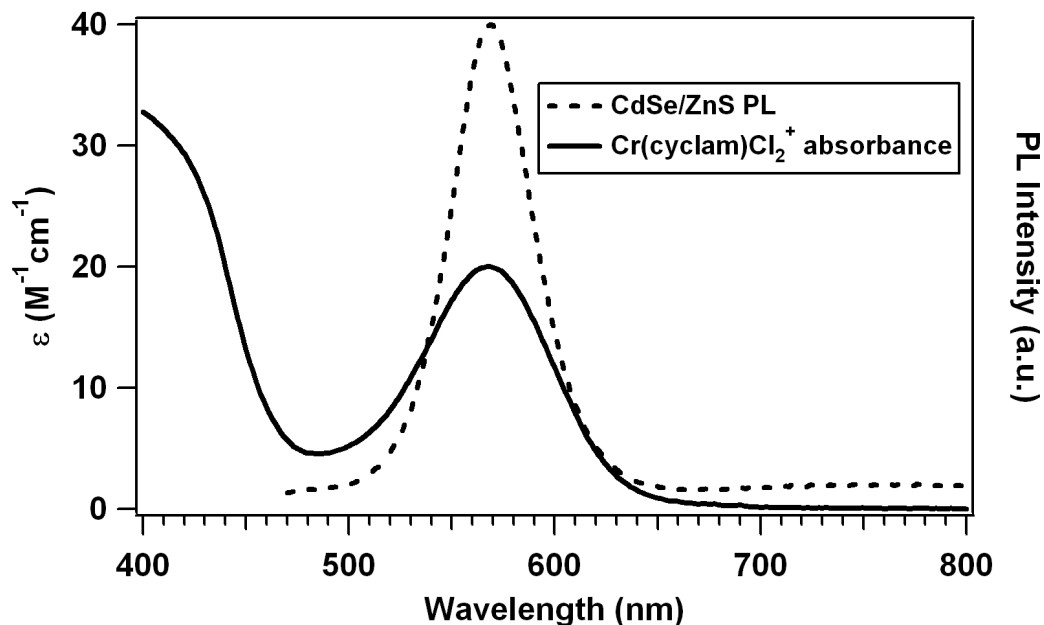
effect was to increase the light harvesting capability of the complex, which leads to an enhancement in the rate of photochemically released nitric oxide (see Figure 1.11.)^{1h} Although these bichromophoric systems represent a considerable improvement in light absorption over **2**, they do not display appreciable absorbance at long wavelengths (>600 nm). As aluded to in the previous chapter, QDs represent a new class of chromophores displaying strong light absorbing capabilities, both via single photon excitation (SPE)³ and two photon excitation (TPE)⁴. The focus of this work is to exploit both attributes displayed by QDs, namely the ability to serve as visible range photosensitizers of an NO donor complex using SPE *and* TPE of the QDs with NIR light. Here I will disucss the suitability of the QDs as a photochemical sensitizers of complexes like **1** and **2**. In this context, Chapter IV is concerned specifically with complex **1** and its electronic interaction with the QDs.

B. Experimental

QDs having core diameters of about 3.8 nm were synthesized using the hot-injection method and then coated with a relatively thick shell (6 monolayers) of ZnS as described in chapter II.^{5,6} This particular size was initially chosen because the photoluminescence (PL) from such core/shell QDs have ideal overlap with the Q₁ absorbance band of **1** (Figure 4.1). Detailed photophysical investigations were initially conducted with **1** as a quencher due to its relative photochemical inertness and ideal spectral characteristics.

Aqueous solubility of the QDs was accomplished by exchange of the original hydrophobic surface capping groups with dihydrolipoic acid (DHLA).⁷ The QDs used here have optical properties, e.g. narrow PL linewidths (FWHM = 45 nm) and PL quantum yields (~ 2 %), that are comparable to those observed in other studies of similarly prepared QDs in aqueous solution.⁷ Samples of QDs or sample mixtures of QDs and varying concentrations of **1** were diluted directly in 10 mm optical path cuvettes and sparged with argon to remove oxygen. All samples described here are diluted in phosphate buffer (15 mM, pH 8.2). Measurements were taken immediately after dilution for each sample at room temperature.

Figure 4.1. Spectrum showing the overlap of the water soluble core/shell CdSe/ZnS QD photoluminescence with the Q₁ absorbance band of [*trans*-Cr(cyclam)Cl₂]⁺Cl in aqueous solution.

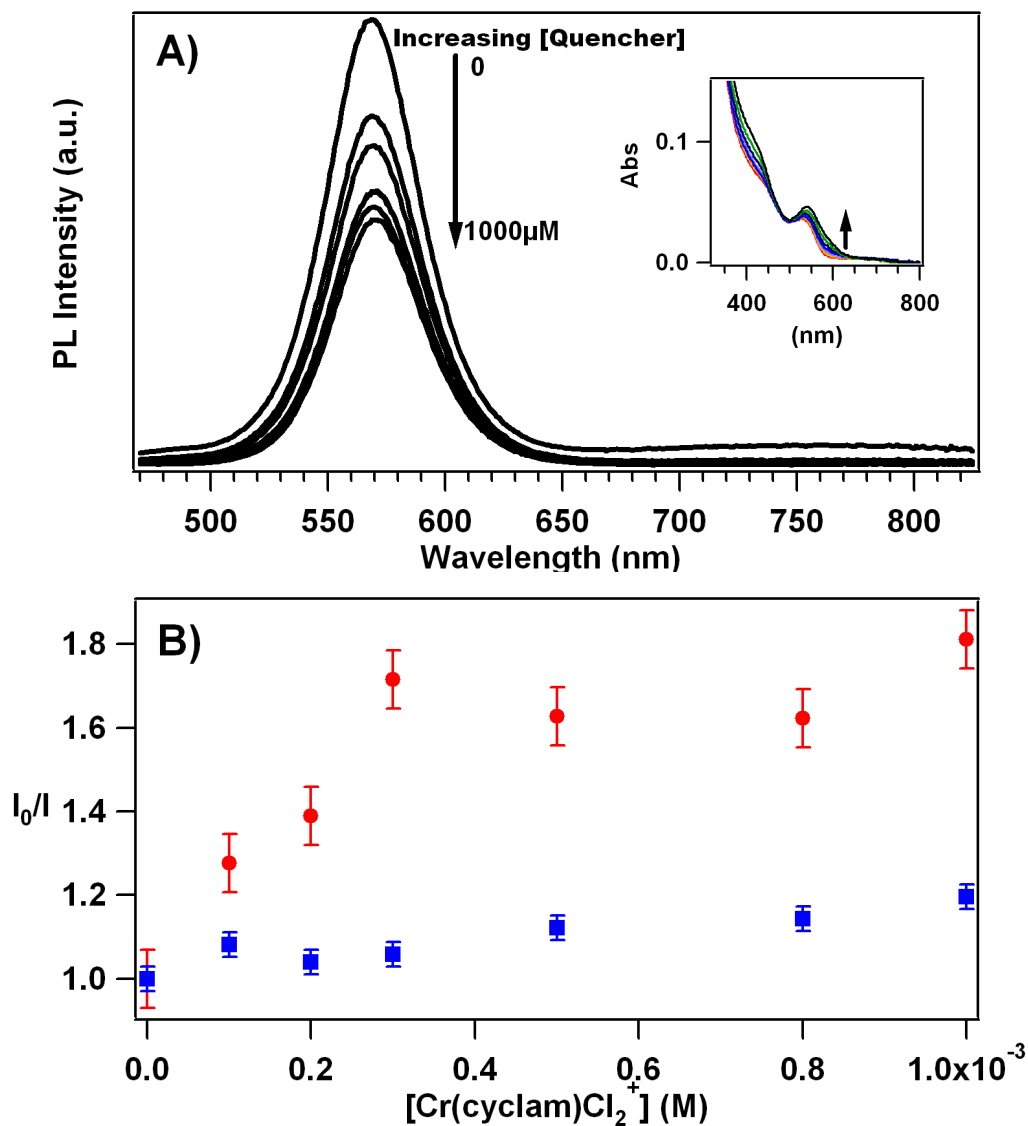


C. Results and Discussion

i. Photoluminescence Quenching of QDs by [trans-Cr(cyclam)Cl₂]Cl

The PL behavior of solutions containing a fixed concentration (~190 nM) of QDs and varied concentrations of **1** (0 to 1000 μ M) is shown in Figure 4.2. A general trend was observed showing a decrease in QD PL intensity as the quencher concentration is increased (Figure 4.2A). About ~50 % of the peak PL intensity was quenched in the solution containing 1000 μ M of **1**. As shown in the top trace of Figure 4.2B, a plot of I_0/I (Stern-Volmer analysis; I being the PL intensity at the λ_{max}) does not give the linear relationship expected for dynamic quenching of a molecular donor by a molecular acceptor.⁸ Instead this plot levels off at quencher concentrations $> \sim 500 \mu\text{M}$. This behavior suggests that more than one emitting state may be involved, a behavior in analogy to that often encountered in the fluorescence quenching behavior of tryptophan residues in proteins.⁸ For the latter systems, buried tryptophans are less quenched (or not at all) than are the surface fluorophores, which are more accessible to contact with a quencher. This results in a persistent fluorescence signal due to the fraction of tryptophans that are not accessible to the quencher. Within this framework, the PL quenching data shown in Figure 4.2 suggests that there are multiple emitters, only some of which are quenched by the added **1**.

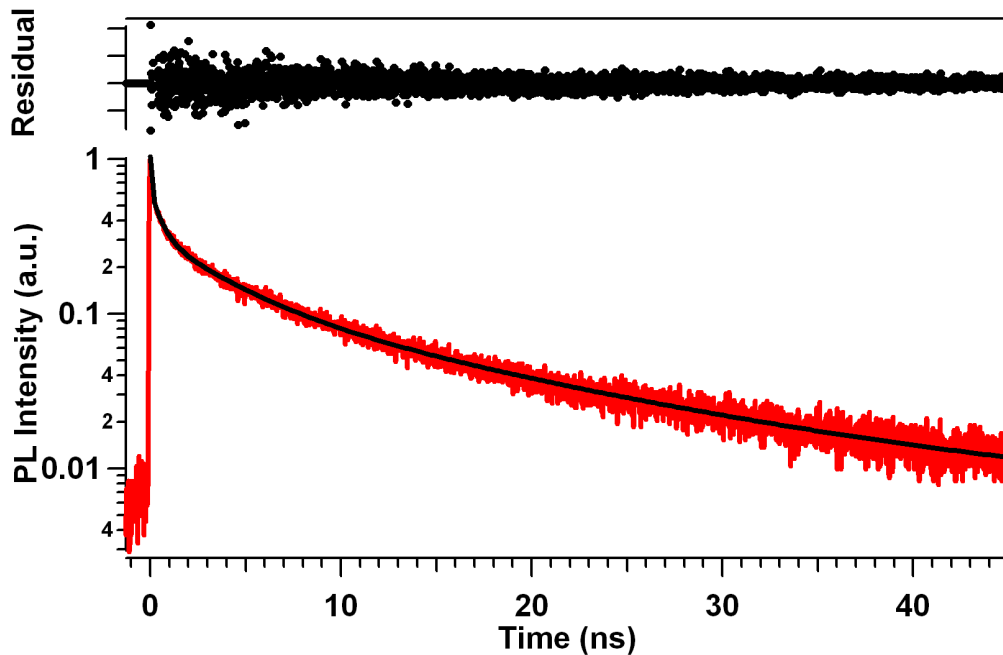
Figure 4.2. A) Top: Photoluminescence spectra of the QDs showing changes due to increasing concentration of **1**. Each trace represents an independently prepared sample having a constant QD concentration (190 nM) and varied **1** concentration (0–1000 μM). The QD PL is excited at 460 nm where the absorbance of **1** is negligible at the concentrations used here. Inset shows the UV-vis absorbance of each sample. Arrow indicates increasing [**1**]. B) Bottom: Stern Volmer type plot where I is the PL intensity of the QDs at the PL λ_{max} and I_0 is the PL intensity of the QDs in the absence of **1**. The upper set of points (red dots) indicate samples which were acquired in 15 mM phosphate buffer, while the lower set (blue squares) were acquired under otherwise identical solutions with 250 mM added KCl.



The time-resolved PL behavior of the QD solutions, both with and without added **1**, was recorded in order to obtain more information about the observed quenching effect. Without quencher, the QD PL decay is multi-exponential as is common for such QD systems⁹ (Figure 4.3), and an acceptable fit to these data (random noise in the residuals) was obtained using the relationship described in Eq. 4.1 with $n = 4$. The lifetimes and amplitude thereby generated are listed in Table 4.1.

$$I(t) = \sum_{i=1}^n \alpha_i \exp(-t/\tau_i) \quad (4.1)$$

Figure 4.3. Time resolved PL of water soluble QDs used in this study in aqueous solution (190 nM). QDs are excited with ~ 120 fs pulses tuned to 460 nm. QD PL is monitored at $\lambda_{\text{max}} = 570$ nm. The trace through the data represents a fit according to Eq. 4.1 with $n = 4$ (see text). A residual plot above the data demonstrates the “goodness of fit”.



Multi-exponential luminescence decay kinetics such as seen in Figure 4.3 are indicative of the heterogeneous nature of QDs in an ensemble measurement.¹⁰ Although one possibility is that the QDs represent a distribution of QD sizes, the relatively narrow band shapes of the absorption and emission bands belie this. It is notable that of the four components needed to fit the temporal PL, one appears to be very short (instrument limited at 55 ps) but to have the largest amplitude. The remaining components include two of intermediate lifetimes and a long lived component (15 ns) that can be attributed to the intrinsic QD lifetime associated with radiative decay of the band edge excited state, as seen by others.¹¹

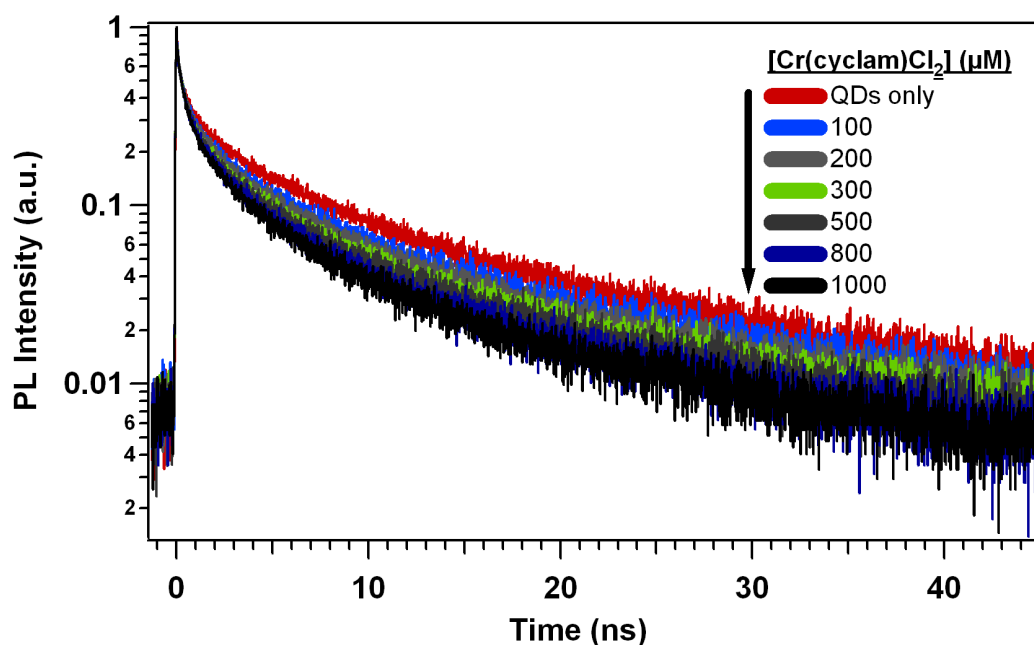
Addition of the quencher **1** has a pronounced effect on the observed temporal behavior of QD PL luminescence, as shown in Figure 4.4. It is clear from these curves that the PL decay occurs with a faster rate in the presence of **1**. The fitting parameters for the temporally resolved PL are given in Table 4.1. The component of the signal due to a response limited fast component (≤ 55 ps) was held constant in the fitting routine. All three resolvable components are observed to decrease with increasing concentration of **1**. Furthermore, the amplitude of the second component, α_2 , increases at the expense of the longest component, α_4 . This behavior suggests that the presence of **1** introduces an alternate decay pathway for the QD excited state.

The steady state and time-resolved PL data demonstrate that the added [*trans*-Cr(cyclam)Cl₂]Cl quenches the photoluminescence of the water-soluble CdSe/ZnS core/shell quantum dots and does so in a concentration dependent

Table 4.1. Computed lifetimes and amplitudes (using Eq. 4.1) for the QD emission data with various concentrations of the *trans*-Cr(cyclam)Cl₂⁺ salt.

[1] (μM)	$(\tau \text{ in ns})$								$\sum \alpha_i \tau_i$
	α_1	τ_1	α_2	τ_2	α_3	τ_3	α_4	τ_4	
0	0.39	0.055	0.31	0.500	0.21	3.54	0.12	15.4	2.8
100	0.39	0.055	0.33	0.499	0.20	3.17	0.10	14.1	2.2
200	0.39	0.055	0.35	0.466	0.21	2.85	0.10	13.0	2.1
300	0.39	0.055	0.36	0.454	0.20	2.67	0.09	12.1	1.8
500	0.39	0.055	0.37	0.476	0.20	2.72	0.09	11.4	1.8
800	0.39	0.055	0.36	0.467	0.20	2.38	0.09	9.9	1.6
1000	0.39	0.055	0.36	0.469	0.20	2.30	0.09	9.4	1.5

Figure 4.4. Comparison of QD time resolved PL as a function of increasing concentrations of **1** (same samples used to generate steady state data in Figure 4.2).



manner. The Stern-Volmer type plot of Figure 4.2B, (I_0/I) vs [1], is nonlinear and levels off at concentrations of **1** greater than 500 μM . Such behavior is inconsistent with collisional ("dynamic") quenching of the optically excited QDs, which would be linear throughout the concentration range according to the

traditional Stern-Volmer treatment.⁸ Instead, some form of "static" quenching, perhaps by the formation of ion pair complexes between the *trans*-Cr(cyclam)Cl₂⁺ cations and the negative surface of the water soluble QD is suggested. Based on Eq. 4.2, one can calculate a limiting

$$\frac{I_0}{I} = 1 + K_{SV}[Q]; K_{SV} = k_q \tau_0 \quad (4.2)$$

slope of the plot shown in Figure 4.2B. In the linear region of low quencher concentration, one can extract a K_{SV} value of 1950 M⁻¹. If one assumes that the PL decrease occurs via dynamic quenching of the longest lived component of the QD PL, ($\tau_0 = \tau_4 = 15.4$ ns), the 30% quenching at 300 μ M concentration would correspond to a quenching rate (k_q) value of $\sim 10^{11}$ M⁻¹ s⁻¹, significantly faster than diffusion limits in this medium. As has been suggested by Maurel *et al.*, such a high K_{SV} value for quenching of CdSe QDs is strongly indicative of formation of a ground-state complex prior to photo-excitation.¹² Whereas in that report, the ground-state complex is formed by direct binding of one or more quenchers to the CdSe surface, electrostatics must play a dominant role in the present system. These core/shell CdSe/ZnS QDs have been modified by exchanging the surface ligands with the chelating dithiol ligand DHLA. Since DHLA is a carboxylic acid, water-solubility is induced by the ionization of the carboxylate group in the mildly basic medium (pH 8.2, 15 mM phosphate buffer solution). Thus, under these conditions the surface of the core/shell/ligand QDs are negatively charged. One can estimate, based on the number of available zinc atoms on the surface of QDs used here, that each QD could accommodate as many as ~ 600 DHLA

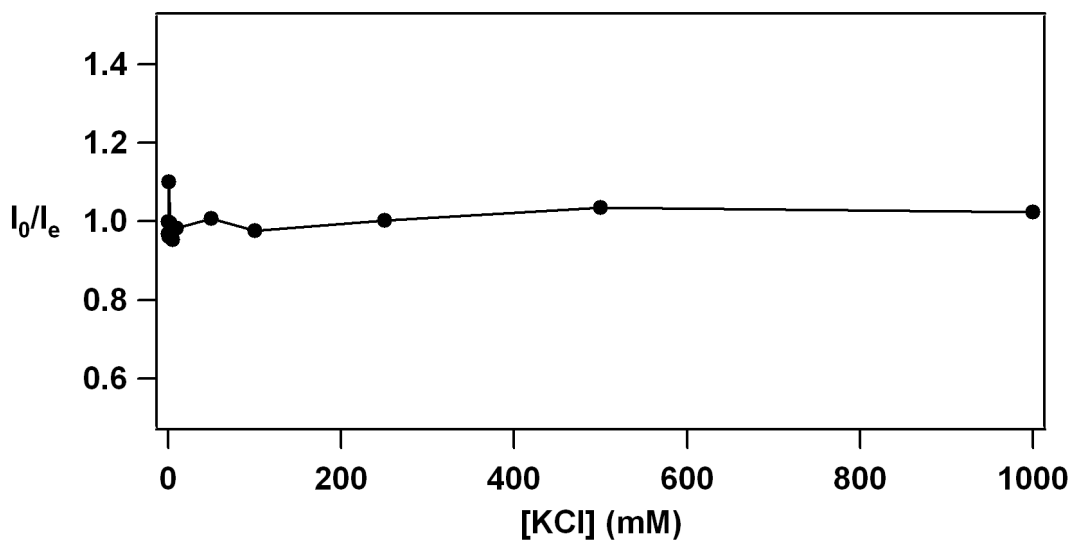
ligands¹³ (assuming one DHLA per every two zinc surface atoms) and based on earlier studies^{13a} would expect that >85 % of the surface ligand sites have been exchanged with DHLA. If indeed the surface is covered by DHLA, one might expect only partial ionization even at pH 8.2. In alkaline solutions, the negatively charged surface should be strongly attractive to cations such as *trans*-Cr(cyclam)Cl₂⁺. Thus, electrostatic (ion pairing) of a quencher at the surface presents the opportunity for an alternate nonradiative decay mechanism for the QD excited state following optical excitation.

If the electrostatically driven assembly of the Cr(III) complex cations on the QD surfaces is indeed responsible for PL quenching, this can be tested by increasing the ionic strength of such solutions by adding another electrolyte. Figure 4.2B shows that added potassium chloride (250 mM KCl) dramatically attenuates the PL quenching by **1**, presumably by screening the electrostatic interaction between the negatively charged QDs and the cationic Cr(III) complex. In a control experiment of the water soluble QDs alone present under otherwise analogous conditions, the effects of added KCl up to 1 M concentration on the QD PL intensities were negligible (Figure 4.5).

The model wherein association of **1** with the QD surface introduces a new non-radiative decay pathway for the QD excited state(s) is further supported by the time- resolved data. Because there are a variety of non-radiative decay mechanisms for these materials, lifetime measurements of ensembles of QDs, as in our case, result in multi-exponential kinetics representative of different excited

state relaxation processes. The changes in the time resolved PL fitting parameters seen as a function of quencher suggest that the interaction with **1** leads to decreases in the longer three decay constants (the shortest decay constant is constrained by the instrumental response), hence accelerating the excited state deactivation of the QD states responsible for these components (see Table 4.1). Lending further support to this argument is the apparent shift in lifetime distribution from the longer components to the shorter components as manifested by a ~25 % drop in the amplitude of the τ_4 component and concomitant increase in the τ_2 component as the concentration of **1** is increased. Notably, quenching of the 15.4 ns component *alone* accounts for over 75% of the total loss in the integrated PL intensity.

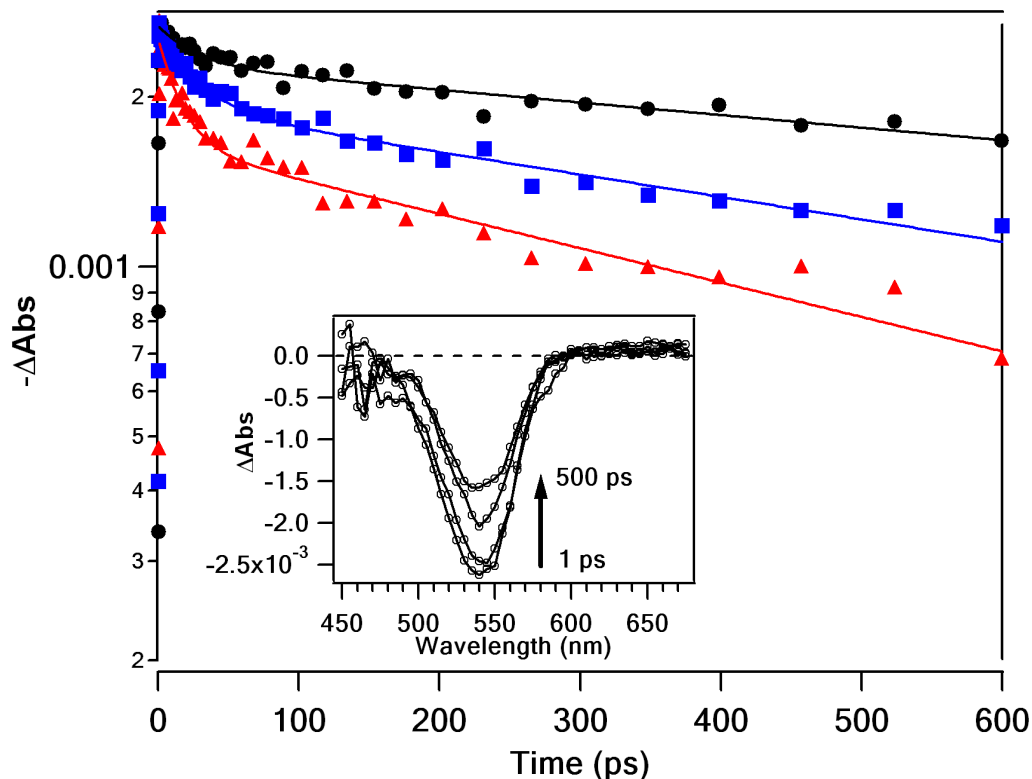
Figure 4.5. Stern-Volmer type plot showing the effect of increasing KCl concentration on the PL intensity of aqueous solutions of QDs. Each point represents an individual sample of QDs diluted to 190 nM in 15 mM phosphate buffer solution (pH 8.2) having various concentrations of KCl added.



ii. Femtosecond Transient Absorbance of 1S Transition in the QDs

Analogous solutions of QDs were examined using femtosecond (fs) transient absorption (TA) spectroscopy to probe the bleaching of the 1S ($[1S(e)-1S_{3/2}(h)]$ transition¹⁰) bleach dynamics of the excited QDs in the absence and in the presence of varied concentrations of added **1**. In these experiments, the concentration of both the QDs and **1** are a factor of ten higher (190 μ M QDs and 0-1000 mM **1**) relative to the PL measurements due to the decreased sample size in the 1 mm pathlength cells used for TA. As observed previously,¹⁰ for the QD sample with no added **1** (Figure 4.6, filled circles) the recovery of the 1S electronic transition displays non-exponential dynamics due to fast carrier trapping in some of the sampled QDs. The fast trapping process occurs with a time constant of \sim 20-40 ps and accounts for roughly 15% of the total signal. The remaining signal decays more slowly with a time constant of roughly \sim 1-2 ns. (A substantial residual bleach remained at the end of this time frame that could not be accessed by this experiment). Introduction of quencher diminished the longer component of the decay, which is manifested in an increase of the relative amplitude of the fast process from 15 to 35% at the highest quencher/QD ratio. This data suggests that the presence of **1** near the QD surface introduces a new, very fast excited decay pathway in the QDs. The residual bleach was also decreased by added **1**.

Figure 4.6. TA dynamics of the QDs measured at 530 nm for 190 μM solutions of QDs with varied concentrations of **1**. The data sets are 0 mM (filled circles), 5 mM (filled squares), and 10 mM (filled triangles) **1**. The lines represent double exponential fits to the data. Inset shows the spectral data for the recovery of the bleach of the QD 1S transition (*without 1* added) at various delay times after the pump pulse.



iii. Mechanism for Quantum Dot PL Quenching

Based on the large spectral overlap between the QD PL and the absorbance of **1** (Figure 4.1), one mechanism for the observed PL quenching would be Förster resonance energy transfer (FRET). In FRET, nonradiative transfer of energy between two interacting dipoles, a donor (D) and an acceptor (A), can occur without physical contact between the two species.^{8,14} This dipole-dipole interaction can occur when the energetic difference between the excited state and ground state of D equals that of A. Such a condition thus requires that there be

spectral overlap between the electronic PL spectrum of D with the electronic absorbance spectrum of A. Furthermore, the strength of the interaction decreases with the inverse of the donor-acceptor separation distance (r) to the sixth power. In this framework, the rate of energy transfer (k_{EN}) as function of r is given by the following expression derived by Förster¹⁴:

$$k_{EN}(r) = \frac{Q_D \kappa^2}{\tau_{D(0)} r^6} \left(\frac{9000(\ln 10)}{128\pi^5 N n^4} \right) \int_0^\infty F_D(\lambda) \varepsilon_A(\lambda) \lambda^4 d\lambda = \frac{1}{\tau_{D(0)}} \left(\frac{R_0}{r} \right)^6; \quad (4.3)$$

where Q_D is the donor quantum yield in the absence of acceptor; $\tau_{D(0)}$ is the donor lifetime in the absence of acceptor; κ is the dipole-dipole orientation factor where for randomly oriented dipoles, $\kappa^2=2/3$; N is Avogadro's number; n is the refractive index of the medium. The integral on the right hand side of Eq. 4.3 is referred to as the J -overlap integral⁸:

$$J(\lambda) = \int_0^\infty F_D(\lambda) \varepsilon_A(\lambda) \lambda^4 d\lambda; \quad (4.4)$$

and, as its name suggests, $J(\lambda)$ takes into account the *spectral* overlap between the PL spectrum of the donor, $F_D(\lambda)$ (area under the curve normalized to unity), and the extinction spectrum of the acceptor, $\varepsilon(\lambda)$ as function of λ , typically in cm.

The term R_0 in Eq. 4.3 is termed the Förster radius and represents the D-A separation distance where the rate of energy transfer, k_{EN} , and the rate of excited state deactivation of D ($1/\tau_{D(0)}$) are equal. The expression for R_0 is then:

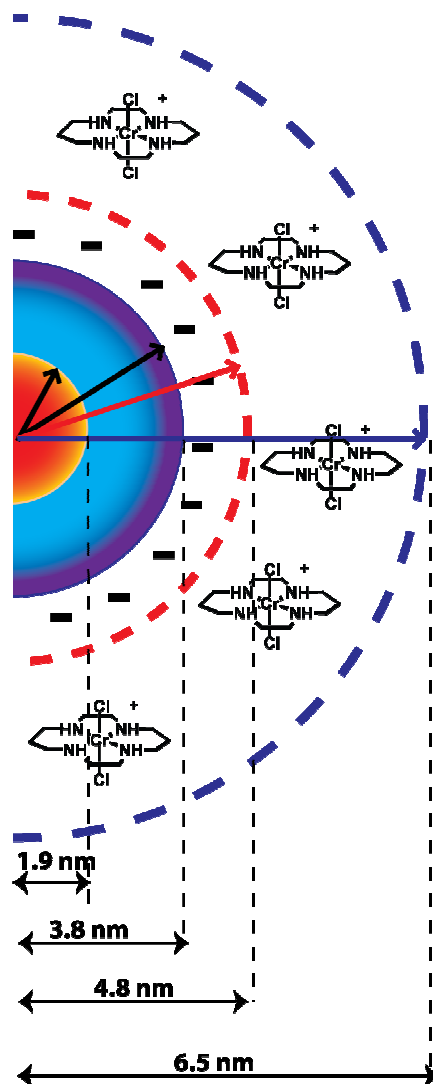
$$R_0 = \left(\frac{9000(\ln 10) \kappa^2 Q_D}{128\pi^5 N n^4} \int_0^\infty F_D(\lambda) \varepsilon_A(\lambda) \lambda^4 d\lambda \right)^{1/6}. \quad (4.5)$$

The Förster formalism has been used to describe the non-radiative energy transfer from QDs to a variety of acceptor molecules, including other QDs,¹⁵ quantum wires,^{15d} dye molecules,¹⁶ and metalloproteins¹⁷. Mattoussi *et al* have demonstrated that using QDs in fluorescence resonance energy transfer (FRET) has the advantage over conventional dyes that the large QD surface area allows multiple acceptor molecules to couple to each QD donor thereby increasing the effective energy transfer efficiency.¹⁸ As a result, donor-acceptor couples having less than ideal spectral characteristics can give rise to an appreciable electronic interaction due to the additive effect of each acceptor.

One of the key factors in the use of the Förster formalism here is the distance of **1** from the QDs. Due to its high sensitivity to the distance between D-A pairs, FRET is sometimes called a “spectroscopic ruler”.⁸ As far as the distance of **1** from the surface of the QDs, some approximations can be made. The DHLA molecules extend no more than ~1 nm out from the surface of the QDs, and thus represent one limit. The hydrodynamic radii for core/shell CdSe/ZnS QDs analogous to those used here have been reported by Dr. Thomas Pons and coworkers at the NRL based on dynamic light scattering (DLS) measurements.¹⁹ For QDs emitting at ~570 nm coated with DHLA, they determined the hydrodynamic radius to be 6-7 nm. This is significantly larger than the geometric radius expected for QDs of this size ($R_{\text{core}} + R_{\text{shell}} = 1.9 \text{ nm} + \sim 6 \times 0.31 \text{ nm/ZnS monolayer}^6 = 3.8 \text{ nm} + R_{\text{DHLA}} = 4.8 \text{ nm}$) even considering the DHLA coating. The difference in the two numbers reflects the sphere of hydration including

counter-ions to which the DLS measurement is very sensitive.^{19,20} It is reasonable to assume that the electrostatic assembly process draws the $\text{Cr}(\text{cyclam})\text{Cl}_2^+$ cations into the hydration sphere of the QDs (Figure 4.7), so a distance of ~ 5 nm from the center of the core is a reasonable estimate.

Figure 4.7. Idealized drawing of $\text{trans-Cr}(\text{cyclam})\text{Cl}_2^+$ cations electrostatically assembled within the hydration sphere of DHLA coated CdSe/ZnS QDs.



Assignment of the other end of the “spectroscopic ruler” becomes somewhat ambiguous in the case of quantum dots. Both the center and the surface of QDs

have been used by others as the end point to describe energy transfer according to FRET in these systems.^{18,21} Further complicating the analysis is the existence of four lifetime components (see Table 4.1), and thus four candidates for τ_D in Eq. 4.3. In one report studying FRET between QDs and Cy3 dyes, although the time-resolved PL of the QDs was reported to contain two components, one of these components was simply ignored in the ensuing analysis.¹⁸

Using the spectral data in Figure 4.1 to calculate $J(\lambda)$, one obtains a R_0 of 2.8 nm for **1** paired with QDs having a PL quantum yield of 0.02. In order to gain some insight into the rate of energy transfer, k_{EN} , several assumptions have to be made. First, R_0 is assumed to represent the distance at which the rate of energy transfer is equal to the rate of QD excited state deactivation represented by only the longest PL component in Table 4.1 ($\tau_{D(0)} = \tau_4$ in Eq. 4.3)). This estimation makes sense because τ_4 accounts for most of the time averaged PL intensity. Furthermore, the decrease in the product, $\alpha_4 \tau_4$, as function of added **1** makes up for >75 % of the total drop in $\sum_i^4 \alpha_i \tau_i$, which makes the assumption that **1** largely effects only the longest lived component a reasonable one. Also for this calculation, the center of the QDs is used as the other end point for r . With these assumptions, the rate of energy transfer can be calculated according to Eq. 4.3 for **1** lying somewhere within the hydration sphere ($4.8 < r < 6.5$ nm). Using this methodology one obtains $2.6 \times 10^6 > k_{EN} > 4.15 \times 10^5 \text{ s}^{-1}$, with k_{EN} decreasing as the distance between the QDs and **1** increases. These rates are 1-2 orders of

magnitude too slow to affect even the longest component of the QD PL. However, if one takes into account the linear enhancement obtained from factoring in multiple acceptors, the analysis becomes more realistic. To determine the number of acceptors needed, the observed quenched rate ($k_{D(Q)}$) must be factored into its components:

$$k_{D(Q)} = k_{D(0)} + k_Q = k_{D(0)} + Nk_{EN}; \quad (4.6)$$

In Eq. 4.6, $k_{D(0)}$ represents the deactivation rate of the QDs without **1** present ($1/\tau_{D(0)}$) and the term N accounts for multiple acceptors contributing the quenching rate k_{EN} . For the highest concentration of **1**, where the maximum quenching is observed, $k_{D(Q)} = 1/t_{D(Q)} = (9.4 \times 10^{-9} \text{ s})^{-1} = 1.1 \times 10^8 \text{ s}^{-1}$ and so $Nk_{EN} = k_Q = 4.5 \times 10^7 \text{ s}^{-1}$. To calculate the number of acceptors, N , needed to account for the observed quenching at a particular distance r (and thus a particular rate, k_{EN}), we have:

$$N = \left(\frac{k_{D(Q)} - k_{D(0)}}{k_{EN}} \right) = \frac{k_Q}{k_{EN}}. \quad (4.7)$$

In order to reduce t_4 to ~ 9.4 ns (the maximum quenching observed) with the range of k_{EN} predicted above, we find from Eq. 4.7 that ~ 18 acceptors would be needed at a distance of $r = 4.8$ nm and ~ 110 would be needed at $r = 6.5$ nm.

Based on steric considerations and a hard packing sphere model^{7a,22}, one can estimate the maximum number of **1** surrounding each QD using the following expression:

$$N_{Complex} = 0.65 \left(\frac{(R_2^3 - R_{QD}^3)}{R_c^3} \right). \quad (4.8)$$

In Eq. 4.8, R_{QD} is the QD radius excluding the organic coating; R_c is the physical dimension of **1** (estimated as 0.90 nm based on crystallographic data); and $R_2 \sim R_{QD} + 2R_c$. Using 3.8 nm for the QD radius, the maximum number of **1** that can encircle a single QD is found to be ~110.

So based on the earlier calculations (Eqs. 4.3-4.7), ~110 molecules situated at the edge of the hydration sphere of a QD would account for the observed quenching of τ_4 at the highest concentration of **1** investigated. Based on Eq. 4.8, no further quenching would be observed for this system because no more molecules can be packed around each QD (assuming only those quenchers that are “first-nearest-neighbors” contribute, a reasonable assumption due to the strong r dependence of FRET). This predicts that the quenching of the QDs should level off, which is exactly what is observed in Figure 4.2B! Thus, the FRET model largely accounts for the concentration dependent PL quenching of the QDs by **1**.

iv. Complications Due to “Surface Effects”?

The results obtained from the femtosecond transient absorbance (TA) of the bleach of the 1S QD transition are difficult to explain within the same framework as that presented above. Obviously, the changes observed in Figure 4.6 occur on a time-scale faster than that seen in the time-resolved PL (tr-PL) data. On the other hand, this technique samples the entire ensemble of QDs, while the PL only samples those QDs which decay with a considerable radiative component. It is

well known that samples of QDs are composed of “bright” and “dark” species.²³ The multi-component decay of the PL seen here is consistent with independent signals from different species within the “bright” portion of the ensemble. In this context, considering that the steady-state PL quantum yield of these materials is relatively low (0.02), a large percentage of the QDs in the ensemble are “dark”. Because the absorbance measurement samples all of the QDs, “bright” and “dark”, the signal in the TA experiment is dominated by the non-emissive QDs. For this reason, it is difficult, and possibly fortuitous to compare the two experiments. Clearly added **1** has a concentration dependent effect both on the “bright” QDs (tr-PL) *and* the “dark” QDs (TA). However, the PL quenching is dominated by the action of **1** on the longest lived or “brightest” QDs. The TA experiment is limited to sub-nanosecond dynamics and although a long component is clearly seen as a residual bleach, changes to components longer than ~1-2 ns cannot be quantified. That said, it is clear from Figure 4.6 that addition of **1** depletes the long component of the decay, which is consistent with the observations seen in the time-resolved PL experiment.

Undoubtedly, the interaction of the QDs with **1** is considerably more complicated than can be quantified by the FRET analysis outlined above. From the TA data it appears that **1** accelerates excited state deactivation on time-scales exceeding 50 ps. Decay of the 1S bleach on the sub-nanosecond timescale is traditionally associated with surface trapping of one of the excited carriers in a portion of the QDs in a sample.²⁴ It would appear that **1** introduces a new

component, or enhances an existing one, associated with such a trapping process. In fact, some evidence for a “surface effect” of **1** on the QD PL is present in the steady-state PL data of Figure 4.2A. Clearly, the PL spectrum of the QD sample with no **1** present contains a weak, broad component red shifted from the sharp band edge transition. This broad transition is routinely attributed to radiative decay of surface trapped carriers. With the lowest concentration of added **1**, this component completely disappears. It is possible that this effect is caused by the appearance of a new competitive deactivation process introduced by **1**'s presence near the QD surface. The changes seen in the TA dynamics (Figure 4.6, <100 ps) with added **1** may reflect this new process.

D. Conclusions

The PL quenching behavior of QD in response to added **1** was consistent with energy transfer from the optically excited QDs to **1**. The concentration dependence of the PL quenching was quantified in-terms of the formation of electrostatic assemblies between the cationic **1** and the anionic QD surface. Although the electronic interaction between the QDs and **1** is clearly complicated, with a simple FRET analysis, it was found that the “brightest” QDS are quenched by molecules of **1** lying at the edge of the QD sphere of hydration (~6.5 nm from the QD core center). Furthermore FRET is capable of predicting the leveling off of the PL quenching due to saturation of the surface of the QDs with **1**, as estimated by independent calculations based on sterics. This system demonstrates that QDs can function as effective sensitizers to *trans*-chromium(III) cyclam

complexes, and clearly exemplifies the advantage of obtaining enhanced energy transfer efficiency when there are multiple acceptors for every one QD donor.

E. References

1. (a) Bourassa, J.; DeGraff, W.; Kudo, S.; Wink, D. A.; Mitchell, J. B.; Ford, P. C. *J. Am. Chem. Soc.* **1997**, *119*, 2853-2860. (b) Conrado, C.; Bourassa, J.; Egler, C.; Weckler, S.; Ford, P. C. *Inorg. Chem.* **2003**, *42*, 2288-2293. (c) Conrado, C. L.; Weckler, S.; Egler, C.; Magde, D.; Ford, P. C. *Inorg. Chem.* **2004**, *43*, 5543-5549. (d) Weckler, S.; Mikhailovsky, A.; Ford, P. C. *J. Am. Chem. Soc.* **2004**, *126*, 13566-13567. (e) Weckler S. R.; Hutchinson, J.; Ford, P. C. *Inorg. Chem.* **2006**, *45*, 1192-1200. (f) DeLeo, M. A.; Ford, P. C. *J. Am. Chem. Soc.* **1999**, *121*, 1980-1981. (g) DeLeo, M. A.; Ford, P. C. *Coord. Chem. Rev.*, **2000**, *208*, 47-59. (h) DeRosa, F.; Bu, X.; Ford, P. C. *Inorg. Chem.*, **2005**, *44*, 4157-4165.
2. DeRosa, F.; Bu, X.; Pohaku, K.; Ford, P. C. *Inorg. Chem.* **2005**, *44*, 4166-4174.
3. (a) Leatherdale, C.; Woo, W.-K.; Mikulec, F.; Bawendi, M. G. *J. Phys. Chem. B.* **2002**, *106*, 7619-7622. (b) Schmelz, O.; Mews, A.; Basché, T.; Herrmann, A.; Müllen, K. *Langmuir* **2001**, *17*, 2861-2865. (c) Yu, W.; Qu, L.; Guo, W.; Peng, X. *Chem. Mater.* **2003**, *15*, 2854-2860.
4. Larson, Daniel R.; Zipfel, W. R.; Williams, R. M.; Clark, S. W.; Bruchez, M. P.; Wise, F. W.; Webb, W. W. *Science* **2003**, *300*, 1434-1436.
5. (a) Murray, C. B.; Norris, D. J.; Bawendi, M. G. *J. Am. Chem. Soc.*, **1993**, *115*, 8706-8715. (b) Talapin, D. V.; Rogach, a. L.; Kornowski, A.; Haase, M.; Weller, H. *Nano Lett.*, **2001**, *1*, 207-211. (c) de Mello Donega, C.; Hickey, S. G.; Wuister, S.; Vanmaekelbergh, D.; Meijerink, A. *J. Phys. Chem. B*, **2003**, *107*, 489-496.
6. Dabbousi, B. O.; Rodriguez-Viejo, J.; Mikulec, F. V.; Heine, J. R.; Mattoussi, H.; Ober, R.; Jensen, K. F.; Bawendi, M. G. *J. Phys. Chem. B*, **1997**, *101*, 9463-9475.
7. (a) Mattoussi, H.; Mauro, J. M.; Goldman, E. R.; Anderson, G. P.; Sundar, V. C.; Mikulec, F. V.; Bawendi, M. G. *J. Am. Chem. Soc.*, **2000**, *122*, 12142-12150. (b) Cheng, C. – T.; Chen, C. – Y.; Lai, C. – W.; Liu, W. – H.; Pu, S. – C.; Chou, P. – T.; Chou, Y. – H.; Chiu, H. – T. *J. Mater. Chem.* **2005**, *15*, 3409 – 3414.
8. Lakowicz, J. R. *Principles of Fluorescence Spectroscopy*, 2nd Ed., Kluwer Academic, New York, **1999** and references therein.

9. (a) Kloepfer, J. A.; Bradforth, S. E.; Nadeau, J. L. *J. Phys. Chem. B* **2005**, *109*, 9996-10003. (b) Selmarten, D.; Jones, M.; Rumbles, G.; Yu, P.; Nedeljkovic, J.; Shaheen, S. *J. Phys. Chem. B* **2005**, *109*, 15927-15932.
10. Klimov, V. I.; McBranch, D. W.; Leatherdale, C. A.; Bawendi, M. G. *Phys. Rev. B* **1999**, *60*, 13740-13749.
11. (a) Crooker, S. A.; Barrick, T.; Hollingsworth, J. A.; Klimov, V. I. *Appl. Phys. Lett.* **2003**, *82*, 2793-2795. (b) Javier, A.; Magana, D.; Jennings, T.; Strouse, G. F. *Appl. Phys. Lett.* **2003**, *83*, 1423-1425.
12. Maurel V.; Laferrière, M.; Billone, P.; Godin, R.; Scaiano, J. C. *J. Phys. Chem. B* **2006**, *110*, 16353-16358.
13. (a) Bowen Katari, J. E.; Colvin, V. L.; Alivisatos, A. P. *J. Phys. Chem.* **1994**, *98*, 4109-4117. (b) Becerra, L. R.; Murray, C. B.; Griffin, R. G.; Bawendi, M. G. *J. Chem. Phys.* **1994**, *100*, 3297-3300.
14. Förster, T. *Discuss. Faraday Soc.* **1959**, *27*, 7-17.
15. a) Kagan, C. R.; Murray, C. B.; Bawendi, M. G. *Phys. Rev. B*, **1996**, *54*, 8633-8643. b) Crooker, S. A.; Hollingsworth, J. A.; Tretiak, S.; Klimov, V. I. *Phys. Rev. Lett.*, **2002**, *89*, 186802-1 – 186802-4. c) Achermann, M.; Petruska, M. A.; Crooker, S.A.; Klimov, V. I. *J. Phys. Chem. B*, **2003**, *107*, 13782-13787. d) Lee, J.; Govorov, A. O.; Kotov, N. A. *Nano Lett.*, **2005**, *5*, 2063-2069. e) Wargnier, R.; Baranov, A. V.; Maslov, V. G.; Stsiapura, V.; Artemyev, M.; Pluot, M.; Sukhanova, A.; Nabiev, I. *Nano Lett.*, **2004**, *4*, 451-457.
16. a) Clapp, A. R.; Medintz, I. L.; Mattoussi, H. *ChemPhysChem*, **2006**, *7*, 47-57 and references therein.
17. Ipe, B. I.; Niemeyer, C. M. *Angew. Chemie, Int. Ed.*, **2006**, *45*, 504-507.
18. Clapp, A. r. Medintz, I. L.; Mauro, J. M.; Fisher, B. R.; Bawendi, M. G.; Mattoussi, H. *J. Am. Chem. Soc.*, **2004**, *126*, 301-310.
19. Pons, T.; Medintz, I. L.; Mattoussi, H. *Proc. SPIE*, **2006**, *6096*, 60961H-1 – 60961H-10.
20. Ipe, B. I.; Shukla, A.; Lu, H.; Zou, B.; Rehage, H.; Niemeyer, C. M. *ChemPhysChem*, **2006**, *7*, 1112-1118.
21. Dayal, S.; Królicki, R.; Lou, Y.; Qiu, X.; Berlin, J. C.; Kenney, M. E.; Burda, C. *Appl. Phys. B* **2006**, *84*, 309-315.

22. (a) Cebula, J.; Ottewill, R. H.; Ralston, J.; Pusey, P. N. *J. Chem. Soc., Faraday Trans.* **1981**, *177*, 2585-2612. (b) Pompa, P. P.; Chiuri, R.; Manna, L.; Pellegrino, T.; del Mercato, L. L.; Parak, W. J.; Calabi, F.; Cingolani, R.; Rinaldi, R. *Chem. Phys. Lett.* **2006**, *417*, 351-357.
23. Ebenstein, Y.; Maokari, T.; Banin, U. *Appl. Phys. Lett.* **2002**, *80*, 4033-4035.
24. Klimov, V. I.; McBranch, D. W.; Leatherdale, C. A.; Bawendi, M. G. *Phys. Rev. B* **1999**, *60*, 13740-13749.

5. Chapter V. Photochemistry of Electrostatic Assemblies Between Quantum Dots and [*trans*-Cr(cyclam)(ONO)₂]BF₄. Sensitized Release of Nitric Oxide.

“Reproduced in part with permission from The Journal of the American Chemical Society, submitted for publication. Unpublished work copyright 2007 American Chemical Society.”

A. Introduction

As discussed previously, a main focus of research in this laboratory and by others has been the study of photoreactions of various transition metal nitrosyl and nitrito complexes with the goal of developing thermally stable precursors that release nitric oxide (NO) upon electronic excitation.¹ Photochemical techniques are attractive given the opportunity to control the location and timing of the signal leading to release of the NO. In order to enhance the photosensitivity of such compounds, one direction that this line of research has taken is the preparation of molecular constructs consisting of a metal complex incorporating the NO containing moiety plus an antenna chromophore to collect the light via either single photon excitation (SPE)² or two photon excitation (TPE).³ Energy or electron transfer from the antenna to the NO precursor center would then lead to net NO release.

In this context, interest has turned to the use of nanocrystal quantum dots (QDs) as possible photosensitizing chromophores. QDs offer several potentially important advantages, among them are high optical cross-sections for both SPE⁴ and TPE⁵ and the ability to tune the optical properties by simply varying the QD

diameter.⁶ Furthermore, the presence of multiple surface ligand sites provides the opportunity to prepare modified quantum dots incorporating various functionalities tethered to the ligands, examples being, desirable solubility properties,⁷ biological specificity⁸ and the nitric oxide precursor. In fact there are a limited number of recent studies in which researchers have exploited some of these attributes in order to build nanomaterial-NO donor hybrids that are capable of delivering NO either thermally⁹ or photochemically¹⁰. In this latter photochemical study, the nanomaterials function only as delivery vessels and do not improve the photochemical attributes of the NO donor.¹⁰ On the other hand, recent studies have also shown that functionalized QDs can be used as photosensitizers for organic reactions¹¹ or singlet oxygen generation, and that is the present goal.¹²

Analogous to the studies of Chapter IV, the following sections will describe the photophysical and photochemical attributes of electrostatic assemblies of DHLA coated CdSe/ZnS QDs and $[\text{Cr}(\text{cyclam})(\text{ONO})_2](\text{BF}_4)_2$ (**2**). Photolysis of this assembly leads to enhanced NO generation as compared to **2** alone, indicating that the QDs are serving as antennas to sensitize photoreactions of **2**.

B. Experimental

i. Materials

All measurements were done in dilute phosphate buffered (15 mM, pH 8.2) solutions of QDs and **2**. The water soluble QDs used in these studies were

prepared in the same way and are from the same batch of hydrophobically coated CdSe/ZnS QDs used in chapter IV. The synthesis of these QDs having core diameters of about 3.8 nm with a relatively thick shell (6 monolayers) of ZnS and DHLA coating is described in chapter II.¹³ The resulting water soluble QDs displayed a photoluminescence maximum centered at 570 nm (FWHM = 48 nm) with $\phi_{\text{PL}} = \sim 2\%$ (Top traces in Figure 5.2B and C).

ii. Single and Two Photon Excited Photoluminescence

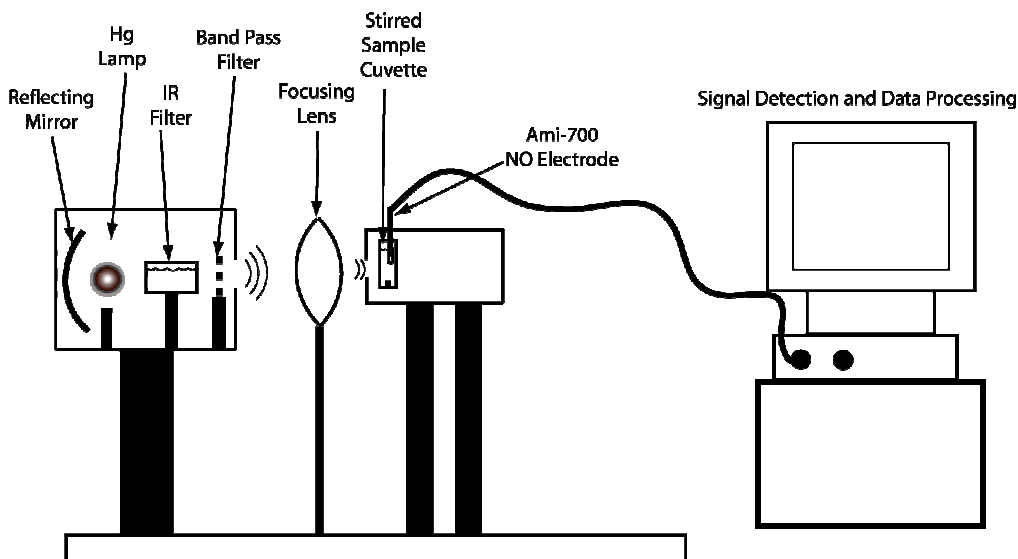
For the photoluminescence (PL) and two photon excited photoluminescence (TPE-PL) measurements, samples of QDs or sample mixtures of QDs and varying concentrations of **2** were diluted directly in 10 mm optical path cuvettes. For all but excitation at 366 nm (which was used to approximate the conditions used for CW photolysis) all solutions were sparged with argon to remove oxygen. The measurements were taken immediately after dilution for each sample. Samples were excited at 366 nm (SPE), 546 nm (SPE), or 800 nm (TPE). The spectral resolution was 1 nm for the TPE data and for the SPE data used to resolve small spectral shifting. Otherwise, the spectral resolution was ~ 4 nm.

For experiments with 366 nm excitation, the PL spectra were corrected for the appreciable absorbance of **2** at this wavelength. Spectra were corrected for inner-filter effects by approximating the influence of the absorbance of **2** as reducing the incident light to the QDs. Therefore the intensity of each spectrum was corrected via multiplication by a factor of $10^{(\text{Abs of } \mathbf{2})}$ at each given wavelength.

iii. Continuous Wave Photolysis and Nitric Oxide Detection

Two procedures were used for the photolysis experiments in conjunction with the NO sensitive electrode (amiNO – 700, Innovative Instruments, Inc.). All experiments were done under aerated conditions. The experimental set-up for NO detection (Figure 5.1) involves an electrode immersed in a cuvette filled with phosphate buffered solution (15 mM, pH 8.2) that is being stirred and is continuously irradiated by the output of a high pressure Hg arc lamp spectrally selected by band pass filter (typically 320–390 nm, where the transmittance >10 %).

Figure 5.1. Diagram of continuous wave photolysis and NO detection experimental set-up.



Procedure A. Injection Method: Under subdued light conditions, the NO electrode was placed into a 10 mm pathlength cuvette that was equipped with a stir flea and filled (~4 mL) with phosphate buffer (15 mM, pH 8.2). The electrode response was allowed to equilibrate in the stirred solution for approximately 10

minutes in the dark. The light was then turned on and care was taken to ensure the electrode tip itself was not illuminated. Once a stable electrode background was established, an aliquot of **2** was added and the electrode response monitored. In the case of mixtures of **2** with the QDs, following electrode equilibration in the stirred buffer solution with the light on, an aliquot of QDs was injected first and allowed to mix for ~100-200 s and then an aliquot of **2** was added.

Procedure B. Pre-Mixing Method: Under subdued light conditions, the NO electrode was placed into a 10 mm pathlength cuvette which was equipped with a stir flea and filled (4 mL) with a solution of **2** alone, or mixtures of **2** and QDs, diluted in phosphate buffer (15 mM, pH 8.2). The electrode response was allowed to equilibrate in the stirred solution for approximately 10 minutes in the dark. The light was then turned on and care was taken to ensure the electrode tip itself was not illuminated. The electrode response was monitored over timed light exposure periods (20-30 s) as indicated.

C. Results and Discussion

i. Photoluminescence Quenching of QDs by 2

As shown in Figure 5.2, the photoluminescence intensity from phosphate buffered solutions of QDs (~130-190 nM) decreases when progressively higher concentrations of **2** (0-1000 μ M) are added to the solution. A very modest red shift of the emission maximum (~3 nm) was also observed (Figure 5.3). This quenching occurs irrespective of the excitation wavelength (compare B and C in

Figure 5.2. Optical data for solutions of QDs (190 nM) mixed with varied concentrations of **2** (0-1000 μM). A) Absorbance data for mixtures of QDs (190 nM) and **2** (0-630 μM). Arrows indicate 366 nm excitation used in B) and 546 nm excitation used in C). B) PL spectra of QDs (190 nM) and mixed with varied concentrations of **2** (0-630 μM) obtained with 366 nm excitation. Spectra have been corrected for inner-filter effects due to absorbance of **2** at this wavelength. C) PL spectra of QDs (190 nM) and mixed with varied concentrations of **2** (0-1000 μM) obtained with 546 nm excitation.

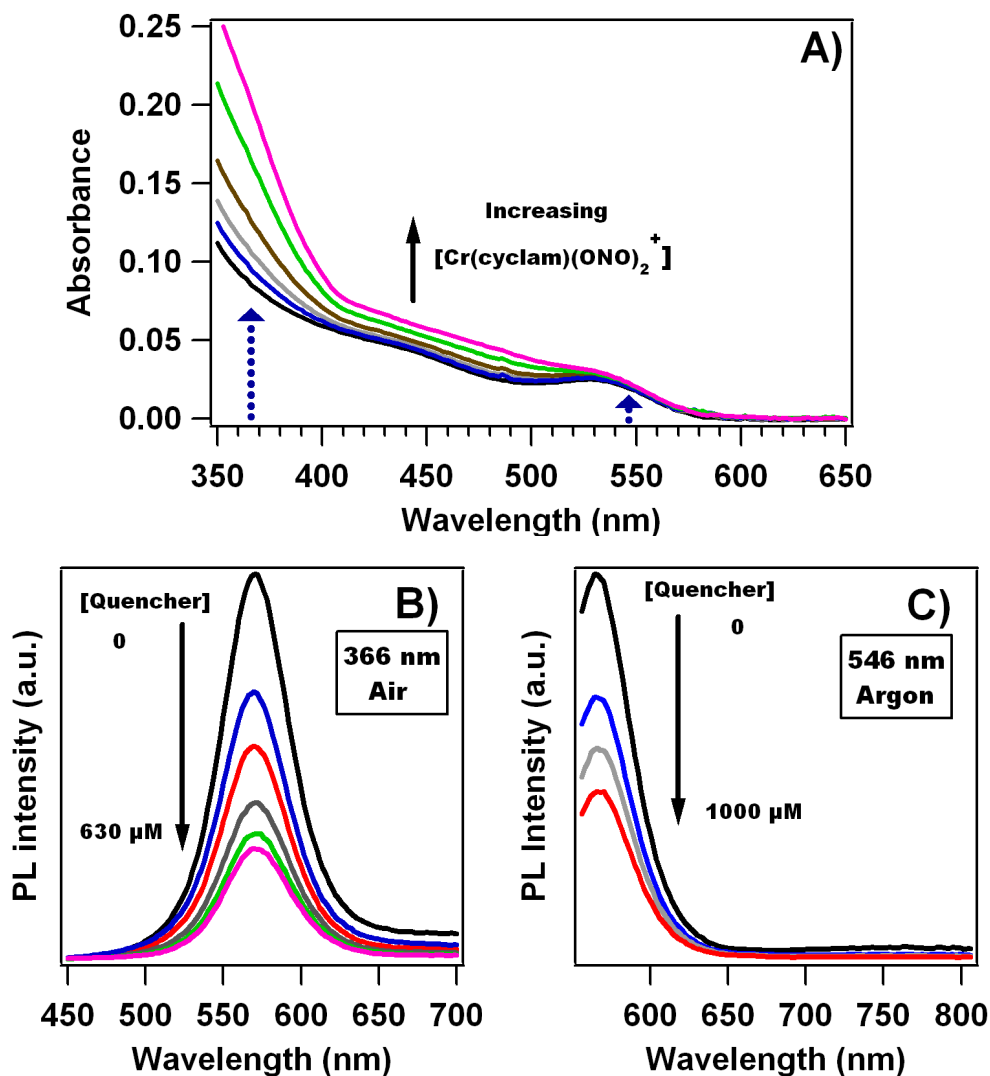
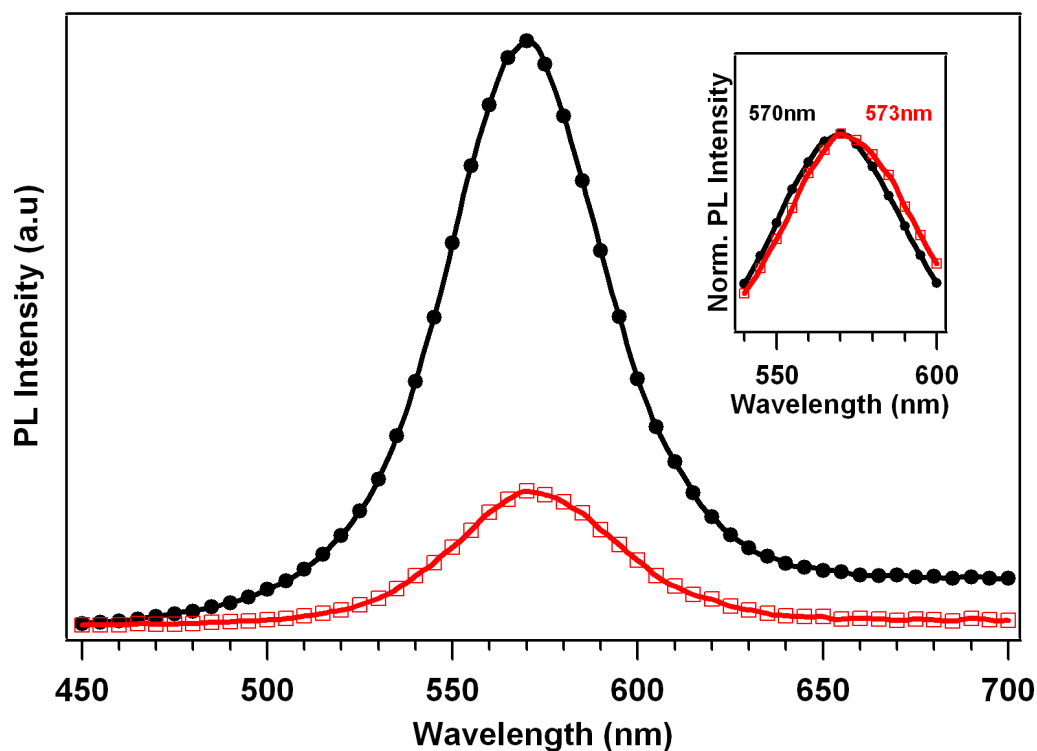


Figure 5.2), however the quenching by **2** over the entire concentration range appears stronger upon UV excitation of the QDs as compared to excitation at 546 nm. For comparison, at $\sim 500 \mu\text{M}$ **2**, the QD PL is quenched by 60 % upon UV excitation versus only 55 % with visible excitation. It should be noted that in the

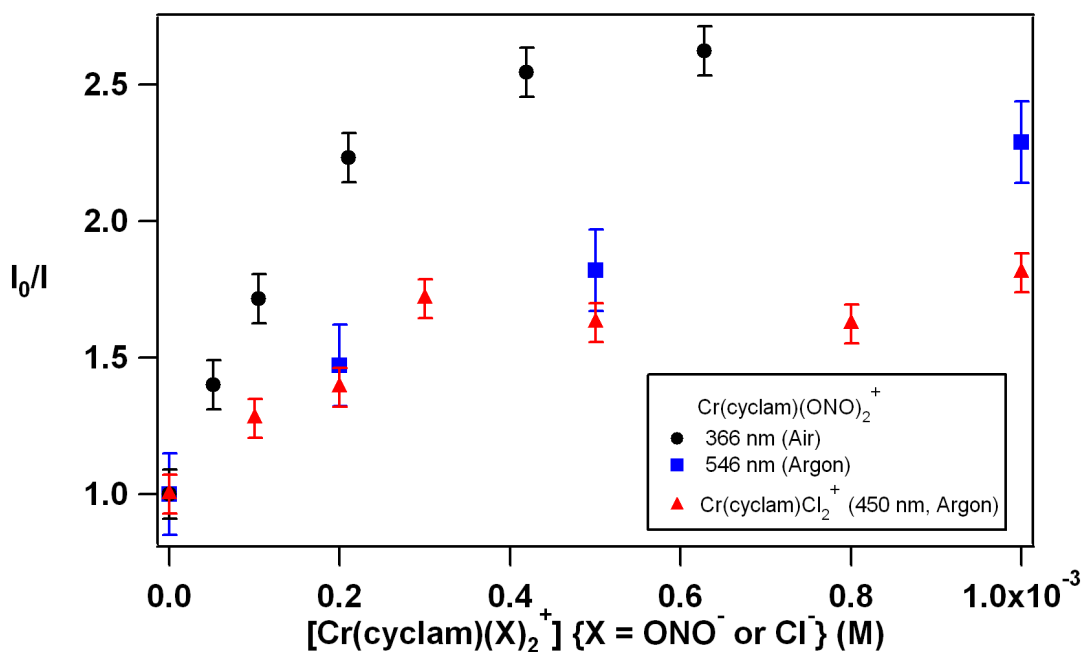
former case, the samples were studied under air atmosphere to approximate the conditions used during the ensuing photochemical experiments. At this point it is unclear what, if any, affect air (presumably O₂) has on the PL of these particular QDs. It has been shown in this laboratory¹⁴ and by others¹⁵ that various QD preparations (solution and solid state) are observed to undergo changes in both PL spectral position and intensity as a function of extended light irradiation in the presence of O₂. Although similar changes are not expected under the low light intensities used for the PL experiment done here, a thorough future investigation of the PL behavior of these particular QDs under exposure to various light intensities and atmospheres is merited.

Figure 5.3. Spectra comparing the PL of phosphate buffered solutions (15 mM, pH 8.2) of QDs alone (190 nM, solid circles) or mixed with **2** (630 μ M, open squares). Inset is a blow up showing the spectra normalized to the peak maxima.



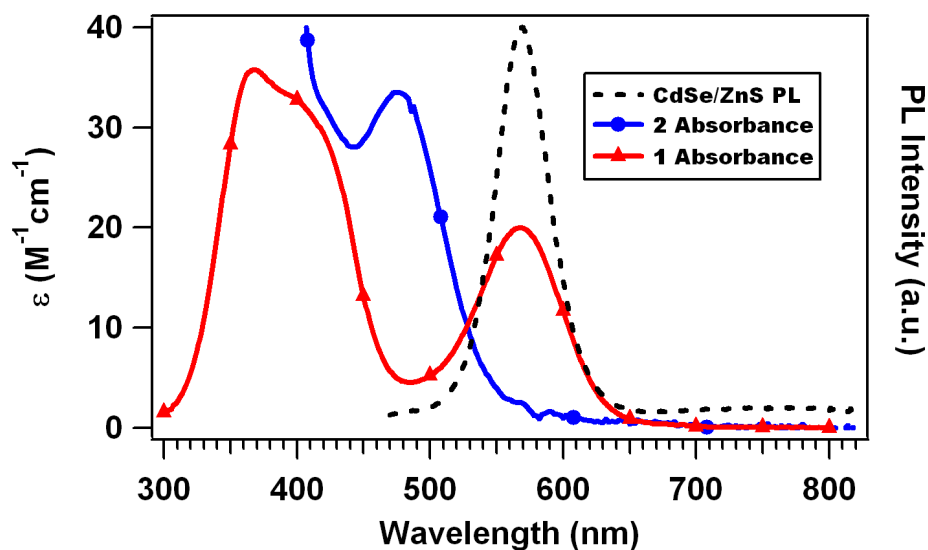
As was shown in chapter IV, similar partial quenching of the QD photoluminescence with the analogous dichloro complex $trans\text{-Cr}(\text{cyclam})\text{Cl}_2^+$ (**1**) is observed. A detailed investigation of the ionic strength dependence of the quenching behavior and the effects observed on the multiexponential decay of the quantum dot excited state lifetimes led to the conclusion that this PL quenching was due to ion pairing between the cationic Cr(III) complex and the anionic quantum dot surface as illustrated in Figure 4.7. Qualitatively, based on the results of Figure 5.2 and the similarity in charge and size between **1** and **2**, a similar electrostatic assembly process must be responsible for the PL quenching observed in mixtures of the QDs and **2**. Again, non-radiative energy transfer from the QDs to **2** would account for the observed changes.

Figure 5.4. Stern-Volmer plot for solutions of QDs in phosphate buffer (15 mM, pH 8.2) at constant concentration (~190 nM) with varied concentrations of Cr(III) complex. I is the PL intensity at the λ_{max} and I_0 is the corresponding PL intensity of QDs without any complex added.



Although the qualitative effect of QD PL quenching is the same with both the dichloro and dinitrito Cr(III) complexes, the mixtures with the latter are quenched to larger extent at equivalent concentrations, and substantially more so in the case of UV excitation of mixtures containing QDs and **2**. Figure 5.4 demonstrates this with a Stern-Volmer type plot that compares the extent of PL quenching for the two experiments described above with **2** and the PL quenching observed for mixtures of QDs and the dicholor analogue, **1**. One interesting point is that all the plots appear to level off at approximately the same concentration of $\sim 500 \mu\text{M}$. This was explained in terms of saturation of the QD hydration sphere with the cationic metal complexes.

Figure 5.5. Spectral overlap of the DHLA coated CdSe/ZnS QDs PL with the absorbance of **1** and **2**. All spectra taken in phosphate buffer (15 mM, pH 8.2).



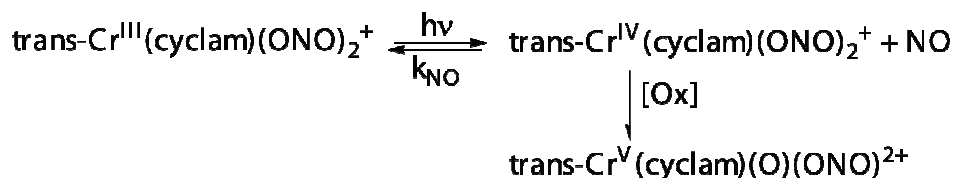
At this point, it is unclear why the dinitrito analogue is a more effective quencher. However, these results tend to counter the proposed mechanism presented in chapter IV for quenching of the QDs by **1** according to the Förster

formalism.¹⁶ Figure 5.5 compares the spectral overlap of the CdSe/ZnS PL with the absorbance of both **1** and **2** in phosphate buffered solution. Clearly, the overlap is much lower with the absorbance band of **2**, and this poorer overlap would be predicted to lower the efficiency of energy transfer according to Förster's predictions. As was suggested in the chapter IV, although the PL quenching data for mixtures of the QDs and **1** could be reasonably explained according to a FRET model, the electronic interaction between the QDs and the Cr(III) complexes is clearly much more complicated. Further quantitative studies are necessary to elucidate the nature by which these species interact.

ii. Electrochemical Detection of Sensitized NO Production

The quenching of the photoluminescence from the QDs is also accompanied by enhanced photoreaction at the Cr(III) centers as indicated by the release of NO presumably owing to the known photoreaction of **2** in aerated solution illustrated by Figure 5.6.^{2c} A nitric oxide specific electrode was used to probe the potential

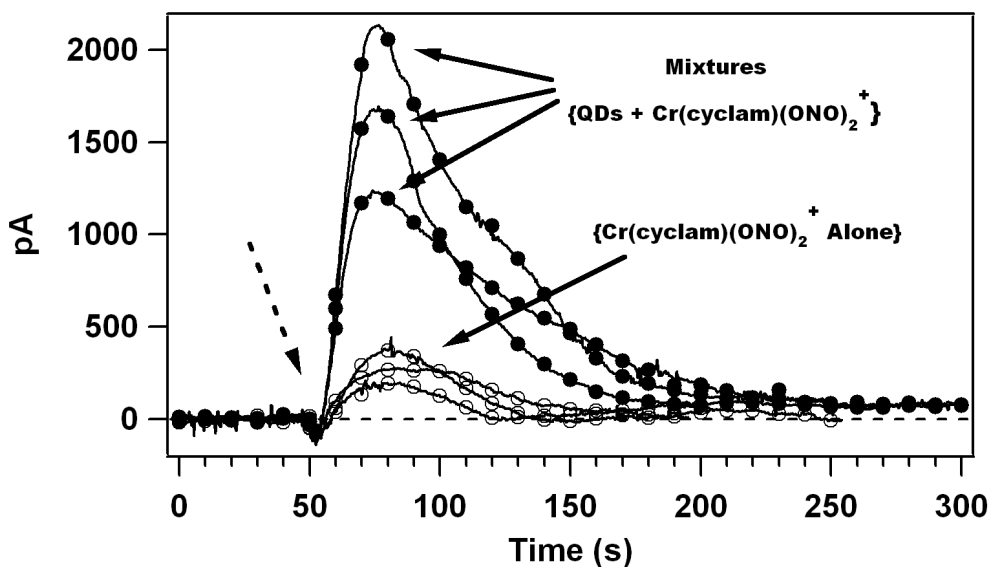
Figure 5.6. Photoreaction of **2** under aerated conditions.



photoreaction accompanying the observed QD quenching.^{4c} In analogy to the experiments by DeRosa *et al*, initial experiments were conducted using injections of aliquots of **2** or QDs followed by **2** into a stirred buffer solution in which the NO electrode had already been pre-equilibrated with the light on (*Procedure A*).^{2d}

Figure 5.7 compares the electrode response when **2** was injected into a solution that contains QDs (100 nM) versus the control phosphate buffer solution that did not contain the water soluble quantum dots (Three independently prepared solutions were measured)

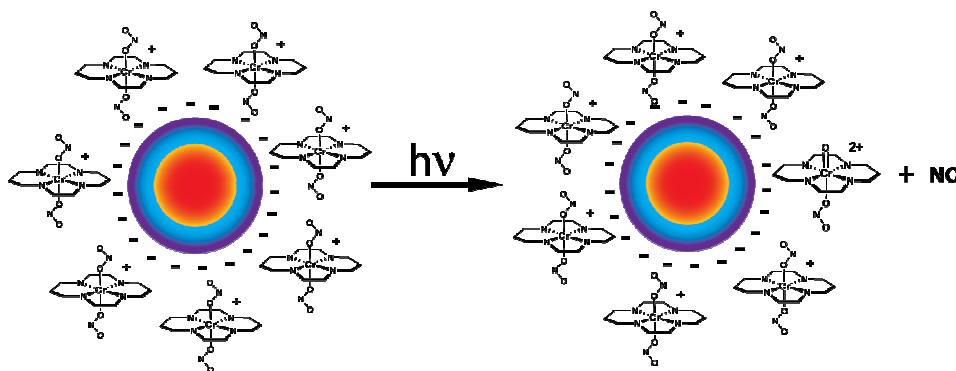
Figure 5.7. NO amperograms comparing electrode response to continuously stirred and irradiated (320-390 nm BP) phosphate buffered solutions with (solid circles) or without (empty circles) QDs (100 nM) following injection of **2** to give a final concentration of 200 μM . Injection is indicated by dashed arrow.



in each case and the concentration of **2** in all six solutions was 200 μM .) With or without QDs, injection of **2** resulted in a positive response from the electrode, measured in picoamps, followed by a slower decay to a value slightly above the initial baseline. However, when the QDs were present, the response maximum of the NO dependent signal was considerably higher, with the latter being on average roughly 6 fold more when the QDs were present. These results are consistent with faster NO production in the presence of the QD antennas due to the enhancement of the light harvesting ability of the system as illustrate in Figure 5.8. It should be

noted that the initial addition of QDs to the buffer solution (data not shown) did not elicit a response from the electrode.

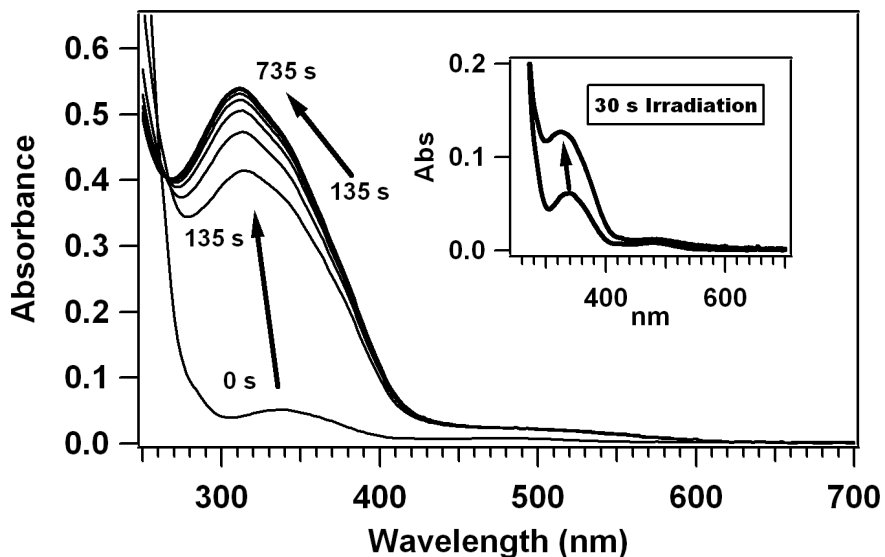
Figure 5.8. Photochemical release of NO from electrostatic assemblies of QDs and *trans*-Cr(cyclam)(ONO)₂⁺.



A comment should be made regarding the rapid drop in electrode response seen for all the samples in Figure 5.7, which based on previous experiences with this electrode, is much faster than would be expected from simply autooxidation of NO. First, the light is always on for the entire observation period, so the decrease in response is *not* due to a cessation of NO production. In fact, during this early period of photolysis, only ~25% of **2** was consumed judging from the absorbance change observed for analogous samples irradiated for 30 s compared to that after exhaustive photolysis of **2** (Figure 5.9).

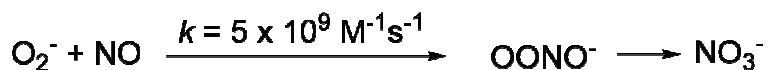
Similar NO amperograms to those seen in Figure 5.7 were observed by DeRosa and De Leo when studying related dinitrito Cr(III) cyclam complexes, suggesting that this phenomenon is special to this particular photochemical system.^{2c,d} Based on the known mechanism for photodecomposition of **2** quantified by De Leo, the trapping of the initial Cr(IV) photoproduct by O₂

Figure 5.9. Absorbance spectra of a sample of **2** (221 μM) irradiated (320-390 nm BP) until a limiting spectra was reached. Inset shows the corresponding changes observed for a sample irradiated for only 30 s.



(referred to as ‘Ox’ in Figure 5.6) produces one equivalent of superoxide (O_2^-). The ensuing diffusion limited reaction of between O_2^- and NO (Figure 5.10) depletes the NO as it is formed during photolysis of **2**. Eventually the rate of NO depletion by reaction with O_2^- , presumably due to build-up of O_2^- in the continuously photolyzed solution, exceeds its rate of production, and the steady state concentration of NO quickly drops. In all of the experiments, the signal

Figure 5.10. The diffusion limited reaction of the superoxide anion with NO forming the peroxyntirite anion which spontaneously rearranges to the nitrate anion.

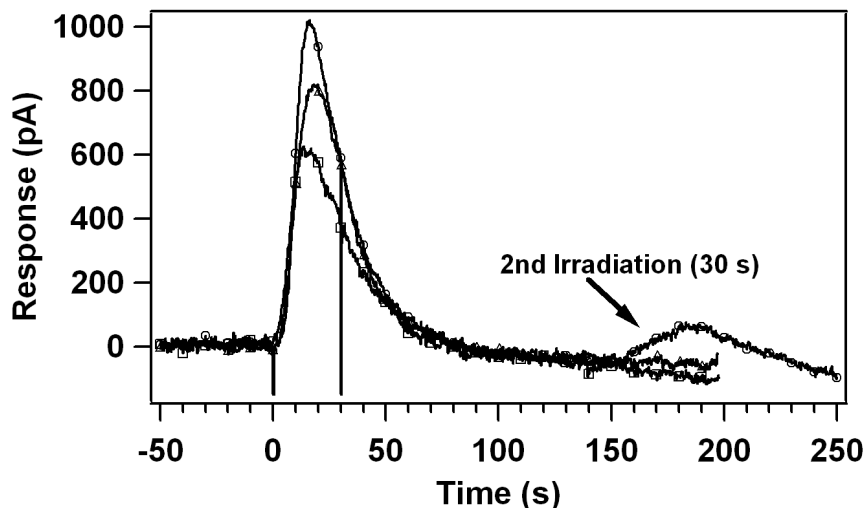


did not completely decay while the light remained on, but rather stabilized at a level just above baseline, consistent with the establishment of an equilibrium

between photochemical NO production and the reactions leading to its decomposition.

Figure 5.7 also demonstrates that although qualitatively similar, identically prepared solutions did not elicit identical responses from the electrode during photolysis. Great care was taken during the experiment to keep all external variables the same, i.e. stirring rate, injection speed and position, electrode position within the cell, etc. In an attempt to address this variability, *Procedure B* was adopted in which **2** or mixtures of **2** and the QDs are pre-equilibrated with the electrode in the dark with constant stirring. In this case, the light is simply turned on following electrode stabilization, and under these conditions, mixing was expected to be homogeneity and the variability contributed by the injection was removed. For these experiments, light irradiation was limited to 20-30s, and the “on” and “off” points were marked (sharp features) for one of the samples (Figure 5.11). As compared to experiments performed using *Procedure A*, somewhat higher signals were observed for photolysis of **2** at similar concentrations although the variability from sample to sample remained under these new conditions (Figure 5.11). Also shown in Figure 5.11 is the effect of a second irradiation period (30 s duration) in one of the samples. Rather than duplicate the initial electrode response, the second irradiation caused a much weaker and slower response, consistent with the action of superoxide lingering in the solution from the earlier photolysis period.

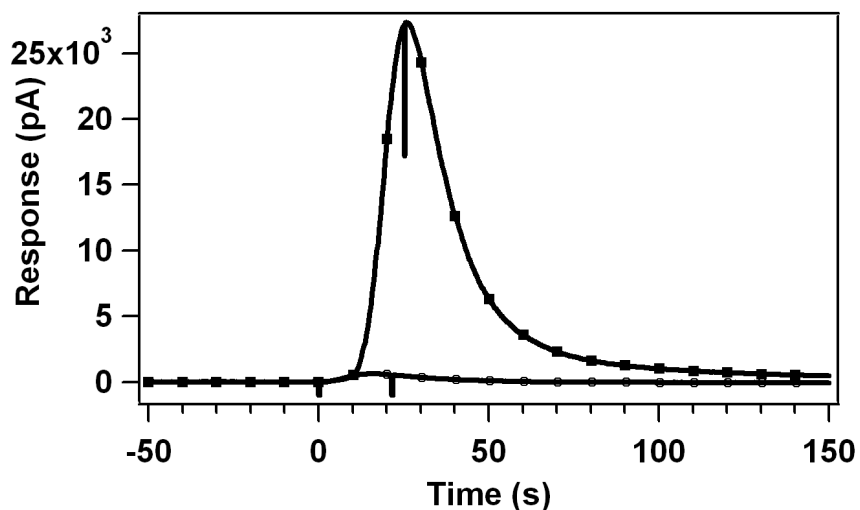
Figure 5.11. NO amperograms for three continuously stirred, irradiated (320-390 nm BP) solutions of **2** (221 mM) generated using *Procedure B*. Sharp lines mark the light “on” and “off” points. For one sample (open circles), following decay of the initial signal, a second irradiation period was conducted.



Quite surprisingly however, the enhancement in electrode response obtained from irradiating solutions of **2** containing QDs was much more dramatic, on average 50 fold higher than for **2** alone (Figure 5.12). One possibility is that due to the extended pre-equilibration time used for the *Procedure B*, the samples are completely homogeneous at this point. Furthermore, the long mixing times for mixture of the QDs and **2** would favor completion of the electrostatic assembly process, thus maximizing the number of complexes of **2** within the radius needed for sensitization to take place. In any case, if one compares the magnitude of the observed response to that obtained from calibrations with acidified nitrite, the peak maximum in Figure 5.12 for the QD (120 nM) and **2** (221 μ M) mixture coincides with a NO concentration of \sim 150 nM, which was produced in $<$ 30 s! This value is given here only as a rough estimate to give the reader an idea of the

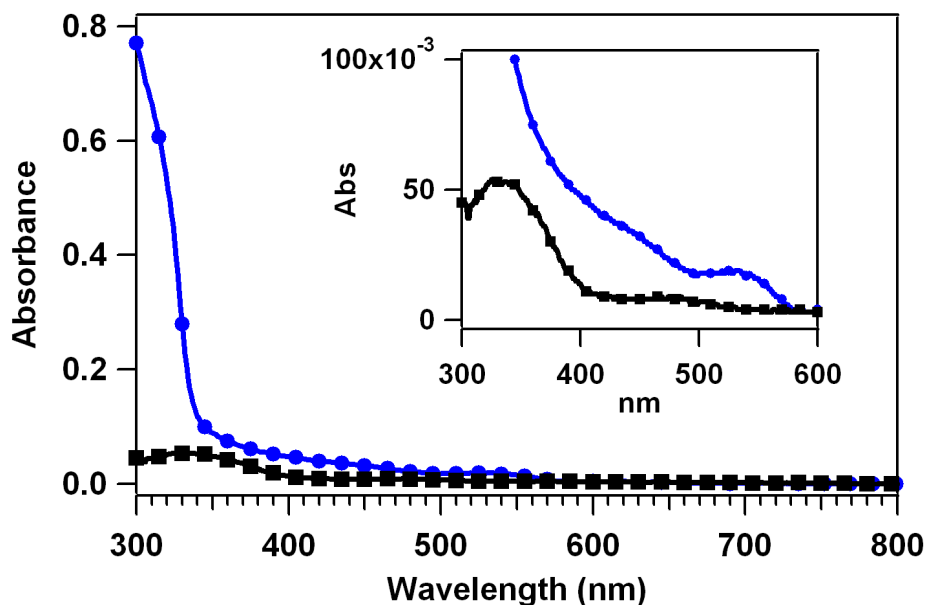
response speed and magnitude. During discussions with Dr. Roberto da Silva, a visiting professor from the University of São Paulo, Brazil it was noted that the electrode response is pH sensitive. Thus, the acidified nitrite calibration can only be used as a rough estimate. Furthermore, the peak heights in these amperograms likely underestimate the total NO produced due to the ever increasing rate of its decomposition via autooxidation with molecular oxygen and reaction with O_2^- .

Figure 5.12. NO amperograms obtained during ~20 s irradiation period of dilute phosphate buffered solutions of **2** (221 mM) with (filled squares) and without (open circles) the presence QDs (120 nM). Sharp features are marks indicating the light was turned “on” at 0 s and light “off” at ~20s.



Unfortunately, as is clear from both Figure 5.7 and Figure 5.11, the NO specific electrode tends to exhibit some variability that cannot be eliminated. For this reason, it was not possible to completely quantify the enhancement effect attributed to the QDs. However, an obvious cause for the considerable enhancement incurred with the QDs is due to their considerably higher absorbance at all wavelengths at the concentrations used here. Figure 5.13 compares the UV-

Figure 5.13. Comparison of the absorbance spectra of phosphate buffered solutions of 100 nM QDs (circles) and 200 μ M **2**. Inset shows blow up of 300–600 nm spectral range.



Visible absorbance spectrum of independent phosphate buffered solutions of the QDs (100 nM) and **2** (200 μ M) at the concentrations typically used for the NO electrode experiments discussed above. For the photolysis experiments described above, a UV band pass filter having maximal transmittance at the 366 nm line of the Hg arc lamp was used. At 366 nm, the extinction coefficient of these water soluble CdSe/ZnS QDs is $\sim 690,000 \text{ M}^{-1}\text{cm}^{-1}$, compared to a value of $\sim 200 \text{ M}^{-1}\text{cm}^{-1}$ for **2** at the same wavelength. The data in Figure 5.13 exemplify the high extinction coefficients of the QDs; although [**2**] is 2000 times that of the QDs in the mixtures described above, the absorbance is clearly dominated by the QD chromophores across the spectral range investigated. Over the wavelength range of the filter (320–390 nm, where the transmittance $>10\%$), the QDs absorb 2 to 10 times as much light as **2**, and the magnitude of enhanced NO production in

their presence indicates that optical excitation of the QDs results in efficient sensitization of the photochemically active excited state of **2**.

All experiments for detection of NO described so far were done using irradiation with UV light (320-390 nm). It is clear from Figure 5.2C that the QD PL is quenched in the presence of **2** when 546 nm excitation is used. However, so far, all attempts to quantify NO production from mixtures of the QDs and **2** during photolysis with a visible band pass filter (460-600 nm) were unsuccessful. For the case of **2** alone, only a very weak signal is observed (<150 pA). At this point, the inability to detect NO using light with energy for which QD PL quenching clearly occurs can only be explained by a concentration issue. In fact, when use of an interference filter to select out the 366 nm Hg line alone (which also diminishes the overall light intensity substantially) was attempted, no signal was observed for photolysis of **2** alone with a concentration of ~200 nM (comparable to the experiments described previously). Based on these results, it became clear that although sensitized NO release likely occurs with visible as well as UV excitation, the concentrations used for these experiments must be raised and carefully tuned to optimize the response of the NO electrode. This work is currently being pursued by Alexis D. Ostrowski in this laboratory.

iii. Two Photon Sensitization in Assemblies of QDs with

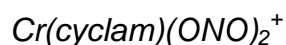
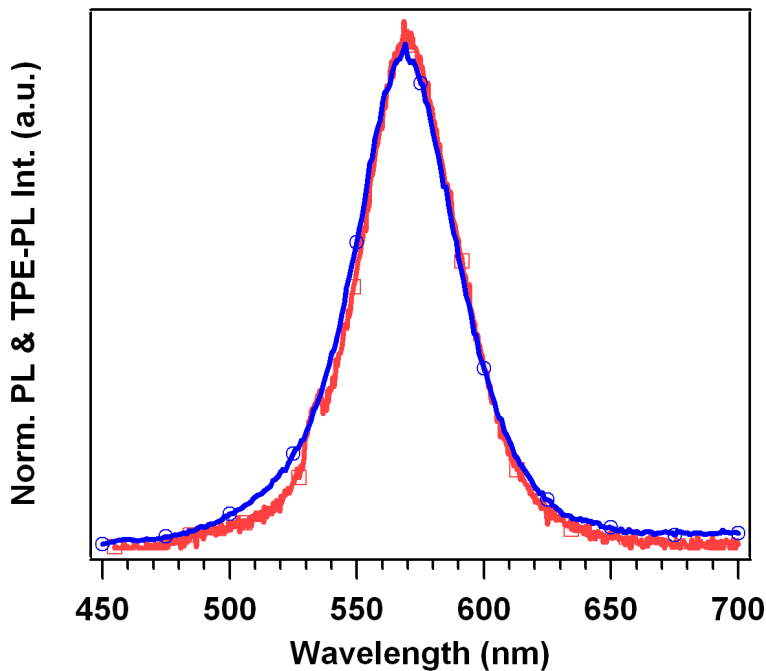


Figure 5.14 compares the PL spectrum of the DHLA coated CdSe/ZnS QDs using 400 nm excitation with the two photon excited photoluminescence (TPE-

PL) spectrum of the same QDs. The TPE-PL was obtained using the 800 nm output of a tunable Ti:sapphire laser operated at 80 MHz with an average pulse width of ~ 120 fs. The two spectra in Figure 5.14 are virtually indistinguishable, consistent with photon emission from the same emitting state following excitation above the band gap with either single photon excitation (SPE) at 400 nm or two photon excitation (TPE) at 800 nm. A slight broadening of the SPE generated PL, especially on the blue edge, is evident. One explanation for this result is that the TPE-PL may preferentially sample a fraction of the total size distribution within the sample.

Figure 5.14. Comparison of the SPE (400 nm, cw; blue open circles) and TPE (800 nm, 120 fs pulses; red open squares) generated photoluminescence of the DHLA coated CdSe/ZnS QDs used in this study. Both samples were diluted in phosphate buffer (15 mM, pH 8.2).

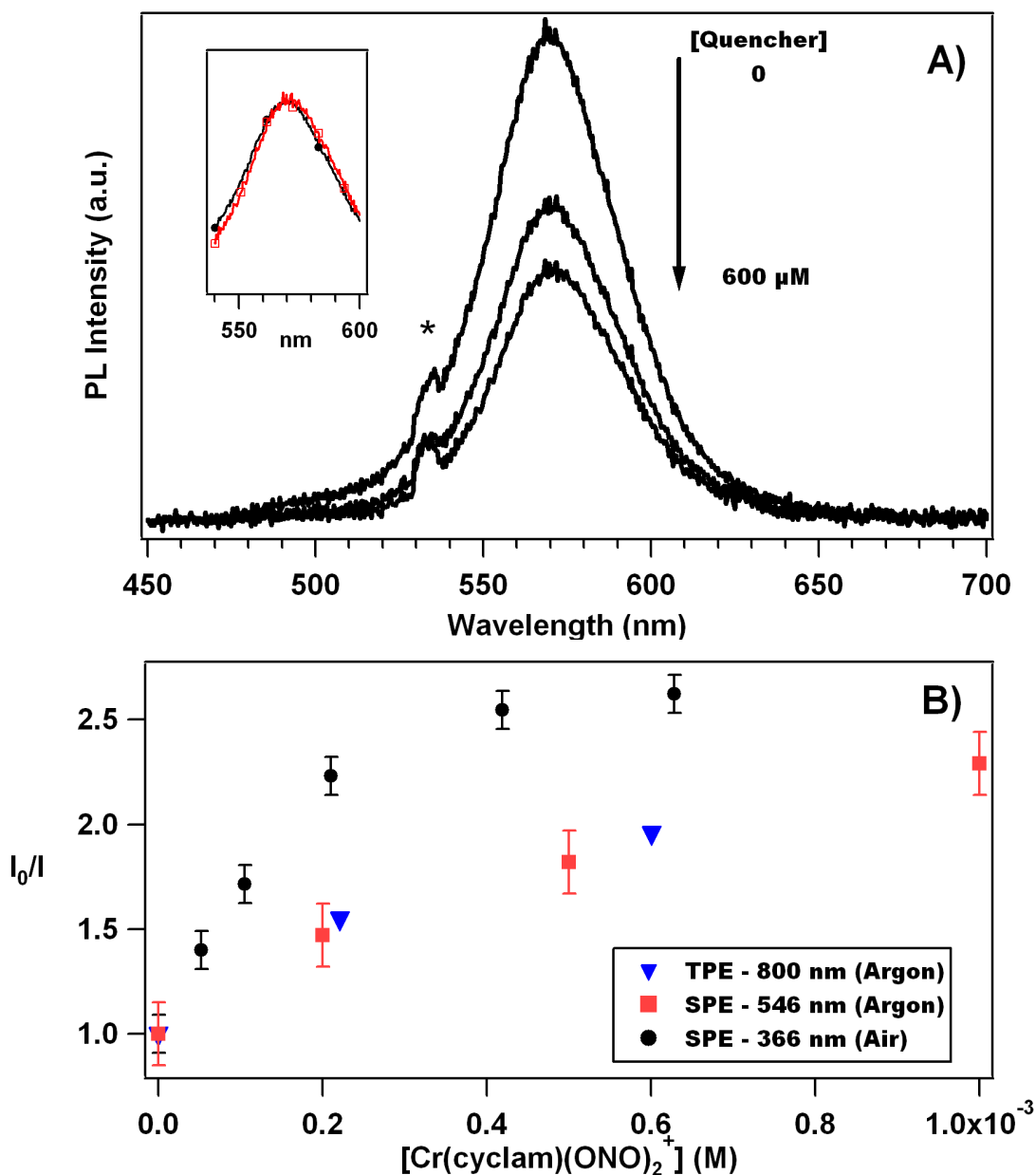


The two photon absorption (TPA) cross-section for the QDs studied here was obtained by the method of Hu and Webb¹⁷ as described in chapter II, in which the

integrated TPE-PL intensity of the QDs (120 nM) is compared to that of obtained from a 13.5 μM fluorescein reference sample (H_2O , pH 11) which has a SPE quantum yield of 0.92 and a TPA cross-section of 36 GM at 800 nm.¹⁷ Using these values for the standard, along with the SPE quantum yield of the QDs (0.02), a TPA cross-section of 10,300 GM is calculated for the water soluble QDs. This value is in close agreement with that reported by Larson *et al* for similarly sized QDs dissolved in water⁵ and is consistent with the large TPA cross-sections predicted for semiconductor quantum dots.¹⁸

The results with the QDs alone demonstrated that these materials have strong TPA cross-sections in the near-IR, and that excitation via TPE generates what appears to be the same emitting state as that obtained in the single photon case. Thus, mixtures of the QDs and **2** were investigated to determine if the TPE-PL of the QDs is also quenched by **2**. Figure 5.15 demonstrates that the TPE-PL was clearly quenched by added **2** in a concentration dependent manner analogous to that observed for SPE. In fact, the TPE-PL quenching data closely follows the data obtained previously for excitation at 546 nm (Figure 5.15B). The similarity of the data obtained is remarkable; notably, the small red shift of the QD PL observed with SPE at high [**2**] (Figure 5.3) is also reproduced in the TPE-PL data (inset Figure 5.15A). These results give strong evidence that two photon excitation of the QDs achieves sensitization of **2** via a process equivalent to that observed for **2** and **1** via single photon excitation.

Figure 5.15. A) TPE-PL spectra of solutions of QDs (120 nM) with varied concentrations of **2** (220 and 600 μM) generated by excitation with 120 fs pulses of 800 nm light (80 MHz). (*) Astrisk marks an instrumental artifact present in all of the TPE-PL data. Inset compares normalized TPE-PL spectra of the QDs in the absence of (black filled circles) and presence of **2** at a concentration of 600 μM (red open squares) exemplifying red shift that accompanies quenching. B) Stern-Volmer type plot comparing the TPE-PL quenching data generated with pulsed NIR excitation, to the analogous experiments using cw excitation in the UV and visible range.



Although attempts were made to perform the analogous experiments to detect TPE sensitized NO production in mixtures of the QDs with **2**, it was not possible to analytically detect the NO evolved under the conditions used. As similar problems were incurred when attempting to detect photochemically produced NO from **2** under low light intensities, it is likely that a similar issue precluded NO detection in the TPE case as well. Based on the relatively weak signals seen in Figure 5.7 and Figure 5.11, it is clear that the photolysis experiments (both SPE and TPE) are all conducted at concentrations that constitute the detection limit of the NO electrode for decomposition of **2**. However, another point should be made. The data in Figure 5.15B (and also in Figure 5.4) suggests that there may be some inherent difference in the photophysical interactions between the QDs and the Cr(III) complexes upon UV excitation as compared to excitation in the visible or the NIR. Clearly, UV excitation leads to a more pronounced quenching than is observed with lower energy excitation. Unfortunately, without further investigation of the detailed mechanism by which the two systems interact, it is difficult to identify what is special about the UV excitation except that it is capable of accessing higher energetic states in the excited state manifolds for both the QDs and the metal complexes. Whether such higher energy is needed in order to access the NO labilizing excited state remains an open question at this point.

D. Conclusions

These results demonstrate that QDs can function effectively as sensitizers of photochemical reactions of complexes that are electrostatically bound near the QD

surfaces. Furthermore, the ability to generate NO from **2** using QDs as light absorbing antenna brings us one step closer to using **2** and other similar photochemically active transition metal based NO donors as pro-drugs due to the large enhancement in their light absorbing capability.

E. References

1. examples are: (a) Ford, P. C.; Bourassa, J.; Miranda, K. M.; Lee, B.; Lorkovic, I.; Boggs, S.; Kudo S.; Laverman L. *Coord. Chem. Rev.* **1998**, *171*, 185-202. (b) Tfouni, E.; Krieger, M.; McGarvey, B. R.; Franco, D. W. *Coord. Chem. Rev.* 2003, *236*, 57-69. (c) Sauaia, M. G.; De Lima, R. G.; Tedesco, A. C.; Da Silva, R. S. *J. Am. Chem. Soc.* **2003**, *125*, 14718-14719. (d) Pavlos, C. M.; Xu, H.; Toscano, J. P. *Cur. Topics Med. Chem.* **2005**, *5*, 635-645. (e) Eroy-Reveles, A A.; Leung, Y.; Mascharak, P. K. *J. Am. Chem. Soc.* **2006**, *128*, 7166-7167.
2. (a) Bourassa, J.; DeGraff, W.; Kudo, S.; Wink, D. A.; Mitchell, J. B.; Ford, P. C. *J. Am. Chem. Soc.* **1997**, *119*, 2853-2860. (b) Conrado, C. L.; Weckslers, S.; Egler, C.; Magde, D.; Ford, P. C. *Inorg. Chem.* **2004**, *43*, 5543-5549. (c) DeLeo, M. A.; Ford, P. C. *J. Am. Chem. Soc.* **1999**, *121*, 1980-1981. (d) DeRosa, F.; Bu, X.; Ford, P.C. *Inorg. Chem.* **2005**, *44*, 4157-4165 and references therein.
3. a) Weckslers, S. R.; Mikhailovsky, A.; Ford, P. C. *J. Am. Chem. Soc.* **2004**, *126*, 13566-13567. (b) Weckslers, S. R.; Mikhailovsky, A.; Korystov, D.; Ford, P. C. *J. Am. Chem. Soc.* **2006**, *128*, 3831-3837.
4. (a) Leatherdale, C. A.; Woo, W.-K.; Mikulec, F. V.; Bawendi, M. G. *J. Phys. Chem. B.* **2002**, *106*, 7619-7622. (b) Schmelz, O.; Mews, A.; Basché, T.; Herrmann, A.; Müllen, K. *Langmuir* **2001**, *17*, 2861-2865. (c) Yu, W. W.; Qu, L.; Guo, W.; Peng, X. *Chem. Mater.* **2003**, *15*, 2854-2860.
5. Larson, Daniel R.; Zipfel, W. R.; Williams, R. M.; Clark, S. W.; Bruchez, M. P.; Wise, F. W.; Webb, W. W. *Science* **2003**, *300*, 1434-1436.
6. Alivisatos, A. P. *J. Phys. Chem.* **1996**, *100*, 13226-13239.
7. Uyeda, H. T.; Medintz, I. L.; Jaiswal, J. K.; Simon, S. M.; Mattoussi, H. *J. Am. Chem. Soc.*, **2005**, *127*, 3870-3878.
8. examples are (a) Gao, X.; Yang, L.; Petros, J. A.; Marshall, F. F.; Simons, J. W.; Nie, S. *Curr. Opin. Biotech.* **2005**, *16*, 63-72 and references therein. (b) Delehanty, J. B.; Medintz, I. L.; Pons, T.; Brunel, F. M.; Dawson, P. E.; Mattoussi, H.. *Bioconjugate Chem.* **2006**, *17*, 920-927
9. Rothrock, A. R.; Donkers, R. L.; Schoenfish, M. H. *J. Am. Chem. Soc.* **2005**, *127*, 9362-9363.

10. Caruso, E. B.; Petralia, S.; Conoci, S.; Giuffrida, S.; Sortino, S. *J. Am. Chem. Soc.* **2006**, ASAP published on the web 12/29/2006.
11. (a) Wijtmans, M.; Rosenthal, S. J.; Zwanenburg, B.; Porter, N. A. *J. Am. Chem. Soc.* **2006**, 128, 11720-11726. (b) Warriar, M.; Lo, M. K. F.; Monbouquette, H.; Garcia-Garibay, M. A. *Photochem. Photobio.* **2004**, 3, 859-863
12. (a) Samia, A. C. S.; Chen, X.; Burda, C. *J. Am. Chem. Soc.* **2003**, 125, 15736-15737. (b) Shi, L.; Hernandez, B.; Selke, M. *J. Am. Chem. Soc.* **2006**, 128, 6278-6279. (c) Bakalova, R.; Ohba, H.; Zhelev, Z.; Nagase, T.; Jose, R.; Ishikawa, M.; Baba, Y. *Nano Lett.* **2004**, 4, 1567-1573. (d) Bakalov, R.; Ohba, H.; Zhelev, Z.; Ishikawa, M.; Baba, Y. *Nat. Biotech.* **2004**, 22, 1360-1361. (e) Clarke, S.; Hollmann, C. A.; Zhang, Z.; Suffern, D.; Bradforth, S. E.; Dimitrijevic, N. M.; Minarik, W. G.; Nadeau, J. L. *Nat. Mater.* **2006**, 5, 409-417. (f) Ipe, B. I.; Lehnig, M.; Niemeyer, C. M. *Small* **2005**, 1, 706-709. (g) Lovric, J.; Cho, S. J.; Winnik, F. M.; Maysinger, D. *Chem. Biol.* **2005**, 12, 1227-1234.
13. (a) Murray, C. B.; Norris, D. J.; Bawendi, M. G. *J. Am. Chem. Soc.*, **1993**, 115, 8706-8715. (b) Talapin, D. V.; Rogach, A. L.; Kornowski, A.; Haase, M.; Weller, H. *Nano Lett.*, **2001**, 1, 207-211. (c) de Mello Donega, C.; Hickey, S. G.; Wuister, S.; Vanmaekelbergh, D.; Meijerink, A. *J. Phys. Chem. B*, **2003**, 107, 489-496. (d) Dabbousi, B. O.; Rodriguez-Viejo, J.; Mikulec, F. V.; Heine, J. R.; Mattoussi, H.; Ober, R.; Jensen, K. F.; Bawendi, M. G. *J. Phys. Chem. B*, **1997**, 101, 9463-9475. (e) Mattoussi, H.; Mauro, J. M.; Goldman, E. R.; Anderson, G. P.; Sundar, V. C.; Mikulec, F. V.; Bawendi, M. G. *J. Am. Chem. Soc.*, **2000**, 122, 12142-12150.
14. Neuman, D. *unpublished results*.
15. (a) Nazzal, A. Y.; Wang, X.; Qu, L.; Yu, W.; Wang, Y.; Peng, X.; Xiao, M. *J. Phys. Chem. B*. **2004**, 108, 5507-5515. (b) Wang, Y.; Tang, Z.; Correa-Duarte, M. A.; Pastoriza-Santos, I.; Giersig, M.; Kotov, N. A.; Liz-Marzán, L. M. *J. Phys. Chem. B*. **2004**, 108, 15461-15469. (c) Myung, N.; Bae, Y.; Bard, A. J. *Nano. Lett.*, **2003**, 3, 747-749,
16. Förster, T. *Discuss. Faraday Soc.* **1959**, 27, 7-17
17. Webb, W.W.; Xu, C., *J. Opt. Soc. Am. B* **1996**, 13, 481-491.
18. Blanton, S. A.; Hines, M. A.; Schmidt, M. E.; Guyot-Sionnest, P. *J. Luminescence* **1996**, 70, 253-268.

19. Mitchell, J. B.; Wink, D. A.; DeGraff, W.; Gamson, J.; Keefer, L. K.; Krishna, M. C. *Canc. Res.* **1993**, *53*, 5845-5848.
20. Hardman, R. *Environ. Health Persp.* **2006**, *114*, 165-172 and references therein.

6. Chapter VI. Conclusions and Future Potential

Although recent work demonstrates that QDs are effective in producing highly reactive singlet oxygen, the active molecule in traditional photodynamic therapy (PDT),¹ the current study is the first example of the use of water soluble semiconductor QDs as photo-activators for drug delivery that targets the hypoxic environment often encountered in tumor cells.² The proposed photochemotherapy applications will require excitations at long wavelengths (red or near infrared) possibly via TPE and likely could be targeted with other nitric oxide precursors as well. Two photon excitation (TPE) already shows great promise for the current system as demonstrated by the quantum dot TPE-PL quenching by **2**. A current collaboration with Professor Elia Tfouni (University of Sao Paulo, Brazil) is directed towards developing related ruthenium nitrosyl complexes³ with functionalities that are capable of binding the QD surface or being conjugated with a preexisting QD surface modality.

The general concept outlined here in the use of quantum dots as photosensitizers for photochemically active transition metal complex can be extended, it would seem, to virtually any system. Of course, a careful quantitative investigation of the mechanism(s) involved in for instance, enhanced NO release from the *trans*-Cr(cyclam)(ONO)₂⁺ cation in the presence of QDs, is still needed. Proper choice of system, e.g. matching the particular photochemically active complex with the ideal QD system (core material, core versus core/shell system,

etc) will depend on the required energetics for photochemical sensitization. Clearly, simple energy transfer in terms of a FRET based model is not the only active mechanism in the system described in this dissertation. Therefore, other energetic nuances of the system besides spectral overlap, for instance positions of the QD valence and conduction bands as well as positions of surface related *inter-gap* states relative to the redox states of the dinitrito Cr(III) complex must be considered. Although there are a few investigations detailing the former⁴, a quantitative investigation of these particular QDs must be conducted since the relevant energy levels are presumably sensitive to the surface composition. On the other hand, relatively little work is reported on the redox properties of the dinitrito Cr(III) complexes. Although the position of the Cr^{III}/Cr^{II} couple has been investigated in a variety of cyclam derivatives with various axial ligands⁵, less is known about the Cr^{IV}/Cr^{III} couple which is more pertinent here. A thorough investigation regarding the redox chemistry of this system and may uncover the true nature of the QD/Cr(III) cyclam interaction.

Another important aspect that will require consideration is the design of stable QD/NO-donor conjugates. Although the long term stability of the electrostatic assemblies described in chapters IV and V has not yet been studied, it is unlikely that such a system would remain intact for extended periods *in vivo*. Whereas Mattoussi *et al* report a relatively stable electrostatic assembly of DHLA coated QDs and positively charged proteins, the proteins in that work are engineered with an extended polycationic tail that presumably magnifies the electrostatic

attraction.⁶ Such a system could be envisioned here, but a covalent assembly may be preferable for many applications. Considering the extensive studies in chapter III, the technology for direct covalent attachment of various molecular species and macromolecules to nanomaterial surfaces has not yet reached a level of sophistication needed for broad application. For QDs, the short alkyl chain based surface coatings/linkers such as those investigated here, although ideal for the short separation distances needed for FRET, are considered less than optimum with respect to the QD and mQD long term stability in aqueous dispersions.⁷ For the present system, FRET does not appear to be the only active mechanism allowing photosensitization. Although any electronic communication between the QDs and the acceptor species will have some distance dependence, future studies should not be limited to ultra short QD stabilizers. Rather one should consider QD stabilizing modalities like amphiphilic polymers⁸, dendrimers⁹, or cross-linked functionalized alkyl chains^{7b} due to their demonstrated enhancement of the long term stability of QDs in solution and in solution phase reactions.

Clinical use of quantum dot based supramolecular structure, such as the QD sensitized NO donors discussed here, will also require evaluation of 1) QD stability, 2) QD thermal toxicity, and 3) the target specificity of the new functional nanomaterial. With respect to the first two points, the limited data available to date indicate that the cytotoxicity of QDs is strongly correlated to their stability, with for example core/shell structures such as those used here *generally* having less toxic effects,¹⁰ However, because much of the limited data has not been

collected by toxicologists, careful systematic investigation of the various QD preparations available using well established and standardized procedures will be required to elucidate their deleterious effects.

With regards to the target specificity for *in vivo* applications, extensive work in the development of QDs as bioimaging agents shows that a variety of tissue/biomolecule specific targeting strategies can be effective¹¹, and thus modified QDs have considerable promise as site-specific agents for photochemical drug delivery. These studies exemplify the greatest potential for QDs and nanomaterials as a whole in biomedical applications. As wet-chemical approaches to the preparation of many nanomaterials have become the route of choice, the freedom to tune chemical functionality of the new materials is virtually endless. This allows one to design multimodal nanostructures with application specific optical, solubility, targeting, and activation properties, and which at the same time exist on a size-scale comparable to various cellular species. For this reason, nanomaterials are already seeing extensive application in the biomedical field, with quantum dots and other inorganic nanoparticles leading the headlines in cellular imaging¹², whereas nanosized polymeric materials and liposomes receiving considerable attention for new drug-delivery strategies¹³.

Clearly, the research described here-in, though provocative and exciting, only scratches the surface of what will likely be a bright future for QDs in biomedical applications. Further studies for the development of quantum dot based systems,

particularly those suited to serve as photosensitizers for NO delivery, are continuing in this laboratory.

References

1. (a) Samia, A. C. S.; Chen, X.; Burda, C. *J. Am. Chem. Soc.* **2003**, *125*, 15736-15737. (b) Shi, L.; Hernandez, B.; Selke, M. *J. Am. Chem. Soc.* **2006**, *128*, 6278-6279. (c) Bakalova, R.; Ohba, H.; Zhelev, Z.; Nagase, T.; Jose, R.; Ishikawa, M.; Baba, Y. *Nano Lett.* **2004**, *4*, 1567-1573. (d) Bakalov, R.; Ohba, H.; Zhelev, Z.; Ishikawa, M.; Baba, Y. *Nat. Biotech.* **2004**, *22*, 1360-1361. (e) Clarke, S.; Hollmann, C. A.; Zhang, Z.; Suffern, D.; Bradforth, S. E.; Dimitrijevic, N. M.; Minarik, W. G.; Nadeau, J. L. *Nat. Mater.* **2006**, *5*, 409-417. (f) Ipe, B. I.; Lehnig, M.; Niemeyer, C. M. *Small* **2005**, *1*, 706-709. (g) Lovric, J.; Cho, S. J.; Winnik, F. M.; Maysinger, D. *Chem. Biol.* **2005**, *12*, 1227-1234.
2. Mitchell, J. B.; Wink, D. A.; DeGraff, W.; Gamson, J.; Keefer, L. K.; Krishna, M. C. *Canc. Res.* **1993**, *53*, 5845-5848.
3. Tfouni, E.; Krieger, M.; McGarvey, B. R.; Franco, D. W. *Coord. Chem. Rev.* **2003**, *236*, 57-69 and references therein.
4. (a) Brus, L. E. *J. Chem. Phys.* **1983**, *79*, 5566-5571. (b) Sykora, M.; Petruska, M. A.; Alstrum-Acevedo, J.; Bezel I.; Meyer, T. J.; Klimov, V. I. *J. Am. Chem. Soc.* **2006**, *128*, 9984-9985. (c) Wang, C.; Shim, M.; Guyot-Sionnest, P. *Science* **2001**, *291*, 2390-2392.
5. Guldi, D.; Wasgestian, F.; Meyerstein, D. *Inorg. Chim. Acta.* **1992**, *194*, 15-22.
6. Mattoussi, H.; Mauro, J. M.; Goldman, E. R.; Anderson, G. P.; Sundar, V.C.; Mikulec, F. V.; Bawendi, M. G. *J. Am. Chem. Soc.*, **2000**, *122*, 12142-12150.
7. (a) Parak, W. J.; Gerion, D.; Pellegrino, T.; Zanchet, D.; Micheel C.; Williams, S. C.; Boudreau, R.; Le Gros, M. A.; Larabell, C. A.; Alivisatos, A. P. *Nanotech.* **2003**, *14*, R15-R27 and references therein. (b) Jiang, W.; Mardyani, S.; Fishcer, H.; Chan, W. C. W. *Chem. Mater.* **2006**, *18*, 872-878.
8. examples are: (a) Wu, X.; Liu, H.; Liu, J.; Haley, K. N.; Treadway, J. A.; Larson, J. P.; Ge, N.; Peale, F.; Bruchez, M. P. *Nat. Biotech.* **2003** *21*, 41-46. (b) Ballou, B.; Lagerholm, B. C.; Ernst, L. A.; Bruchez, M. P.; Waggoner, A. S. *Bioconj. Chem.* **2004**, *15*, 79-86. (c) Gao, X.; Cui, Y.; Levenson, R. M.; Chung, L. W. K.; Nie, S. *Nat. Biotech.* **2004**, *22*, 969-

976. (d) Bakalova, R.; Zhelev, Z.; Ohba, H.; Baba Y. *J. Am. Chem. Soc.* **2005**, *127*, 11328-11335.
9. Guo, W.; Li, J. J.; Wang, Y. A.; Peng, X. *Chem. Mater.* **2003**, *15*, 3125-3133.
10. Hardman, R. *Environ. Health Persp.* **2006**, *114*, 165-172 and references therein.
11. examples are (a) Gao, X.; Yang, L.; Petros, J. A.; Marshall, F. F.; Simons, J. W.; Nie, S. *Curr. Opin. Biotech.* **2005**, *16*, 63-72 and references therein. (b) Delehanty, J. B.; Medintz, I. L.; Pons, T.; Brunel, F. M.; Dawson, P. E.; Mattoussi, H.. *Bioconjugate Chem.* **2006**, *17*, 920-927.
12. (a) Kawasaki, E. S.; Player, A. *Nanomedicine* **2005**, *1*, 101-109 and references therein. (b) Michalet, X.; Pinaud, F. F.; Bentolila, L. A.; Tsay, J. M.; Doose, S.; Li, J. J.; Sundaresan, G.; Wu, A. M.; Gambhir, S. S.; Weiss, S. *Science* **2005**, *307*, 538-544 and references therein.
13. Cuenca, A. G.; Jiang, H.; Hochwald, S. N.; Delano, M.; Cance, W. G.; Grobmyer, S. R. *Cancer* **2006**, *107*, 459-466 and references therein.

I. Appendix I. Photoenhancement in CdSe QDs in the Presence of NO

A. Introduction

Even in highly crystalline materials, the nature of the surface with respect to optimum surface reconstruction and complete electronic passivation holds the key to obtaining materials with high radiative recombination efficiencies. It has become common practice to coat CdSe cores with a thin shell (1-5 monolayers typically) of a higher semiconductor with a higher band-gap such as ZnS or CdS.¹⁻³ The fluorescence quantum yield can be thus raised from a few percent for the original, organically capped material, to several tens of percent (10-50%) for the coated particles. The higher band gap material functions by preventing migration of electronically excited carriers to the surface where they may trap or become involved in redox reactions with molecules on or near the surface. The overcoat has also been shown to enhance the over-all stability of the quantum dots (QDs) with respect to oxidation and photo-degradation.²

Even with the improvements in particle quality and electronic passivation, the photoluminescence properties of the nanoparticles are observed to be highly sensitive and vary from report to report. A large number of investigations have shown both photoenhancement and quenching in solid thin films and in dispersions of semiconductor nanoparticles. The changes observed can be divided into two main categories, 1) reversible, and 2) irreversible. In the latter case,

continuous irradiation with above band-gap light of thin films in the presence of air⁴ or moisture⁵, or in solution in the presence of methanol⁶ or air⁷ leads to an increase in the photoluminescence intensity. In this case, the observed effect is attributed to permanent photo-induced changes in the surface structure, either by rearrangement and/or loss of surface passivants, or by oxidation to form CdO and SeO₂. Both of these mechanisms are supported by X-ray photoelectron spectroscopy (XPS) and time-of-flight secondary ion mass spectrometry (ToF-SIMS) studies in which the surface structure was investigated at different stages of photolysis.⁸ Additionally, purely chemical treatments either with sodium borohydride⁹ or dissolved oxygen¹⁰ have been shown to have similar photoluminescence enhancement effects attributed to oxidation of the surface of the nanoparticles.

Only a few reports have shown examples of reversible type photo-enhancement behavior. Jones *et al* found that the photoluminescence of previously irradiated solutions of CdSe and excess stabilizer (trioctylphosphine oxide, TOPO) dropped in intensity, eventually falling below the original, “pre-brightened”, level.⁶ This process was observed to be extremely slow. A similar “darkening” following irradiation was observed by Zhelev *et al*, whom in addition found no changes in the corresponding optical absorbance spectra during either the photo-enhancement or darkening periods.¹¹ These examples are indicative of generation of photostationary state, which clearly does not involve the permanent photo-chemistry typified by experiments described previously.

Single particle photoluminescence experiments have shown that particles exhibit luminescence intermittency or blinking.¹² The widely excepted explanation for the on/off behavior is Auger ionization of the particles due to the generation of multiple excitons within a single particle. This leads to trapping of carriers at or near the particle surface, generating trap states that, following another photo-excitation, decay nonradiatively. Additionally, correlated atomic force microscopy and single-particle fluorescence microscopy have shown that a significant portion of the particles in a sample (sometimes exceeding 50 % of the ensemble) are dark.¹³ Yet, until recently there has been know experimental evidence linking the distribution of bright and dark particles seen in single-particle work with the photoenhancement effects of ensembles. A recent report by Muller *et al* shows that when the environment of a sample of CdSe is quickly purged with air, particles that were originally dark under vacuum are turned on, while the ones that were already emissive become brighter.¹⁴ This suggests that the effects described for ensemble measurements are due, at least partially, to tuning of the relative population of bright and dark particles in the ensemble. Our results are consistent with a similar photo-induced surface-substrate interaction that turns dark particles on, increasing the total quantum yield for the ensemble. Reactive substrates near the surface can stabilize trap states that would otherwise allow localization of an ejected charge carrier.

B. Experimental

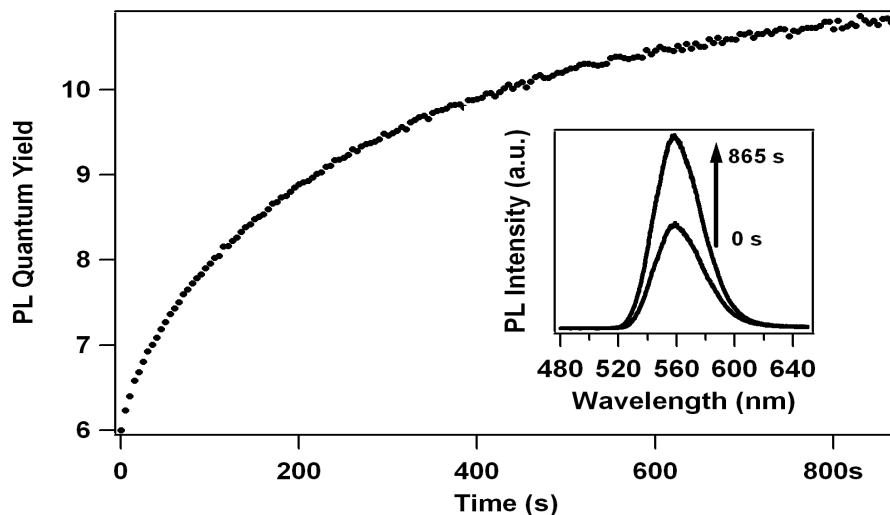
CdSe-HDA quantum dots (QDs) were synthesized using the single source precursor route as described in chapter II. Solutions of QDs in spectroscopy grade toluene (Burdick and Jackson) were prepared in sealed cells under argon or nitric oxide.

C. Results and Discussion

A typical photoluminescence (PL) intensity response of a toluene solution of CdSe-HDA (~350 nM) containing ~12 mM dissolved nitric oxide gas is shown in Figure I.1. Over a ~850 s period of continuous photolysis with the 488 nm output of an argon ion laser, the PL intensity was observed to increase by nearly a factor of 2, corresponding to an increase in quantum yield from 6 to ~11 %. Careful analysis of the spectral data before and after the photolysis showed that the band-edge emission has narrowed slightly decreasing the asymmetry seen in the original spectrum under argon. Inspection of the corresponding UV-vis absorbance spectra showed negligible changes in the QD absorbance.

The changes that were observed here in the shape and positions of the optical spectra following irradiation are very small compared to what is seen in thin films^{4,5} irradiated in air where large blue shifts, 15-20 nm, and substantial fluctuations in line-widths were observed. In both of these investigations, the authors hypothesized that the enhancement and the blue shift is driven by permanent photo-chemistry at the surface of nanoparticles, resulting in a

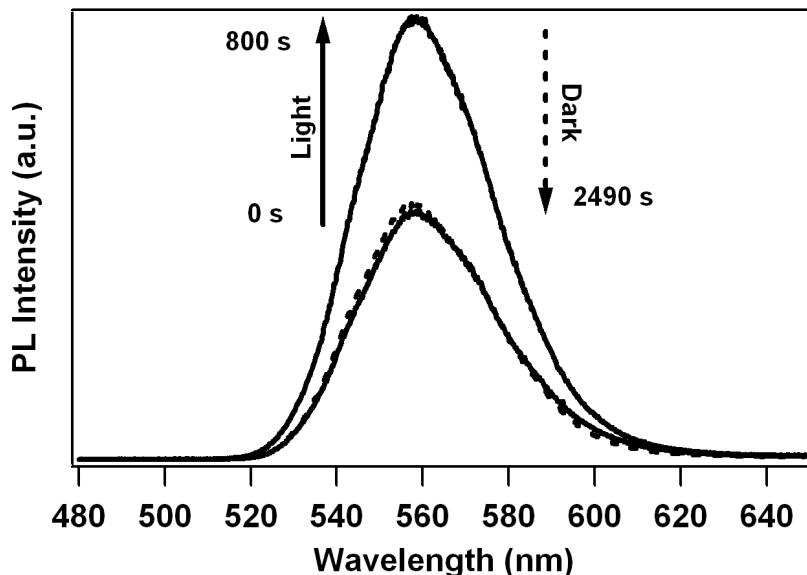
Figure I.1. Change in the PL quantum yield of a ~ 350 nM solution of CdSe-HDA QDs in toluene with 12 mM dissolved nitric oxide (NO). The sample is continuously stirred while being irradiated with the 488 nm line of an Ar^+ laser (13 mW average power). Inset shows the PL spectrum before and after 865 s of continuous photolysis.



substantial oxide layer that effectively decreases the particle size. This mechanism does not appear to play a major role in our experiments. First, we saw no substantial shift in energy of the emission maximum. Second, the enhancement in our experiments was shown to reverse when the illumination was removed. Over the course of minutes to hours, the photo-enhanced luminescence slowly decreased in intensity (Figure I.2). The time constant for this darkening process was found to vary widely from experiment to experiment. A similar slow relaxation process was observed by Jones *et al* for solutions of CdSe containing excess surfactant (TOPO).⁶ In those experiments, the small changes in peak position and linewidths were also observed to relax, at least partially, when the illumination is was removed. These reports, combined with what was observed here under NO suggest that the enhancement and darkening processes are due

largely to a tuning between a dark and bright state of the ensemble, and only to a smaller extent, if at all to permanent surface chemistry.

Figure I.2. Spectral data comparing effects of light irradiation (800 s, 488 nm at 13 mW) followed by a period of darkness (2490 s) on a ~ 350 nM solution of CdSe-HDA QDs dissolved in toluene with 12 mM NO.



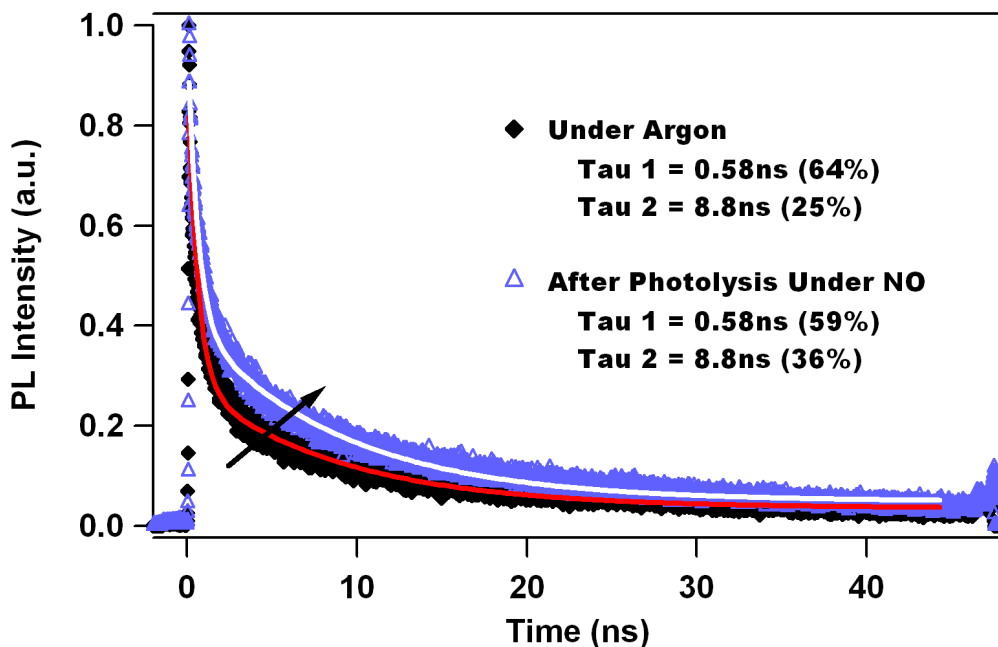
To further investigate any changes that may occur on the surface, we monitored the infrared absorbance of the CdSe solution under NO after illumination. While free NO has a small extinction coefficient for the N-O stretch at 1875 cm^{-1} ($\sim 20\text{ M}^{-1}\text{cm}^{-1}$), metal bound NO species show strong signatures for the NO stretch between $1400\text{--}2000\text{ cm}^{-1}$ depending on the character of the binding.¹⁶ However, no new features were detected in the region of $1600\text{--}2300\text{ cm}^{-1}$ (limited by the dichloromethane solvent). Only a weak, broad band centered at 1875 cm^{-1} and a sharp signal at 2223 cm^{-1} were observed. These bands can be assigned to free NO and N_2O , respectively, the latter being a common impurity in

the NO used here. There was no evidence for formation of a new metal-NO species on the surface.

In support of a brightening mechanism that is governed by the activation of otherwise dark particles, the PL lifetime was monitored before and after the photolysis experiment (Figure I.3). The luminescence decay was fit to a double exponential decay, consistent with previous measurements on these systems.¹⁷

Under argon, the fast,

Figure I.3. PL lifetimes measured for a solution of ~350 nM CdSe-HDA QDs dissolved in toluene initially under argon (blue triangles) and following cw photolysis (865 s, 488 nm at 13 mW) with 12 mM dissolved NO added (black squares). Samples were excited with 120 fs pulses tuned to 400 nm (2 MHz).



sub-nanosecond component (0.58 ns) comprises 64 % of the total luminescence intensity, while the slower component (8.8 ns) makes-up only 25 % of the signal. It should be noted that on the time-scale of this experiment, the luminescence signal has not decayed completely. Using these fitting parameters, ~11 % of the

luminescence intensity has a lifetime longer than 50 ns. Following illumination under NO, there are substantial changes in the decay parameters. The largest change is observed in the 8.8 ns component which increases in amplitude to 36 % of the total signal. This is equivalent to a 44 % increase in the contribution of the long component to the luminescence intensity. In reference 17, the fast and long components are assigned to relaxation from the charged exciton (CE) and band edge exciton (BEE) states, respectively. The longer component was not assigned in that work, likely due to experimental limitations. Yet, luminescence decays obtained on a nanosecond system for CdSe nanoparticles of similar size dispersed in toluene had previously been observed to contain a short component convoluted with the pulse (<10 ns), and a longer component on the order of 60-100 ns whose amplitude comprised 10-20 % of the total signal.¹⁸ To date, this “much longer lived” feature remains unassigned. Yet, we see that the photo-enhancement seen in the steady-state is directly related to the increase in contribution of the strongly emitting BEE. This suggests a shift in the ensemble distribution, increasing the number of bright particles.

The origin of dark particles has been discussed in the context of luminescence intermittency, where bright particles are observed to blink on and off. This phenomenon has been attributed to charging of some of the particles most likely due to localization of a carrier at a structural/electronic defect at the surface. Brus *et al* demonstrated that a significant number of particles are positively charged using electrostatic force microscopy.¹⁹ When excited, charged particles are

expected to relax non-radiatively, and are thus largely non-emissive. These “dark” particles effectively reduce the observed emission quantum yield in an ensemble measurement.¹³ Taking this into account in the present investigation suggests that the brightening effect described above maybe due to the “turning on” of otherwise dark particles. We suggest that this is accomplished by some photochemically activated process between the dark QDs and the reactive NO molecules in solution. Support for this mechanism comes from recent results by Muller *et al.* showing conversion of dark to bright particles by exposing a sample to air.¹⁴

D. References

1. Hines, M. A.; Guyot-Sionnest, P. *J. Phys. Chem.*, **1996**, *100*, 468.
2. Peng, X.; Schlamp, M. C.; Kadavanich, A. V.; Alivisatos, A. P. *J. Am. Chem. Soc.*, **1997**, *119*, 7019.
3. Dabbousi, B. O.; Rodriguez-Viejo, J.; Mikulec, F. V.; Heine, J. R.; Mattoussi, H.; Ober, R.; Jensen, K. F.; Bawendi, M. G. *J. Phys. Chem. B.*, **1997**, *101*, 9463.
4. Nazzal, A. Y.; Wang, X.; Qu, L.; Yu, W.; Wang, Y.; Peng, X.; Xiao, M. *J. Phys. Chem. B.*, **2004**, *108*, 5507.
5. Cordero, S. R.; Carson, P. J.; Estabrook, R. A.; Strouse, G. F.; Buratto, S. K. *J. Phys. Chem. B.*, **2000**, *104*, 12137.
6. Jones, M.; Nedeljkovic, J.; Ellingson, R. J.; Nozik, A. J.; Rumbles, G. *J. Phys. Chem. B.*, **2003**, *107*, 11346.
7. Wang, Y.; Tang, Z.; Correa-Duarte, M. A.; Pastoriza-Santos, I.; Giersig, M.; Kotov, N. A.; Liz-Marzán, L. M. *J. Phys. Chem. B.*, **2004**, *108*, 15461.
8. Asami, H.; Abe, Y.; Ohtsu, T.; Kamiya, I.; Hara, M. *J. Phys. Chem. B.*, **2003**, *107*, 12566.
9. Jang, E.; Jun, S.; Chung, Y.; Pu, L. *J. Phys. Chem. B.*, **2004**, *108*, 4597.
10. Myung, N.; Bae, Y.; Bard, A. J. *Nano. Lett.*, **2003**, *3*, 747.
11. Zhelev, Z.; Jose, R.; Nagase, T.; Ohba, H.; Bakalova, R.; Ishikawa, M.; Baba, Y. *J. Photochem. Photobio. B.*, **2004**, *75*, 99.
12. Nirmal, M.; Dabbousi, B. O.; Bawendi, M. G.; Macklin, J. J.; Trautman, J. K.; Harris, T. D.; Brus, L. E. *Nature*, **383**, 802.
13. Ebenstein, Y.; Maokari, T.; Banin, U. *Appl. Phys. Lett.*, **2002**, *80*, 4033.
14. Muller, J.; Lupton, J. M.; Rogach, A. L.; Feldmann, J.; Talapin, D. V.; Weller, H. *Appl. Phys. Lett.*, **2004**, *85*, 381.
15. Cumberland, S. L.; Hanif, K.; Javier, A.; Khitrov, G. A.; Strouse, G. F.; Woessner, S. M.; Yun, C. S. *Chem. Mater.*, **2002**, *14*, 1576.

16. Ford, P. C.; Lorkovic, I. M. *Chem. Rev.*, **2002**, *102*, 993; *and references therein*.
17. Javier, A.; Magana, D.; Jennings, T.; Strouse, G. F. *Appl. Phys. Lett.*, **2003**, *83*, 1423.
18. Neuman, D. *Unpublished results*. Luminescence lifetimes were measured using the 3rd Harmonic of a pulsed Nd:YAG. The pulse width was roughly 10 ns (FWHM), and thus the sub-nanosecond and 8.8 ns components were strongly convoluted with the pulse itself.
19. Kraus, T. D.; Brus, L. E. *Phys. Rev. Lett.*, **1999**, *83*, 4840.